The influence of ionized impurities on the transport properties of a two-dimensional electron gas

Please check the document version of this publication:

• A submitted manuscript is the version of the article upon submission and before peer-review. There can be important differences between the submitted version and the official published version of record. People interested in the research are advised to contact the author for the final version of the publication, or visit the DOI to the publisher's website.
• The final author version and the galley proof are versions of the publication after peer review.
• The final published version features the final layout of the paper including the volume, issue and page numbers.

[Link to publication](#)

Download date: 17. Nov. 2023

THE INFLUENCE OF IONIZED IMPURITIES
ON THE TRANSPORT PROPERTIES OF A
TWO-DIMENSIONAL ELECTRON GAS

P.M. KOENRAAD

THE INFLUENCE OF IONIZED IMPURITIES
ON THE TRANSPORT PROPERTIES OF A
TWO-DIMENSIONAL ELECTRON GAS

PROEFSCHRIFT

Ter verkrijging van de graad van doctor aan de Technische Universiteit Eindhoven, op gezag van de Rector Magnificus, prof. ir. M. Tels, voor een commissie aangewezen door het College van Dekanen in het openbaar te verdedigen op vrijdag 16 februari 1990 te 14.00 uur

door

PAULUS MARIA KOENRAAD

geboren te Vught

Dit proefschrift is goedgekeurd door de promotor:

prof. dr. J.H. Wolter

en de copromotor:

dr. ir. F.A.P. Blom

aan

anne-marie

CONTENTS

CHAPTER 1

GENERAL INTRODUCTION

1.1 INTRODUCTION

This thesis deals with the study of the physical properties of two–dimensional electron gases such as realized in GaAs/Al$_x$Ga$_{1-x}$As heterostructures. The possibility of formation of such a two–dimensional electron gas (2DEG) is strongly related to the inclusion of intentionally doped sublayers. The commonly used dopant impurity for these layers is silicon. As a donor it provides the necessary electrons to form the 2DEG.

With present day epitaxial growth techniques like Molecular Beam Epitaxy (MBE) and Metal Organic Chemical Vapor Deposition (MOCVD) one can carefully adjust the position and confinement of doping atoms and electrons in GaAs and Al$_x$Ga$_{1-x}$As. Nowadays it is possible to obtain two–dimensional electron gases as well as two–dimensional doping layers. This has led to an intensive study of physical effects related to the 2DEG. In order to get a good insight in these new physical effects it is necessary to have a good understanding of the interaction between electrons and ionized doping atoms. With present growth techniques this interaction between the electrons and the ionized donors can be controlled in detail. From transport measurements one can get information on how the doping atoms are incorporated in the semiconductor material and how they behave as scattering centers.

Although the study of homogeneously doped crystals is a very old field there are still serious problems to be solved. For instance, even the simple problem of silicon as a doping atom of Al$_x$Ga$_{1-x}$As is still not well understood. While in Al$_x$Ga$_{1-x}$As with x < 0.25, silicon acts as a normal shallow donor, i.e. the activation energy is in the order of several meV, for x > 0.25 silicon acts as a deep donor, the so–called DX–center. This DX–center is responsible for the Persistent Photo Conductivity (PPC) effect[1] observed in Al$_x$Ga$_{1-x}$As when

$0.25 < x < 0.6$. There is still no clear understanding of the behaviour of the DX–center, for instance the electron occupancy of the center as a function of the AlAs mole fraction and temperature.

By confining the silicon donors to a very narrow range of a few atomic distances, a phenomena which is called δ–doping, one can reach very high doping densities in which case it is very interesting to investigate how the DX–center behaves. At present there is a vivid discussion on this point. For instance, Etienne and Thierry–Mieg[2] did not observe any DX–centers in highly δ–doped $Al_{0.3}Ga_{0.7}As$, while from bulk doped $Al_{0.3}Ga_{0.7}As$ it is known that silicon predominantly forms DX–centers. On the other hand Zrenner et al.[3] reported evidence for the presence of the DX–center in highly δ–doped GaAs structures.

The study of the physical properties of the two–dimensional electron gas (2DEG) has revealed new and remarkable effects. In particular in a $GaAs/Al_xGa_{1-x}As$ heterostructure where the ionized donors are separated from the 2DEG by an undoped $Al_xGa_{1-x}As$ spacer, the 2DEG has been studied extensively. When in 1980 von Klitzing et al.[4] studied the Hall effect in a 2DEG in a Si–MOSFET they observed precisely quantized plateaus in the Hall resistivity. The plateaus occur when the Fermi level passes through the Landau levels. For this striking discovery he was awarded the Nobel prize in 1985. Although the discovery of this so–called Integer Quantum Hall Effect (IQHE) is already ten years old there is still no commonly accepted theory.

To explain the IQHE the most common picture is that the quantization arises from the interaction between the electrons in the 2DEG and the ionized scatterers. Localization[5,6], percolation models[7,8], gauge arguments[9], and edge channels concepts[10] are used to explain the exact quantization of the Hall plateaus. In view of these various models it is very interesting to study the influence of the interaction between the 2DEG and ionized impurities on the IQHE and try to discriminate between these models.

Another effect, which is sensitive to the interaction between electrons and ionized impurities, is the spin asymmetry in the magneto–resistance of a 2DEG. In high magnetic fields the magneto–resistivity shows two separated peaks: one belonging to the electrons with their spin parallel (up) and another one belonging to electrons with their spin anti–parallel (down) to the magnetic field. Measurements on $GaAs/Al_xGa_{1-x}As$ heterostructures showed that the height of the spin-up peak is different from that of the spin–down spin peak. To explain this

observation it has been proposed[11] that this asymmetry of the spin–up and spin–down peak originates from the interaction of the electrons in the 2DEG with the ionized donors.

In high–mobility $GaAs/Al_xGa_{1-x}As$ heterostructures Tsui *et al.*[12] discovered plateaus in the Hall resistance also at fractional filling factors of the Landau levels. This Fractional Quantum Hall Effect (FQHE) is thought to arise from many–body effects in the 2DEG. It might be the first time that a many–body effect is discovered in a solid state material. Since in these high–quality $GaAs/Al_xGa_{1-x}As$ heterostructures the mean free path of the electrons is very large, it is expected that the FQHE is strongly influenced by the effects which limit the electron mean free path like electron–ionized impurity interaction.

In all these experiments the study of the interaction between the ionized impurities and the 2DEG was done by growing different samples or changing the electron density either by illumination (PPC) or back–gating. In this thesis we describe experiments in which we combined the last two methods to increase the electron density in the 2DEG of a $GaAs/Al_xGa_{1-x}As$ heterostructure. In this way we studied the interaction between the ionized impurities and the 2DEG keeping the electron density in the sample constant.

Contrary to selectively doped heterostructures, in δ–doped structures both the ionized impurities and the electrons are confined to the same two–dimensional layer. The interaction between the electrons and the ionized impurities is strongly increased. These structures are therefore very attractive to study the electron–ionized impurity interaction. We note however that normally very high electron densities are reached in a δ–doped structure and thus more than one electronic subband is filled. The influence of the electron–ionized impurity interaction is not the same in all subbands and depends strongly on the distribution of the electrons and the ionized donors. This is due to a different spatial confinement of the electrons in the different electronic subbands.

From this discussion it is obvious that electron–ionized impurity interaction is the central issue of many interesting physical effects observed thus far in two–dimensional electron gases. The study of this electron–ionized impurity interaction is the subject of this thesis which is organized as follows. In the remainder of the general introduction we introduce the basic physical and technical concepts. They serve as a kind of tools in the following chapters. In chapter 2 we present a three level donor model in order to calculate the occupancy of the DX–center and

the free electron concentration in bulk $Al_xGa_{1-x}As$. In chapter 3 we discuss the influence of parallel conduction in the $Al_xGa_{1-x}As$ layer of a $GaAs/Al_xGa_{1-x}As$ heterostructure on the measured magneto and Hall resistance. In this chapter we also present a model to calculate the influence of parallel conduction. The operation of a back–gate after wavelength dependent illumination is investigated in chapter 4. In chapter 5 we present measurements on the asymmetry of the height of the spin–up and down–peak in the magneto–resistance when the electron-ionized impurity interaction is changed. The influence of electron–ionized impurity interaction on the IQHE and the FQHE is reported in chapter 6. Finally, in chapter 7 we discuss experiments carried out on δ–doped GaAs structures in which we studied the electron–ionized impurity interaction.

Part of this work was performed in collaboration with C. Langerak, J. Perenboom, J. Singleton, and S. Spermon of the High Field Magnet Laboratory in Nijmegen in the group of Prof. H. van Kempen. Some of the sample characterizations were carried out at the Faculty of Electrical Engineering at the Eindhoven University of Technology in the group of Prof. L.M.F. Kaufmann.

1.2 STRUCTURES

At low temperatures electron scattering on charged acceptors and donors is the main scattering mechanism. To increase the electron mobility selective doping, so–called modulation doping[13], has been invented. In this technique the electrons are spatially separated from their parent ionized donors. To grow selectively doped structures, epitaxial growth techniques like Metal Organic Chemical Vapor Deposition (MOCVD) and Molecular Beam Epitaxy (MBE) are the key technologies.

In general, an epitaxial growth process is any process in which chemical elements or compounds are deposited onto a single–crystal under conditions such that the deposited materials become precisely arranged upon the substrate, yielding a single crystal deposited, or epitaxial layer. In the MOCVD growth process a carrier gas (normally H_2) transports the molecules required for the growth of the epitaxial layer flows to the surface of the substrate. The molecules are thermally decomposed at or close to the surface of the substrate. For the growth of $Al_xGa_{1-x}As$ layers the carrier gas contains the metal–organic compounds trimethylgallium ($Ga(CH_3)_3$) and trimethylalluminium ($Al_2(CH_3)_6$) and the hydride

arsine (AsH_3). By mixing these compounds it is possible to grow a desired alloy and by changing the mixture of these compounds in the carrier gas different alloys can be grown on top of each other. In order to n–type dope the $Al_xGa_{1-x}As$ the hydride silane (SiH_4) can be added to the carrier gas. Diethylzink ($Zn(C_2H_5)$) is used for p–type doping. MBE can best be described as a highly controlled ultra-high–vacuum evaporation/deposition process. The vacuum chamber contains several furnaces and a heated substrate on which the epitaxial layers are grown. The evaporation from each furnace is directed towards the substrate and the flux of atoms reach the substrate without being scattered. In the case of the growth of $Al_xGa_{1-x}As$ three of the furnaces contain the elements gallium, aluminum and arsenic. Additional furnaces contain the doping material. Si and Be are used for n and p–type doping, respectively. The rate of evaporation of the source materials, i.e. the flux of atoms or molecules arriving at the substrate, is determined by the temperature of the furnaces. The composition and doping are controlled by opening and closing of the shutters in front of each furnace.

With MOCVD and MBE it is possible to grow a wide variety of alloys with atomically abrupt interfaces between successive alloy films. The major advantage of MBE is the fact that one can grow very clean material with respect to background impurities whereas the flexibility in growing different alloys is regarded as being the major advantage of MOCVD. Review articles on both MOCVD[14] and MBE[15] have been published.

1.2.1   GaAs/$Al_xGa_{1-x}As$ HETEROSTRUCTURE

As described previously MBE and MOCVD are capable of growing GaAs and $Al_xGa_{1-x}As$ thin films with a high degree of control of the doping and alloy composition and with extremely abrupt interfaces. All these abilities are important to grow high–quality heterojunctions. The epitaxial layers of a GaAs/$Al_xGa_{1-x}As$ heterostructure are grown on a high–resistivity (semi–insulating) GaAs substrate, see Fig 1.1. In general the first grown layer is 4 μm high–quality GaAs. With MBE this means that typically less than 10^{15} cm^{-2} ionized acceptors are present due to carbon contamination of the vacuum system and source materials[16]. The second "spacer" layer consists of undoped $Al_xGa_{1-x}As$ with x $\approx$ 0.3. Depending on the desired electron density or mobility of the electrons this spacer layer is between 10 and 1000 Å thick. The third layer is $Al_xGa_{1-x}As$ with the same AlAs
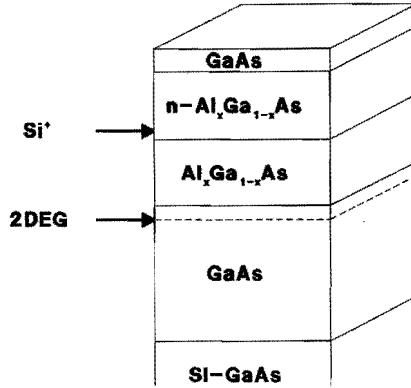
Fig. 1.1:

Schematic layer structure of a GaAs/$Al_x Ga_{1-x}$As heterostructure. The ionized donors in the n–$Al_x Ga_{1-x}$As are separated from the 2DEG, formed at the GaAs/$Al_x Ga_{1-x}$As interface, by the undoped $Al_x Ga_{1-x}$As spacer layer. On top of the heterostructure a small GaAs cap layer is grown in order to protect the $Al_x Ga_{1-x}$As layer.

mole fraction which is silicon doped typically at $N_{si} = 2 \cdot 10^{18}$ cm^{-3}. Due to the different bandgaps of GaAs and $Al_x Ga_{1-x}$As electrons from the silicon donors transfer to the GaAs and thus are separated from their parent ionized donors. The Coulomb interaction between the charged ionized donor atoms in the large gap $Al_x Ga_{1-x}$As and the electrons in the GaAs leads to a confinement at the GaAs/$Al_x Ga_{1-x}$As interface. Since the interface is nearly structurally perfect the separation of electrons and ionized donors results in very high mobilities compared to uniformly doped GaAs.

If the confinement of the electrons at the GaAs/$Al_x Ga_{1-x}$As interface is strong enough, the de Broglie wavelength is comparable to the width of the confining potential. Thus this problem has to be treated quantum mechanically. This means that there is no continuum in allowed energy states of the electrons but several subbands appear. Usually only the lowest subband is populated in high mobility heterostructures. In Fig. 1.2 we show the probability distribution of the electrons in the lowest subband confined at the GaAs/$Al_x Ga_{1-x}$As interface. Since the motion in the direction perpendicular to the interface is quantized the electrons move freely only in the directions along the interface. This means that the electron gas is essentially a two–dimensional electron gas (2DEG). The first

observation of a 2DEG in a GaAs/Al_xGa_{1-x}As heterostructure was reported in 1979 by Störmer *et al.*[17]. The separation between the ionized donors in the Al_xGa_{1-x}As layer and the electrons in the 2DEG at the GaAs/Al_xGa_{1-x}As interface is shown in Fig. 1.2 where the ionized donors are indicated by the black box.

Fig. 1.2:

> The probability distribution of electrons in the lowest subband (solid line) and electrostatic potential (dashed line) in a GaAs/Al_xGa_{1-x}As hetero-structure. The electron density is $3 \cdot 10^{11}$ cm^{-2} and the spacer thickness is 350 Å. The Fermi energy is taken as the origin of the energy scale and the ionized donors are indicated by the black box.

1.2.2   δ–DOPED GaAs STRUCTURE

Contrary to selectively doped heterostructures, in δ–doped structures both the ionized impurities and the electrons are confined to the same two–dimensional layer. Such δ–doped structures can be grown by MBE in a stop and go procedure.
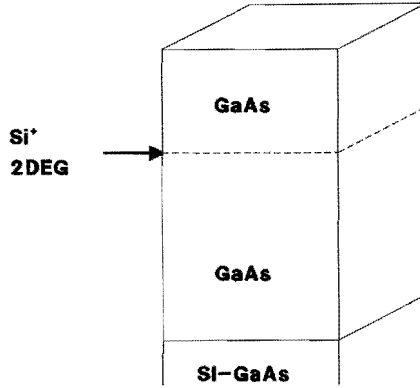
Fig. 1.3:

Schematic layer structure of a δ–doped GaAs structure. The 2DEG is formed at the silicon doping layer between the two GaAs layers.

First a high–quality GaAs layer of 4 μm thick is grown, see Fig. 1.3. The growth is interrupted by closing the Ga shutter thus producing an As–terminated surface. Subsequently the silicon atoms as n–type doping material are introduced, with a sheet concentration of typically $4 \cdot 10^{12}$ cm^{-2}, by opening the shutter of the silicon furnace. In the ideal case the silicon atoms are buried in a single monolayer by the subsequent growth of the second GaAs layer. In practice however, the Si–donor atoms are smeared out over a certain range. For example at a growth temperature of 620 ^{0}C the spreading of the donors is typically 100 Å which corresponds to 40 atomic layers. At high doping concentrations an impurity band is formed because the overlap between neighboring silicon atoms is strong enough. The confining potential of the ionized donors is narrow enough to induce electronic subbands. This means that a 2DEG is formed because the electrons can move freely in the directions along the doping layer but are confined in the direction perpendicular to the doping layer. The first observation of a 2DEG in a δ–doped structure was made in 1984 by Zrenner et al.[18]. In δ–doped structures several subbands are populated due to the high electron density, see Fig. 1.4. In this figure the ionized donors are indicated by the black box. The influence of the electron–ionized impurity interaction is not the same in all subbands and depends strongly on the distribution of the electrons and the ionized donors. This is due to a different spatial confinement of the electrons in the various electronic subbands as is shown in Fig. 1.4.
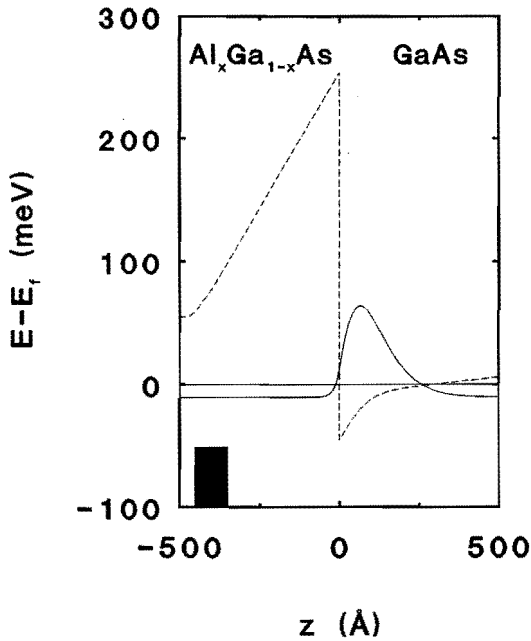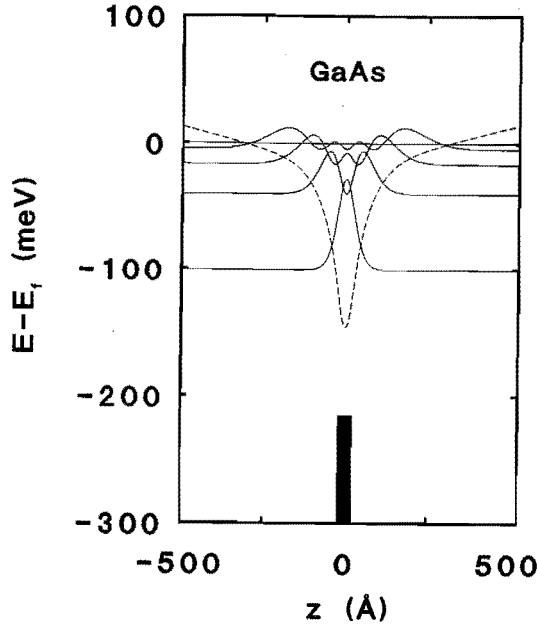
Fig. 1.4:

> The probability distribution of the electrons in the various subbands (solid
> line) and electrostatic potential (dashed line) in a GaAs δ–doped structure.
> The electron density is $4.5 \cdot 10^{12}$ cm^{-2}. The Fermi energy is taken as the origin
> of the energy scale and the ionized donors are indicated by the black box.

1.3 FORMATION OF A TWO–DIMENSIONAL ELECTRON GAS

In order to calculate the energy and wavefunction of electrons in a 2DEG in
δ–doped GaAs or a GaAs/Al$_x$Ga$_{1-x}$As heterostructure we have to solve the Schrö-
dinger equation

$$\mathcal{H}\Psi(\vec{R}) = (\mathcal{H}_0 + U(z))\Psi(\vec{R}) = E\Psi(\vec{R}) \qquad [1.1]$$

where $\vec{R} = (x,y,z)$. The hamiltonian $\mathcal{H}_0$ belongs to an unperturbed periodic host
lattice. The potential U(z) accounts for the difference between the lattice poten-
tial and the underlying periodic potential. Equation [1.1] is usually dealt with

within an effective mass formalism[19-22]. To simplify the calculations in the case of a GaAs/Al$_x$Ga$_{1-x}$As heterostructure one usually takes the effective masses in both the Al$_x$Ga$_{1-x}$As and GaAs region equal. Since the one–electron potential parallel to the GaAs/Al$_x$Ga$_{1-x}$As interface is periodic, the wavefunction $\Psi(\vec{R})$ is written as a product of a z–dependent wavefunction $\varphi(z)$ and a plane wave in the xy–direction, or

$$\Psi(\vec{R}) = \varphi_i(z) \, \psi_{\vec{k}}(\vec{r}) = \varphi_i(z) \, e^{i\vec{k}\cdot\vec{r}} \qquad [1.2]$$

where $\vec{R} = \vec{r} + \vec{z}$ and $\vec{k} = k_x\vec{e}_x + k_y\vec{e}_y$.

It can be shown that the function $\varphi_i(z)$, enveloping $\Psi(\vec{R})$ in the z–direction, fulfills the simple type of equation

$$\left\{ -\frac{\hbar^2}{2m^*}\frac{\partial^2}{\partial z^2} + U(z) \right\} \varphi_i(z) = E_i \, \varphi_i(z) \qquad [1.3]$$

where

$$E = E_i + \frac{\hbar^2(k_x^2 + k_y^2)}{2m^*} \qquad [1.4]$$

and i, the subband index, numbers the various possible solutions of [1.3]. We are generally interested only in the energetically low lying bound states $\varphi_i(z)$. The potential U(z) can be shown to be equal to

$$U(z) = \Delta U_0 \, \theta(z) + U_c(z) + U_{ex}(z) \qquad [1.5]$$

The first term in [1.5] accounts for the conduction band discontinuity, ΔU_0, at the interface between the Al$_x$Ga$_{1-x}$As and the GaAs region in the case of a GaAs/Al$_x$Ga$_{1-x}$As heterostructure. $\theta(z)$ is the Heavyside step function. The term U$_c$(z) describes the electrostatic potential and the last term is an exchange correlation potential.

The electrostatic potential, U$_c$(z), obeys the Poisson equation

$$\frac{\partial^2}{\partial z^2} U_c(z) = \frac{e\rho(z)}{\epsilon_0 \epsilon_r} \qquad\qquad [1.6]$$

The charge distribution, $\rho(z)$, is the sum of the positively charged donors, $n_D(z)$, the negatively charged acceptors, $n_A(z)$, and the electron density of the 2DEG, $n(z)$. Thus

$$\rho(z) = e \left[\, n_D(z) - n_A(z) - n(z)\,\right] \qquad\qquad [1.7]$$

The negatively charged acceptors in the GaAs are charged background impurities within the depletion region. The acceptor depletion width is defined by

$$w_A = \left[\frac{2\epsilon_0\epsilon_r E_{GaAs}}{e^2 N_A}\right]^{1/2} \qquad\qquad [1.8]$$

where E_{GaAs} is the bandgap of GaAs and N_A is background impurity density.

The electron density is given by the sum of the charge distributions of the populated subbands

$$n(z) = \sum_i n_i\, \varphi_i^*(z)\varphi_i(z) \qquad\qquad [1.9]$$

where i is restricted to the subbands below the Fermi–level, E_f. The envelope wavefunctions are normalized according to

$$\int \varphi_i^*(z)\varphi_i(z)\mathrm{d}z = 1 \qquad\qquad [1.10]$$

and the population of subbands lying below the Fermi–level is

$$n_i = \frac{m^*}{\pi\hbar^2}\,(\, E_f - E_i \,) \qquad\qquad (\,T = 0\,K\,) \qquad\qquad [1.11]$$

The factor $m^*/(\pi\hbar^2)$ in [1.11] is the Density Of States (DOS) in a two–dimensional parabolic band taking the spin factor 2 into account. For high electron densities the non–parabolicity of the conduction band has to be taken into account.

In the GaAs/Al$_x$Ga$_{1-x}$As heterostructure the positively charged donors are distributed over a region w$_D$ which is defined by charge neutrality

$$w_D = (n_{2DEG} + n_{depl})/N_D \qquad\qquad [1.12]$$

where n$_{2DEG}$ is the total electron density in the 2DEG, n$_{depl}$ the sheet density of charged acceptors (n$_{depl}$ = N$_A$w$_A$), and N$_D$ is the donor density.

In δ–doped GaAs we assume that all the donors are ionized. The width of the donor distribution is equal to w$_D$. Using relation [1.12] we calculate the electron density in the 2DEG in a δ–doped structure.

We have to include a local exchange correlation potential in order to account for many–body corrections. There are slight differences in the choice of this potential between various authors[23-25].

The Schrödinger and Poisson equation have to be solved selfconsistently because the potential, U(z), in [1.4] according to [1.5], [1.6], [1.7] and [1.9] depends on the envelope wavefunctions $\varphi_i(z)$. Normally the selfconsistent solution is calculated by numerical methods.

A typical solution of this set of equations in the case of a GaAs/Al$_x$Ga$_{1-x}$As heterostructure, with n$_{2DEG}$ = 3· 10^{11} cm^{-2}, is given in Fig. 1.2. In this figure we observe that the envelope wavefunction is mainly situated in the GaAs layer and penetrates the Al$_x$Ga$_{1-x}$As layer only over a very small distance. The solution in the case of δ–doped GaAs is presented in Fig. 1.4. Due to the high electron density in this δ–doped structure, n = 4.5·10^{12} cm^{-2} more than one subband is populated. In all subbands the electrons are distributed symmetrically around the doping layer. The envelope wavefunction of the lowest subband has a strong overlap with the donor distribution whereas this overlap is much weaker for the wavefunctions of the higher subbands.

1.4 SCATTERING MECHANISMS

The electrons in a 2DEG cannot flow freely but are scattered by irregular Coulomb potentials in the crystal. These irregularities originate from the ionized impurities and the lattice vibrations (acoustic or optical phonons). In a GaAs/Al$_x$Ga$_{1-x}$As heterostructure the interface roughness and alloy disorder in the Al$_x$Ga$_{1-x}$As can be taken into account. Several authors[26-30] have calculated

the scattering probability for these scattering mechanisms.

At room temperature the optical phonons dominate the electron scattering process. At intermediate temperatures, 20 K < T < 80 K the acoustic phonon scattering via the deformation potential coupling and piezoelectric coupling are important. At low temperatures the ionized impurities dominate the scattering processes. The ionized impurities are present as charged acceptors and ionized donors. Normally the background impurities in MBE grown GaAs[16] are charged acceptors and the charged donors are the ionized doping atoms in the $Al_xGa_{1-x}As$ layer. In a $GaAs/Al_xGa_{1-x}As$ heterostructure the scattering on these ionized doping atoms is referred to as remote ionized impurity scattering because the doping atoms are separated from the 2DEG by an undoped $Al_xGa_{1-x}As$ spacer. The interface roughness and alloy disorder scattering are only important at high electron densities[28].

Normally one chooses to calculate the electron mobility, which characterizes the relevant scattering mechanisms, by solving the Boltzmann Transport Equation (BTE) in the relaxation time approximation[29]. In the case of a 2DEG the relaxation time τ is calculated from

$$\frac{1}{\tau(\vec{k})} = \int_\Omega (1 - \cos(\theta))\, W(\vec{k},\vec{k}')\, d\Omega \qquad [1.13]$$

where $\vec{k}$ and $\vec{k}'$ are the in and out–going two–dimensional wavevectors and θ is the angle between $\vec{k}$ and $\vec{k}'$. The transition probability, $W(\vec{k},\vec{k}')$, is given by the Fermi Golden Rule

$$W(\vec{k},\vec{k}') = \frac{2\pi}{\hbar} \left| <\Psi_i(\vec{k}',\vec{R})|\mathcal{H}_{int}|\Psi_j(\vec{k},\vec{R})> \right|^2 \delta(E_k - E_{k'}) \qquad [1.14]$$

where $|<\Psi_i(\vec{k},\vec{R})>$ describes the wave function of an electron with a wavevector $\vec{k}$ in subband i and $\mathcal{H}_{int}$ is the hamiltonian describing the scattering interaction.

In a 2DEG the drift mobility is calculated with

$$\mu_d = \frac{e}{m^*} <\tau> = \frac{e}{m^*} \frac{\int \tau(E)\ E\ \left\{-\partial f(E)/\partial E\right\}\ dE}{\int E\ \left\{-\partial f(E)/\partial E\right\}\ dE} \qquad [1.15]$$

where f(E) is the Fermi–Dirac function and $\tau(E(\vec{k})) = \tau(\vec{k})$. The total mobility due to all the scattering processes is calculated using Mathiessen's Rule for independent scattering mechanisms

$$\frac{1}{\mu_{tot}} = \sum_i \frac{1}{\mu_i} \qquad [1.16]$$

From all scattering mechanisms we will only discuss the ionized impurity scattering in detail because in this thesis we are mainly interested in the interaction between the electrons in the 2DEG and the ionized impurities. The interaction hamiltonian in the case of the Coulomb interaction with one single charged impurity is given by

$$\mathcal{H}_{int} = \frac{e^2\ /\ 4\pi\epsilon_0\epsilon_r}{\sqrt{\rho_i^2 + (z-z_i)^2}} \qquad [1.17]$$

where z_i is the position of the charged impurity and ρ_i is the radial distance from the charged impurity, see Fig. 1.3.
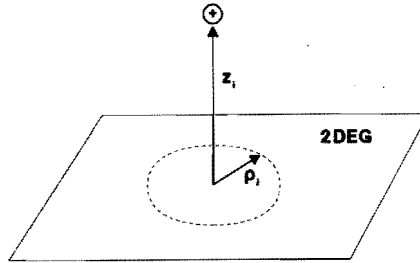
Fig. 1.5:

An ionized impurity at a distance z_i from the $GaAs/Al_xGa_{1-x}As$ interface.

The matrix element of this operator for ionized impurity scattering in the lowest subband is calculated from the following expression

$$<\Psi_0(\vec{k'},\vec{R})|\mathcal{H}_{int}|\Psi_0(\vec{k},\vec{R})> =$$

$$\iint \varphi_0^*(z)e^{-\imath\vec{k'}.\vec{r}}\;\frac{e^2\;/\;4\pi\epsilon_0\epsilon_r}{\sqrt{\rho_i^2 + (z-z_i)^2}}\;\varphi_0(z)e^{\imath\vec{k}.\vec{r}}\;\mathrm{d}\vec{r}\mathrm{d}z \qquad [1.18]$$

We define $\vec{q}$ by the relation $\vec{k'} = \vec{k} + \vec{q}$ where $|\vec{k'}| = |\vec{k}|$ since only elastic scattering processes are considered, see Fig. 1.6.
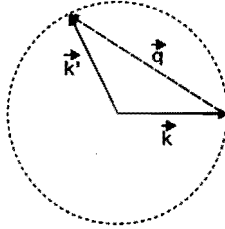
Fig. 1.6:

Collision diagram in the case of elastic scattering.

Thus, $|\vec{q}|$ can be expressed as $q = 2k|\sin(\theta/2)|$. Now [1.18] is rewritten as follows

$$e^2/4\pi\epsilon_0\epsilon_r \int \varphi_0^*(z)\varphi_0(z) \int e^{-\imath\vec{q}.\vec{r}}\;\frac{1}{\sqrt{\rho_i^2 + (z-z_i)^2}}\;\mathrm{d}\vec{r}\mathrm{d}z \qquad [1.19]$$

Due to the rotation symmetry around the impurity we change to integration over radial coordinates. In this case $\mathrm{d}\vec{r} = 2\pi\rho_i\mathrm{d}\rho_i$. Taking the Fourier transform gives

$$2\pi \int e^{-\imath\vec{q}.\vec{r}}\;\frac{1}{\sqrt{\rho_i^2 + (z-z_i)^2}}\;\rho_i\mathrm{d}\rho_i = 2\pi\,\frac{1}{q}\,e^{-q|z-z_i|} \qquad [1.20]$$

Substitution of [1.20] in [1.19] shows that

$$<\Psi_0(\vec{k}',\vec{R})|\mathcal{H}_{int}|\Psi_0(\vec{k},\vec{R})> = \frac{e^2}{4\pi\epsilon_0\epsilon_r}\frac{2\pi}{q}F(q,z_i) \qquad [1.21]$$

where the formfactor is defined by

$$F(q,z_i) = \int |\varphi_0(z)|^2 e^{-q|z-z_i|}\, dz \qquad [1.22]$$

The momentum relaxation time due to a single charged impurity at a distance z_i according to [1.13] is

$$\frac{1}{\tau(k,z_i)} = \qquad [1.23]$$

$$\frac{2\pi}{\hbar}\left[\frac{e^2 Z}{2}\right]^2 \int \frac{F^2(q,z_i)}{(\epsilon_0\epsilon_r q)^2}(1-\cos(\theta(q)))\, dq\, \delta(\epsilon_{\vec{k}+\vec{q}} - \epsilon_{\vec{k}})$$

The momentum relaxation time due to all the charged impurities is given by the integration of [1.23] over the charged impurity distribution, $N(z_i)$

$$\frac{1}{\tau(k)} = \int \frac{1}{\tau(k,z_i)} N(z_i)\, dz_i \qquad [1.24]$$

As discussed in the previous sections there are two regions with charged scattering centers which have a different contribution to the relaxation time, i.e. the positively charged Si–donors and the negatively charged background acceptors in the GaAs layer.

In the case of background impurity scattering the exponent $e^{-q|z-z_i|}$ in the formfactor is nearly equal to 1 and the formfactor is thus $\int |\varphi_0|^2 dz \approx 1$. The influence of the shape of the wavefunction on the relaxation time is only very small.

In the case of remote impurity scattering in a GaAs/Al$_x$Ga$_{1-x}$As heterostructure $(z-z_i) > 0$. If the Fang–Howard wavefunction[31] is used as approximation for $\varphi_0(z)$ the formfactor reduces to

$$F(q,z_i) = \frac{b^3}{(b + q)^3}\, e^{-qz_i} \qquad\qquad [1.25]$$

where $b = 3/<z>$.

Thus the remote impurity scattering depends exponentially on the distance between the 2DEG and the scatterers.

In [1.24] as well as in the rest of literature[26-29] the total distribution of the ionized impurities is taken to calculate the ionized impurity scattering. It has been shown by Van Hall *et al.*[30] that this is wrong in the case of a GaAs/Al$_x$Ga$_{1-x}$As heterostructure because the distribution of the scatterers is already used in the hamiltonian [1.4] from which the envelope wavefunction of the 2DEG is calculated. Thus in their opinion the scattering is only due to the fluctuations in the distribution of the scatterers.

Another effect which has to be taken into account in the calculation of the mobility, is the screening of the scattering potential by the other electrons in the 2DEG. Normally screening is accounted for by replacing ϵ_r in [1.23] by[32] $\epsilon(q) = \epsilon_r\,(1 + q_s/q)$. Various authors calculate the inverse screening length q_s in a different way[26-30]. The screening parameter q_s is dependent on the temperature, the distribution of electrons and scatterers, and the electron density. At a higher electron density q_s increases and thus leads to a longer relaxation time for both remote and background ionized impurity scattering. However, the remote impurity relaxation time increases stronger than the background impurity relaxation time with increasing electron density.

Fig. 1.7 shows the calculated[33] mobility versus electron density at 4.2 K in a GaAs/Al$_x$Ga$_{1-x}$As heterostructure with a spacer of 300 Å. The mobility is limited by the remote ionized (RI) and background ionized (BI) impurities and increases with the electron density. This is due to screening and the fact that the relaxation time is mainly governed by scattering at the Fermi level. This figure also shows that the effect of acoustical phonon (AC) scattering is stronger at higher electron densities. Fig. 1.8 shows that at low temperatures there is no temperature dependence for the ionized impurity scattering. At higher temperatures the mobility starts to increase for both the background and remote ionized impurity scattering. Between 10 K and 100 K acoustical phonon scattering limits the mobility and above 100 K the mobility is limited by optical phonon (OP) scattering.
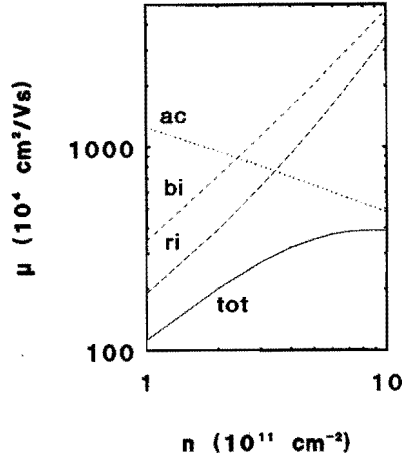
Fig. 1.7:

The electron mobility versus electron density in a GaAs/Al$_x$Ga$_{1-x}$As hetero-structure with a spacer thickness of 300 Å at 4.2 K.
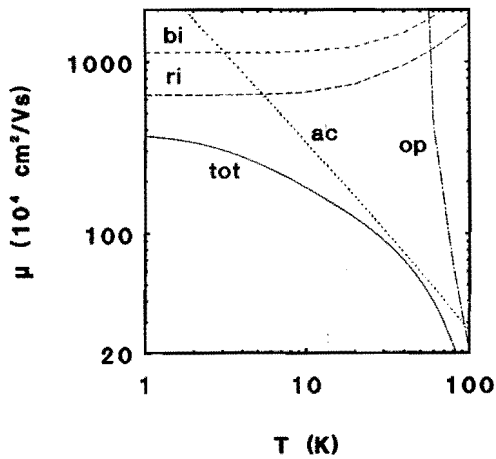
Fig. 1.8:

The electron mobility versus temperature in a GaAs/Al$_x$Ga$_{1-x}$As hetero-structure with a spacer thickness of 300 Å and an electron density of $3 \cdot 10^{11}$ cm^{-2}.

As shown above the mobility is dependent on the electron density and the distance between the ionized impurities and the 2DEG. This means that the relative importance of the scattering mechanisms depends on the the spacer thickness of the sample. Remember that the electron density in the 2DEG of a $GaAs/Al_xGa_{1-x}As$ heterostructure depends on the spacer thickness. Fig. 1.9 shows the dependence of the mobility on the spacer thickness, as calculated by Van Hall *et al.*[30]. The experimental values of the electron density as a function of the spacer thickness were taken from Harris *et al.*[34]. The figure shows that remote ionized impurity scattering dominates the scattering in samples with a small spacer whereas background ionized impurity scattering dominates in samples with a large spacer. In samples with a spacer thickness of ≈ 400 Å the relative importance of three scattering mechanisms; remote ionized impurity scattering, background impurity scattering and acoustical phonon scattering, is nearly equal.
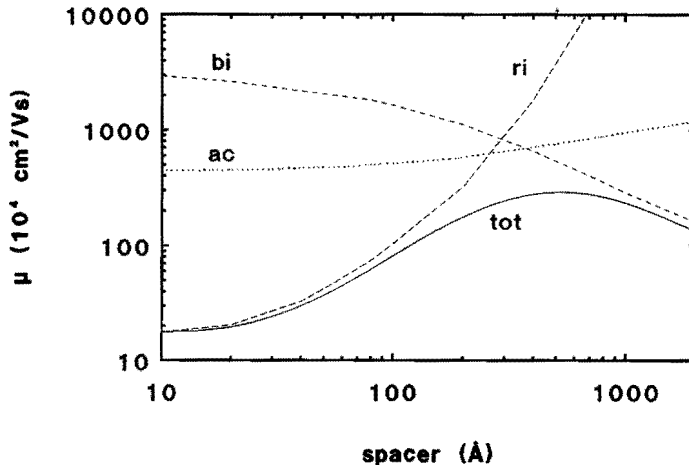
Fig. 1.9:
   The electron mobility versus spacer thickness at 4 K. [v. Hall *et al.*[30]]

1.5 MAGNETO–TRANSPORT

Magneto–transport in homogeneous samples is characterized by a conductivity tensor, $\overset{\leftrightarrow}{\sigma}$, which describes the relation between the current density and the electric field

$$\vec{J} = \overset{\leftrightarrow}{\sigma} \vec{E} \qquad\qquad [1.26]$$

In the case of conduction in two dimensions the resistivity tensor is equal to

$$\overset{\leftrightarrow}{\sigma} = \begin{bmatrix} \sigma_{xx} & \sigma_{xy} \\ -\sigma_{xy} & \sigma_{xx} \end{bmatrix} \qquad\qquad [1.27]$$

when we assume isotropic conduction in the 2DEG. The inverse of the conductivity tensor is the resistivity tensor

$$\overset{\leftrightarrow}{\rho} = \begin{bmatrix} \rho_{xx} & -\rho_{xy} \\ \rho_{xy} & \rho_{xx} \end{bmatrix} \qquad\qquad [1.28]$$

where

$$\rho_{xx} = \sigma_{xx}/(\sigma_{xx}{}^2 + \sigma_{xy}{}^2) \text{ and } \rho_{xy} = \sigma_{xy}/(\sigma_{xx}{}^2 + \sigma_{xy}{}^2)$$

The inverse relations are

$$\sigma_{xx} = \rho_{xx}/(\rho_{xx}{}^2 + \rho_{xy}{}^2) \text{ and } \sigma_{xy} = \rho_{xy}/(\rho_{xx}{}^2 + \rho_{xy}{}^2)$$

Using the Boltzmann–Transport–Equation in the relaxation time approximation the following solution in low magnetic field ($\mu B < 1$), can be derived

$$\sigma_{xx} = \frac{n_{2DEG} \; e^2 \; <\tau>}{m^*} = n_{2DEG} \; e \; \mu_d \qquad\qquad [1.29]$$

where $< ... >$ is the averaged value of τ as [1.15]. The transversal or Hall conductivity is

$$\sigma_{xy} = \frac{n_{2DEG}\ e}{B}\ r_h \qquad\qquad [1.30]$$

where $r_h = <\tau^2>/<\tau>^2$ is the Hall–factor. This Hall–factor is dependent on the scattering mechanism and the degeneracy of the system[35]. Due to the high degeneracy in a 2DEG at low temperatures r_h is almost equal to 1.

In high magnetic fields, ($\mu B > 1$), the motion perpendicular to the magnetic field direction becomes quantized and the two–dimensional DOS consists of equally spaced Landau levels.

If we take the magnetic field perpendicular to the 2DEG, i.e. the z–direction, then the Hamiltonian of an electron in the xy–plane is given by

$$\mathcal{H} = \frac{1}{2m^*}\left[\hbar^2\frac{\partial^2}{\partial x^2} + \left[\hbar\frac{\partial}{\partial y} + eBx\right]^2\right] \qquad\qquad [1.31]$$

The eigenfunctions of this Hamiltonian are

$$\psi_N(x,y) = e^{\iota k_y y}\ \frac{1}{(2^N N!\sqrt{\pi}l)^{1/2}}\ e^{-x^2/2l^2}\ H_N(x/l) \qquad\qquad [1.32]$$

where $l = (\hbar/eB)^{1/2}$ is the cyclotron radius and H_N are Hermite functions of the order N. The eigenvalues are the so–called Landau levels

$$E_N = (N + 1/2)\ \hbar\omega_c \qquad\qquad [1.33]$$

The degeneracy of each Landau level is equal to $1/2\pi l^2 = eB/h$ and they are broadened due to scattering of the electrons.

Due to the fact that electrons have a spin we have to include an extra energy term. The total energy of a 2D–electron in a magnetic field is thus

$$E = E_i + (N + 1/2)\ \hbar\omega_c + \vec{\sigma}_s g\mu_B B \qquad\qquad [1.34]$$

where E_i is the subband energy, $\vec{\sigma}_s$ is the spin vector $(\pm 1/2)$, g the so–called g–factor and μ_B is the Bohr magneton.

The conductivity of a 2DEG in a strong magnetic field was formulated by

Ando *et al.*[36,37]. When semi–elliptic Landau levels are used, the longitudinal conductivity is given by

$$\sigma_{xx} = \int \left[-\frac{\partial f(E)}{\partial E} \right] \frac{e^2}{\pi^2 \hbar} \left[\frac{\Gamma_N^{\frac{1}{2}r}}{\Gamma_N} \right]^2 \left[1 - \left[\frac{E - E_N}{\Gamma_N} \right]^2 \right]^{1/2} dE \qquad [1.35]$$

where Γ_N is the width of the Landau level, $\Gamma_N^{\frac{1}{2}r}/\Gamma_N$ is a measure of the effective range of the scattering potential, and $f(E)$ is the Fermi–Dirac function. The longitudinal conductivity shows Shubnikov–de Haas oscillations as a function of the filling factor. The filling factor is equal to the number of filled Landau levels

$$i = n_{2DEG} / (eB/h) \qquad [1.36]$$

The filling factor can be changed either by the magnetic field or by the electron density. The peak conductivity at half integer filling factors and $T = 0$ K is equal to $(\Gamma_N^{\frac{1}{2}r}/\Gamma_N)^2 e^2/\pi^2\hbar$.

The scattering potential is called short range when the width of the scattering potential is smaller than the cyclotron radius l. In the extreme case of short range scattering the scattering potential can be written as $V_{scat}(\vec{r},z) = V(z)\, \delta(\vec{r})$. For δ–like scattering potentials $(\Gamma_N^{\frac{1}{2}r})^2 = (N + 1/2)\, \Gamma_N^2$ and thus the peak conductivity is equal to $(N + 1/2)\, e^2/\pi^2\hbar$. This relation was also found experimentally[38] in a Si–MOSFET where the scatterers are very near to the 2DEG and can be approximated by δ–like scattering potentials.

When the scatterers are sufficiently long ranged the level widths can be approximated[36] by the following form

$$\Gamma_N^2 \approx 4 < (V(\vec{r})-<V(\vec{r})>)^2 > \qquad [1.37]$$

$$(\Gamma_N^{\frac{1}{2}r})^2 \approx 4 < (l\, \partial V(\vec{r})/\partial y) > \qquad [1.38]$$

where $V(\vec{r})$ is the local potential and $< ... >$ means the average over all configurations of the scatterers, i.e. $\int\int$ .... $N(z)\, dz d\vec{r}$.

Ando studied the range dependence of the peak conductivity by taking a Gaussian scattering potential,

$$V_{scat} = V(z) \exp(-r^2/d^2)/\pi d^2 \qquad\qquad [1.39]$$

He calculated the peak conductivity for several Landau levels, Fig. 1.10. In this figure $\alpha = d/l$. Thus $\alpha = 0$ for short range scattering and $\alpha \to \infty$ for long range scattering. The numerical calculations show that the peak conductivity is strongly reduced for all Landau levels when the scattering becomes long range.
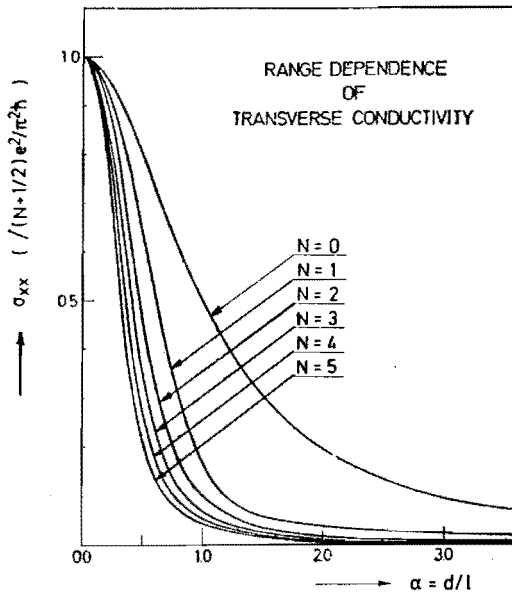
Fig. 1.10:
   The peak conductivity $(\Gamma_N^{tr}/\Gamma_N) / (N+1/2)$ as a function of the range $\alpha = d/l$ of the Gaussian potential. [Ando et al.[36]]

1.6   DENSITY OF STATES IN A LANDAU LEVEL

In the preceding sections we used a semi–elliptic DOS for the Landau levels. This is a good approximation in the case of short range scattering and a large number of scatters per Landau orbit. In a Si–MOSFET the scattering is short range because the scattering centers are situated at the Si/SiO_2 interface and thus are approximated by δ–functions. In the $GaAs/Al_xGa_{1-x}As$ heterostructure this is

not to be expected because remote ionized impurity scattering is the main scattering mechanism at low temperatures. Since the charged donors are separated from the 2DEG by an $Al_xGa_{1-x}As$ spacer, the scattering potentials due to these remote ionized impurities are long range and Gaussian like. The shape and the width of a Landau–level are important when calculating the magneto–conductivity. In the previous section for instance we have shown that the peak conductivity is dependent on the range of the scattering potential. Therefore, in this section we will discuss the influence of scattering centers on the shape of a Landau level.
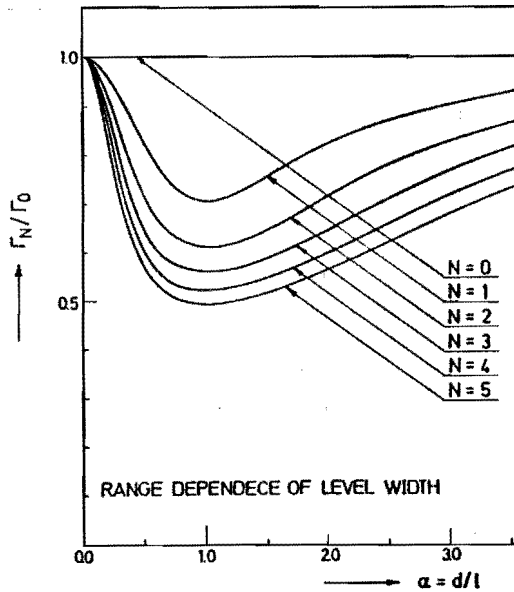
Fig. 1.11:

The level broadening ratio Γ_N/Γ_0 as a function of the range $\alpha = d/l$ of the Gaussian potential. [Ando et al.[36]]

1.6.1 LANDAU–LEVEL WIDTH

Ando and Uemura[36] calculated the dependence of the Landau level width on the range of the scattering potential. In the case that the scattering potentials are Gaussian the width of the lowest Landau level is given by $\Gamma_0 = \Gamma/(1 + \alpha^2)$ with $\Gamma^2 = (2/\pi)\,\hbar\omega_c\,(\hbar/\tau)$. The level width decreases as the range increases, because the model potential becomes weaker when d increases [1.39]. Fig. 1.11 shows the ratio Γ_0/Γ_N as a function of $\alpha = d/l$ for several N. It can be seen that the level width is generally smaller for higher Landau levels and that in both limits $\alpha = 0$ and $\alpha \to \infty$ the width is the same for every Landau level. When the scattering range is comparable to the cyclotron radius the width of the Landau levels differs strongly. This is due to the fact that the extension of the electrons in each Landau level is $l\,(2N + 1)^{1/2}$ and thus the electrons in the higher Landau orbits will feel a scattering potential which has an shorter range, i.e. the scattering potential is smaller compared to the extension of the electron.

1.6.2 SHAPE OF THE LANDAU LEVEL

In the case of a small number of short range scattering potentials per Landau orbit the DOS of a Landau level has been calculated by Brézin et al.[39] and Ando[40]. Their results show that the DOS becomes asymmetric at low concentrations of scatterers per Landau orbit. Fig. 1.12 gives the results for attractive scatterers, i.e. positively charged Coulomb scatterers. The DOS of the lowest Landau level has been calculated for different values of C_i, the number of scatterers per Landau orbit. The dotted line is the analytical result obtained by Brézin et al.[39], the solid line is the numerical result of Ando and the dashed line gives the result obtained by Ando in the single–site approximation. The origin is chosen at $E_0 - (1 + C_i)\,E_B$, with E_B the binding energy of a single scatterer.

These calculations show that the Landau level has a long tail at the low energy side for attractive scatterers. For repulsive scatterers, i.e. negatively charged Coulomb scatterers, the tail is at the high energy side of the Landau level. Two other results are obtained from their calculations; 1) the mean energy value of the Landau level is shifted to a lower energy and 2) at very low concentrations of scatterers per Landau orbit extra peaks are formed in the DOS. The peaks in the DOS are impurity bands at integer values of E_B.
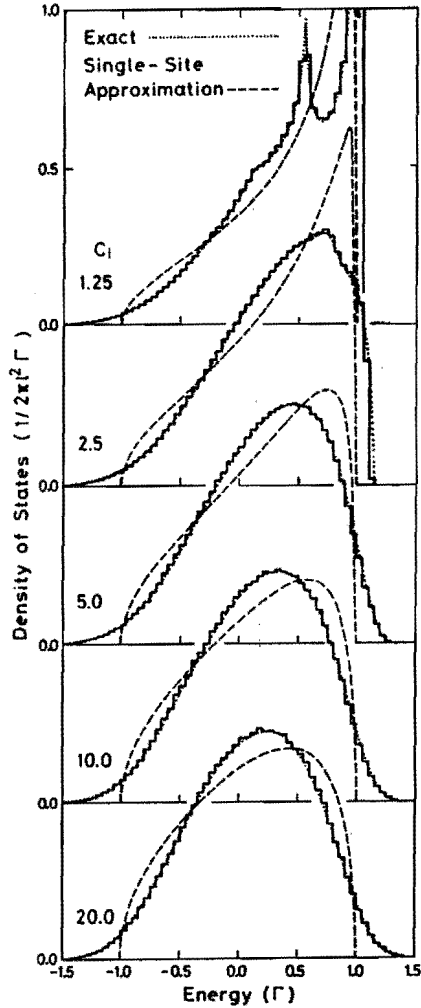
Fig. 1.12:

Histograms of the DOS for the lowest Landau level N = 0. Scatterers with attractive short–range δ–potentials are used. The numbers C_i denote the number of scattering potentials per Landau orbit. The energy is normalized by $\Gamma = 2C_i^{1/2}E_B$ and its origin is chosen at $E_0-(C_i+1)E_B$. The dotted lines are the analytical results obtained by Brézin et al.[39] the dashed and solid lines are results obtained by Ando[40].

1.7   THE INTEGER QUANTUM HALL EFFECT

In 1980 measurements by von Klitzing *et al.*[4] showed that the Hall resistivity of a 2DEG in a Si–MOSFET showed exactly quantized plateaus at integer values of the filling factor, i, according to

$$\rho_{xy} = \frac{1}{i} \cdot \frac{h}{e^2} \qquad\qquad [1.40]$$

This Integer Quantum Hall Effect (IQHE) was later also found in a 2DEG in a GaAs/Al$_x$Ga$_{1-x}$As heterostructure[41], see Fig. 1.13. At integer filling factors where the Hall voltage is quantized the magneto–resistivity is zero.
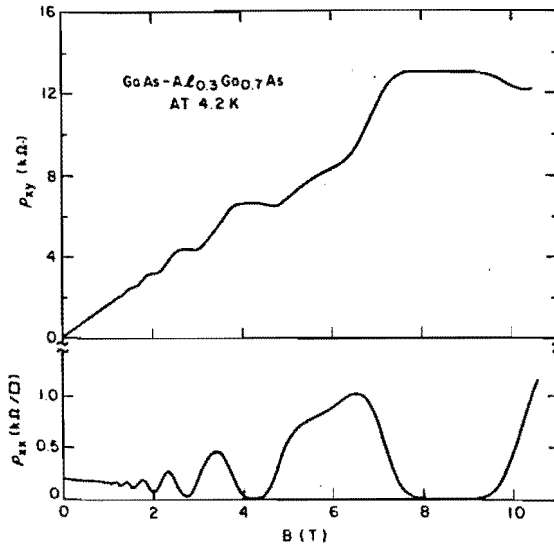
Fig. 1.13:

> Recording of the Hall and magneto–resistivity as a function of the magnetic field in a GaAs/Al$_x$Ga$_{1-x}$As heterostructure with an electron density of 4.2·10^{11} cm^{-2} and a mobility of 7.9·10^4 cm^2/Vs. [Tsui *et al.*[41]]

The commonly accepted model to explain these plateaus assumes the existence of localized states in the wings of the Landau level. By using a gauge argument Laughlin[9] has explained that $\rho_{xy} = h/ie^2$ when the Fermi energy lies in a mobility gap, i.e. an energy range where all electron states are localized.

A possible mechanism of localization in the case of slowly varying potentials was proposed by Kazarinov and Luryi[5], and Iordansky[6]. In high magnetic field and at low temperature the motion of an electron reduces to a classical drift along the equipotential contours. Thus conduction takes place along the open contours and localization takes place along the closed potentials, see Fig. 1.14. Hence the IQHE is explained by a percolation model in this case of long range scattering centers. Ando[8] calculated that in this case localization increases with the range of the scattering potentials.

Another approach to explain localization is the so-called Anderson localization. Anderson localization is due to the quantum interference of electron states
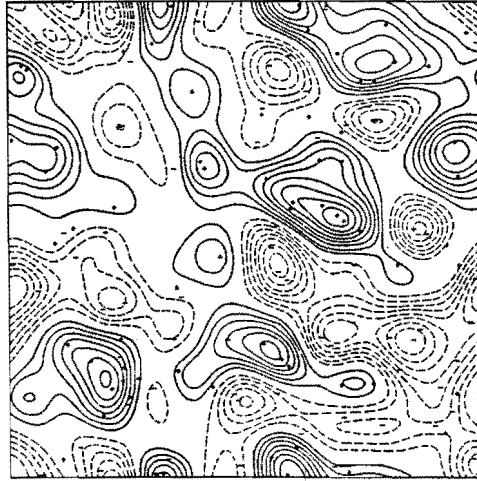
Fig. 1.14:

An example of equipotential lines of the lowest Landau level of a model system with Gaussian scatterers. In this figure − and + represent the positions of repulsive and attractive scatterers. Equipotential lines higher and lower than the center of the Landau level are represented by the dashed and solid lines, respectively. The electrons which move along closed contours at the potential minima or maxima are localized. [Ando[8]]

scattered by randomly placed scattering centers. Wei *et al.*[42,43] were very successful to explain IQHE experiments in $InAs/In_xGa_{1-x}As$ heterostructures with Anderson localization and short range scattering potentials.

Recently Büttiker[10] has proposed a new model for the IQHE. When the Fermi level is situated between two Landau levels the current is driven to edges channels along the lateral borders of the 2DEG because all states in bulk of the 2DEG are localized. He proposed that edge currents flow in opposite directions along each side of the sample. Due to the absence of back–scattering and scattering between the two edge channels the conductivity of each channel is quantized to ie^2/h where i is the number of conducting edge states. Van Houten *et al.*[44] successfully explained experiments in a 2DEG under Quantum Hall conditions using the concept of edge channel conduction.

According to Woltjer *et al.*[7] the IQHE is due to inhomogeneities in the electron density of the 2DEG. He assumes that only at an integer filling factor the magneto– resistivity vanishes, i.e. $\rho_{xx} = 0$. Due to inhomogeneities in the electron density the filling factor is not the same everywhere. In the Quantum Hall region, i.e. when a plateau is observed in the Hall resistance, a percolation path is formed in the 2DEG along which $\rho_{xx} = 0$. When a gradient in the electron density in the 2DEG is present, a current path exists for a certain magnetic field range. In this range ρ_{xx} measured between to contacts is zero and ρ_{xy} is quantized.

1.8   THE FRACTIONAL QUANTUM HALL EFFECT

In high mobility samples of $GaAs/Al_xGa_{1-x}As$ heterostructures Tsui *et al.*[12] found that the Hall resistance also showed plateaus at non–integer filling factors

$$\rho_{xy} = \frac{q}{p} \cdot \frac{h}{e^2} \qquad\qquad [1.41]$$

where p and q are both integers, but q is an odd integer. This Fractional Quantum Hall Effect (FQHE) was observed at filling factors with q = 3, 5, 7, 9. Fractional minima in ρ_{xx} are reported at even higher denominator fractions[45], see Fig. 1.15. Eisenstein[46] also observed plateaus at even filling factors.

The FQHE was explained by Laughlin[47] as due to a many electron effect. From single electron states, each with the same spin, a many electron state was
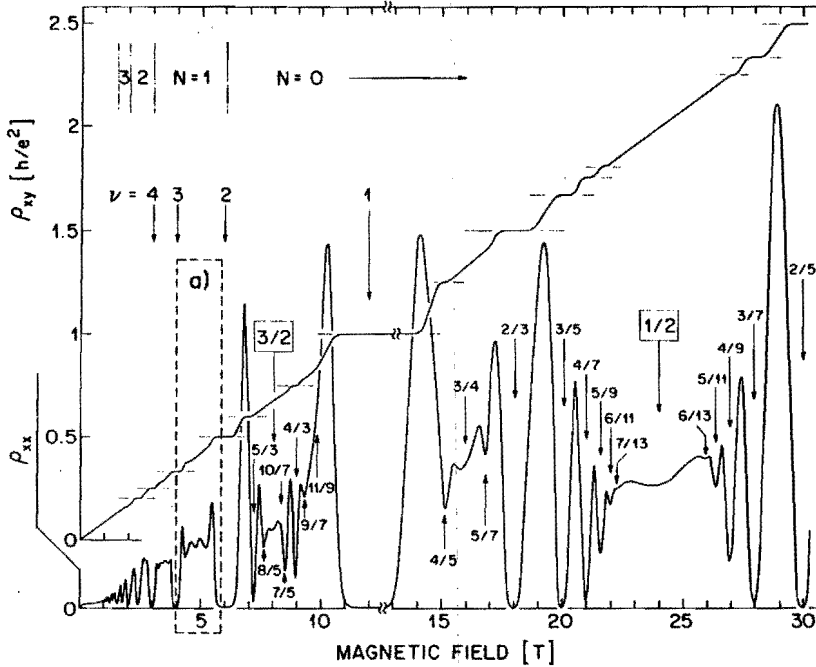
Fig. 1.15:

Measurement of the Hall and longitudinal resistance in a high mobility, $136 \cdot 10^4$ cm^2/Vs, GaAs/Al$_x$Ga$_{1-x}$As heterostructure at an electron density of $3.0 \cdot 10^{11}$ cm^{-2}. [Willet[45]]

constructed which is stable at fractional filling factors of a Landau level. Due to the fact that all electrons have the same spin the Pauli principle excludes all odd denominator fractions[47]. The minima in ρ_{xx} showed an activated behaviour which indicates an energy gap between a ground state and a excited state. The calculation of this energy gap was a major problem which was not solved for many years. Later it was suggested[48] that these many electron ground and excited states can also be constructed from electrons with different spins. Maksym et al.[49] were able to obtain good agreement between the calculated and measured activation energy when they used non–polarized states, i.e. not all electrons contributing to the many electron state have the same spin. Using this idea they were also able to explain the very peculiar dependence of the activation energy on rotation in a magnetic field[50,51]. Eisenstein[46] also used the non–polarized states to

explain the existence of even denominator fractions since the Pauli principle can no longer exclude them.

REFERENCES

1   S.T. Pantiledes, "Deep Centers in Semiconductors", Gordon and Beach Science Publishers (1986).

2   B. Etienne and V. Thierry–Mieg, App. Phys. Lett. $\underline{52}$, 1237 (1988).

3   A. Zrenner, F. Koch, R.L. Williams, R.A. Stradling, K. Ploog, and G. Weimann, Semicond. Sci. Technol. $\underline{3}$, 1203 (1988).

4   K. v. Klitzing, G. Dorda, and M. Pepper, Phys. Rev. Lett. $\underline{48}$, 494 (1979).

5   R.F. Kazarinov, and S. Luryi, Phys. Rev. B $\underline{25}$, 7626 (1982).

6   S.V. Iordansky, Solid State Comm. $\underline{43}$, 1 (1982)

7   R. Woltjer, R. Eppenga, J. Mooren, C.E. Timmering, and J.P. André, Europhys. Lett $\underline{2}$, 149 (1986).

8   T. Ando, Journ. Phys. Soc. Jap. $\underline{53}$, 3101 (1984).

9   R.B. Laughlin, Phys. Rev. B $\underline{23}$, 5632 (1981).

10 M. Büttiker, Phys. Rev. B $\underline{38}$, 9375 (1988).

11 R.J. Haug, K. von Klitzing, and K. Ploog, Phys. Rev. B $\underline{35}$, 5933 (1987).

12 D.C. Tsui, H.L. Störmer, and A.C. Gossard, Phys. Rev. Lett. $\underline{48}$, 1559 (1982).

13 L. Esaki, and R. Tsu, IBM Res. Note, RC–2418, mar. 1969.

14 M.R. Leys, Chemtronics $\underline{2}$, 155 (1987).

15 K. Ploog, "Physics and Applications of Quantum Wells and Superlattices", NATO ASI series B $\underline{170}$, p. 43, ed. E.E. Mendez and K. von Klitzing (Plenum Press, 1987)

16 T.M. Kerr, C.E.C. Wood, S.M. Newstead, and J.D. Wilcox, J. App. Phys. $\underline{65}$, 2673 (1989).

17 H.L. Störmer, R. Dingle, A.C. Grossard, W. Wiegmann, and M.D. Sturge, Solid State Comm. $\underline{29}$, 705 (1979).

18 A. Zrenner, H. Reisinger, F. Koch, and K. Ploog, Proceedings of the "17th International Conference on the Physics of Semiconductors", p. 325, San Francisco, ed. by J.P. Chadi and W.A. Harrison (Springer–Verlag, 1984)

19 J.C. Slater, Phys. Rev. $\underline{11}$, 1592 (1949).

20 F. Stern and S. Das Sarma, Phys. Rev. B $\underline{30}$, 840 (1984).

21 T. Ando, Journ. Phys. Soc. Jap. $\underline{51}$, 3893 (1982).

22 G.A.M. Hurkx and W. v. Haeringen, J. Phys. C $\underline{18}$, 5617 (1985).

23 W. Kohn and L.J. Sham, Phys. Rev. $\underline{140}$, A1133 (1965).

24 L. Hedin and B.I. Lundqvist, J. Phys. C **4**, 2064 (1971).

25 O. Gunnarson and B.I. Lundqvist, Phys. Rev. B **13**, 4274 (1976).

26 K. Hirakawa and H. Sakaki, Phys. Rev. B **33**, 8291 (1986).

27 W. Walukiewicz, H.E. Ruda, J. Lagowski and H.C. Gatos, Phys. Rev. B **30**, 4571 (1984).

28 T. Ando, Journ. Phys. Soc. Jap. **51**, 3900 (1982).

29 B. Lin, thesis University of Princeton (1985).

30 P.J. v. Hall, T. Klaver, and J.H. Wolter, Semicond. Sci. Technol. **3**, 120 (1988) and P.J. v. Hall, Superl. Microstr. **6**, 213 (1989).

31 F. Fang and W.E. Howard, Phys. Rev. Lett. **16**, 797 (1966).

32 P.F. Maldague, Surf. Sci. **73**, 296 (1978).

33 P.J. v. Hall private communication.

34 J.J. Harris, C.T. Foxon, D.E. Lacklison, and K.W. Barnham, Superl. Microstr. **2**, 563 (1986).

35 R.A. Smith, "Semiconductors" (Cambridge University Press, Cambridge, 1978).

36 T. Ando and Y. Uemura, Journ. Phys. Soc. Jap. **36**, 959 (1974).

37 T. Ando, Y. Matsumoto, and Y. Uemura, Journ. Phys. Soc. Jap. **39**, 279 (1975).

38 S. Kawai, T. Igarashi, and J. Wakabayashi, Prog. Theor. Phys. Supp. **57**, 176 (1975).

39 E. Brézin, D.J. Gross, and C. Itzykson, Nucl. Phys. B **235**, [FS11] 24 (1984)

40 T. Ando, Journ. Phys. Soc. Jap. **53**, 3126 (1984).

41 D.C. Tsui and A.C. Gossard, Appl. Phys. Lett. **38**, 550 (1981).

42 H.P. Wei, D.C. Tsui, and A.M.M. Pruisken, Phys. Rev. B **33**, 1488 (1986)

43 Chapter 5 in "The Quantum Hall Effect" ed. by R.E. Prange and S.M. Girvin, (Springer Verlag, 1987).

44 H. van Houten, B.J. van Wees, J.E. Mooij, C.W.J. Beenakker, J.G. Williamson, and C.T. Foxon, Europhys. Lett **5**, 712 (1988).

45 R. Willet, J.P. Eisenstein, H.L. Störmer, D.C. Tsui, A.C. Gossard, and J.H. English, Phys. Rev. Lett. **59**, 1776 (1987).

46 J.P. Eisenstein, Proceedings "Application of High Magnetic Fields in Semiconductor Physics II", Würzburg, p. 106, ed. by G. Landwehr (Springer Verlag, 1989).

47 R.B. Laughlin, Chapter 7 in "The Quantum Hall Effect" ed. by R.E. Prange and S.M. Girvin, (Springer Verlag, 1987).

48 B.I. Halperin, Helv. Phys. Acta $\underline{56}$, 75 (1983).

49 P.A. Maksym, R.G. Clark, S.R. Haynes, J.R. Mallet, J.J. Harris, and C.T. Foxon, Proceedings "Application of High Magnetic Fields in Semiconductor Physics II", Würzburg, p.138, ed. by G. Landwehr (Springer Verlag, 1989).

50 R.G. Clark, J.R. Mallet, S.R. Haynes, P.A. Maksym, J.J. Harris and C.T. Foxon, Proceedings "Application of High Magnetic Fields in Semiconductor Physics II", Würzburg, p. 127, ed. by G. Landwehr (Springer Verlag, 1989).

51 R.G. Clark, S.R. Haynes, A.M. Suckling, J.R. Mallet, P.A. Wright, J.J. Harris, and C.T. Foxon, Phys. Rev. Lett. $\underline{62}$, 1536 (1989).

CHAPTER 2

ANALYSIS OF THE SHALLOW AND DEEP CENTER OCCUPANCIES IN
Si–DOPED $Al_xGa_{1-x}As$ USING A MULTI–LEVEL DONOR MODEL

2.1 INTRODUCTION

The electronic properties of Si–doped $Al_xGa_{1-x}As$ are controlled by the co–existence of a hydrogen–like shallow center and a deep center, the so–called DX center. This deep center, which is dominant for $0.25 < x < 0.6$, is also responsible for the effect of Persistent Photo Conductivity (PPC).

The nature of the deep center is a long–standing problem. Lang *et al.*[1] proposed a Large Lattice Relaxation (LLR) model whereas Saxena[2] used a band structure model to explain the features of the deep center. Hydrostatic pressure experiments showed that the deep center can be induced by pressure[3,4]. From these experiments it has been proposed that the deep center is tied to the L–minimum and that the predominance of either shallow or deep centers depends on the relative positions of their energy levels. The total number of deep and shallow centers has proven to be nearly equal to the amount of Si–doping[5]. Therefore it has been concluded that both centers are induced by the same donor. It has been shown[6,7] that the photo–ionization cross section and the thermal capture and emission energies are the same for the pressure–induced deep centers in GaAs as for the deep centers in $Al_xGa_{1-x}As$.

From photo–ionization measurements it has recently been suggested[8,9] that the deep level does not show LLR but only Small Lattice Relaxation (SLR). This has also been supported by Extended X–ray Absorption Fine Structure (EXAFS) experiments[10]. Far infrared measurements[11] proved that all the deep centers in $Al_{0.4}Ga_{0.7}As$ act as shallow centers after photo–ionization. The maximum attainable electron density in highly Si–doped GaAs should be due to self–compensation. At high doping concentrations, however, the conduction band is filled to such an amount that the deep center, which lies above the conduction band edge,

becomes populated[12,13]. It has also been shown that in GaAs a metastable level is present which can be persistently populated by hot electrons[14]. This level is believed to be the deep center which becomes resonant with the Γ–band for x < 0.22.

These experiments strongly suggest that the shallow donor states can be regarded as excited states of the deep (DX) ground states. Assuming such a donor model implies the use of the statistics of a multi–level donor. Saxena[15] already used a two–level donor model to determine the pressure dependence of the band structure. However, she did not point out the consequences of the use of a multi-level donor for the occupancies of the different levels. In this chapter we show that the shallow and deep center occupancies and the free electron concentration in Si–doped $Al_xGa_{1-x}As$ as function of the composition can consistently be described on the basis of a dependent three–level donor model, properly taking into account the distribution function. This model proves to be also suitable for analyzing the behaviour of a $GaAs/Al_xGa_{1-x}As$ heterostructure under hydrostatic pressure.

2.2 THE MULTI–LEVEL DONOR MODEL

In previous calculations[13,16,17] the occupancies of the shallow and deep centers are given by

$$n_{DX} = \frac{N_{DX}}{1 + \dfrac{1}{g_{DX}} \cdot \exp\left[\dfrac{E_{DX} - E_f}{k_B T}\right]} \qquad [2.1]$$

$$n_s = \frac{N_s}{1 + \dfrac{1}{g_s} \cdot \exp\left[\dfrac{E_s - E_f}{k_B T}\right]} \qquad [2.2]$$

where N_{DX} and N_s are the concentrations of deep and shallow centers, respectively; E_{DX} and E_s are their ionization energies, and g_{DX} and g_s are the degeneracy factors. The shallow and deep centers are then treated as two independent kinds of donors. Tachikawa et al.[3] demonstrated that the electron occupancy of the

deep centers can be calculated in a three–level (independent) donor model, assuming that the deep center is coupled to the L–minimum with E_L–E_{DX} = 120 meV. If, however, a donor is assumed to have more than one level, the total donor occupancy cannot be calculated by assuming independent donors. In a situation where the deep centers are dominant an electron excited from the deep ground state can be trapped at an excited (shallow) state in a dependent donor model. Assuming independent donors, where the dominance of deep centers means that N_{DX} equals the total donor concentration, no trapping at shallow centers is possible because these shallow centers are transferred into deep centers. So the use of [2.1] and [2.2] is not correct as was also pointed out by Morgan[18].

In this chapter we show that the occupancy of the deep center and the free electron concentration can be derived by assuming a donor with one ground state and two excited states. The ionized donor concentration is then given by[19]

$$n_D^+ = \frac{N_D}{1 + \sum_r \left[g_r \exp\left[\frac{E_f - E_{Dr}}{k_B T} \right] \right]} \qquad r = \Gamma, L, X. \qquad [2.3]$$

Using [2.1] the deep center concentration N_{DX} has to be determined for various compositions by deep level transient spectroscopy (DLTS) measurements. In our calculation, using [2.3], deep center occupancies can be calculated without knowing any experimental data concerning the deep centers.

Using a multi–valley effective mass model Chand *et al.*[20] calculated the activation energy when there are different energy levels connected to the Γ, L and X band. Watanabe *et al.*[17] suggested that the variation in activation energy of the donor as a function of composition is due to a variation in the concentration ratio between shallow and deep centers. In the present paper we show that the variation in the activation energy is due to different occupancies of the ground and excited states of the donors. From this model of dependent donor levels it is also easily understood why the deep center activation energy for emission is independent on the AlAs mole fraction[5], while the activation energy for capture decreases with increasing AlAs mole fraction[21]. For x > 0.22 the shallow state becomes the excited state of the deep ground state. After photo–ionization of an occupied deep state, the electron will only return to this deep state if the thermal energy is large enough to overcome the potential barrier between the ionized and

38

	band structure model	$E_L - E_\Gamma$ (x=0.2) meV	$E_L - E_{DL}$ meV	$E_\Gamma - E_{DL}$ (x=0.2) meV
Tachikawa[a]	Casey and Panish[d]	163	120	-43
Lifshitz[b]	Casey and Panish[d]	163	140	-23
Henning[c]	Saxena (T = 0 K)[e]	200	200	0
This work	Casey and Panish[d]	163	160	-3

a   M. Tachikawa, M. Mizuta, H. Kukimoto, and S. Minomura, Jap. Journ. Appl. Phys. **24**, L821 (1985).

b   N. Lifshitz, A. Jayaraman, and R.A. Logan, Phys. Rev. B **21**, 670 (1980).

c   J.C.M. Henning, and J.P.M. Ansems, Semicond. Sci. Techn. **2**, 1 (1987).

d   H.C. Casey and B. Panish, "Heterostructure Lasers" (Academic Press, New York, 1978).

e   J.C.M. Henning, J.P.M. Ansems, A.G.M. de Nijs, J. Phys. C **17**, L–915 (1984)

Table 2.1:

Electronic band parameters for $Al_xGa_{1-x}As$ as used by various authors.

Γ	$E_\Gamma - E_{D\Gamma}$ meV	g_Γ	$E_{cr}(x)$ for T = 300 K[b] eV	$\partial E_{cr}/\partial P$ [c] meV/kbar
Γ	6[a]	2	1.424 + 1.247·x x < 0.45 1.424 + 1.247·x + 1.147(x–0.45)² x > 0.45	11.1
L	160	8	1.708 + 0.642·x	2.8
X	40[a]	6	1.900 + 0.125·x + 0.143·x²	-0.8

a   M. Tachikawa, M. Mizuta, H. Kukimoto, and S. Minomura, Jap. Journ. Appl. Phys. **24**, L821 (1985).

b   H.C. Casey and B. Panish, "Heterostructure Lasers" (Academic Press, New York, 1978).

c   S. Adachi, J. Appl. Phys. **58**, R1 (1985).

Table 2.2:

Band structure parameters for $Al_xGa_{1-x}As$ as used in our calculations.

bound state.

In our calculations we assume a shallow level tied to the Γ–minimum, a deep level tied to the L–minimum and a shallow level tied to the X–minimum. For the constant energy separation E_L–E_{DL} between the L–minimum and the coupled deep center we use a value of 160 meV. From Hall and DLTS measurements values of 120 meV and 140 meV have been found[3,4], respectively. From photo luminescence measurements Henning et al.[8] found that E_L–E_{DL} = 200 meV and Calleja et al.[22] reported 220 meV, so there seems to be a large discrepancy between the various values reported. Comparing these results one has to keep in mind that the deep centers start to dominate the conduction for x > 0.2 because at this composition the deep centers cross the Γ–band. The different values of E_L–E_{DL} are partly due to the differences in the band structure models used by several authors. This is shown in Table 2.1 where for several models E_D–E_Γ at x = 0.2 is given. Taking into account the differences in the several band structure models, the discrepancy in E_L–E_{DL} of about 80 meV reduces to 40 meV in E_Γ–E_{DL}. In our calculations the band structure model reported by Casey and Panish[23] is adopted. In this band structure model, the activation energy of the deep center at x = 0.3 is about 60 meV, a value commonly accepted in calculations on GaAs/Al$_{0.3}$Ga$_{0.7}$As heterostructures. Ishikawa et al.[24] also reported an ionization energy of 60 meV at x = 0.3. For g_r and E_{Dr} we use the values as given in Table 2.2. The temperature dependence of the bandgap, E_{gr}, is taken into account by using the Varshni[25] equation

$$E_{gr}(T) = E_{gr}(T_0) + \left[\frac{T_0^{\,2}}{T_0 + \beta_r} - \frac{T^2}{T + \beta_r} \right] \cdot \alpha_r \qquad\qquad [2.4]$$

where $T_0 = 300$ K and the coefficients α_r and β_r are given by[26]

$$\alpha_\Gamma = 5.41 \cdot 10^{-4} \ \mathrm{eVK^{-1}}$$

$$\alpha_L = 6.05 \cdot 10^{-4} \ \mathrm{eVK^{-1}}$$

$$\alpha_X = 4.60 \cdot 10^{-4} \ \mathrm{eVK^{-1}}$$

$$\beta_{\Gamma,L,X} = 204 \ \mathrm{K}.$$

Fig. 2.1:

Occupancy of the shallow Γ and X donor levels, the deep L level, and the free electron concentration at room temperature as a function of AlAs mole fraction x in comparison with the data reported by Watanabe et al.[5].
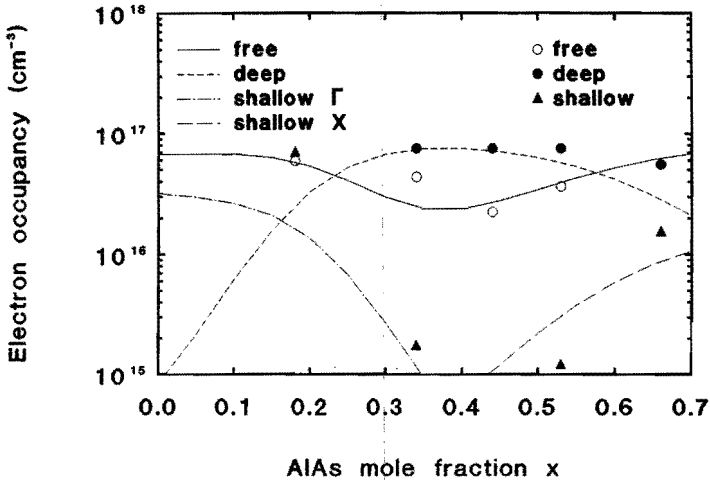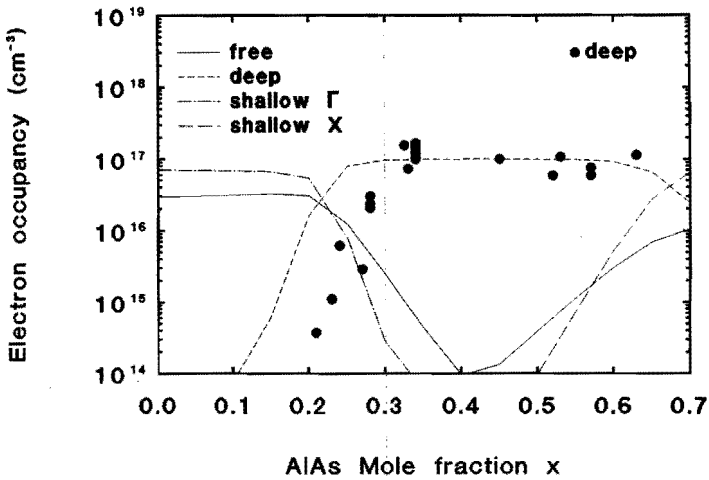

Fig. 2.2:

Occupancy of the shallow Γ and X donor levels, the deep L level, and free electron concentration at T = 100 K as a function of AlAs mole fraction x in comparison with the DLTS data reported by Lang et al.[1].

The electron density in each conduction band, using the Ehrenberg approximation[27], is given by

$$n_r = \frac{N_{cr}}{\frac{1}{4} + \exp\left[\dfrac{E_{cr} - E_f}{k_B T}\right]} \qquad\qquad r = \Gamma, L, X \qquad [2.5]$$

$$\text{with } N_{cr} = \left[\frac{2\pi m_r^* k_B T}{h^2}\right]^{3/2}$$

For the value of electron effective mass in the Γ, L and X conduction band we used those reported by Joyce[28] are used. Neglecting the acceptor concentration, charge neutrality requires

$$n_\Gamma + n_L + n_X = N_D^+ \qquad\qquad\qquad [2.6]$$

After obtaining E_f from [2.3], [2.5] and [2.6] for different AlAs fractions, the occupancy of each state can be calculated by[19]

$$n_{Dr} = N_D^+ \cdot g_r \exp\left[\frac{E_f - E_{Dr}}{k_B T}\right] \qquad\qquad [2.7]$$

The magnitude of the doping concentration N_D does not influence the relative occupancy of the donor levels.

2.3   ANALYSIS OF EXPERIMENTAL DATA

2.3.1   BULK $Al_xGa_{1-x}As$

Fig. 2.1 presents the results of our calculations of the occupancies of the donor levels and the free electron concentration at room temperature. For the doping concentration a value of $N_D = 1 \cdot 10^{17}$ cm^{-3} is used. The deep center concentration (DLTS), the shallow donor concentration (C–V) and the free electron concentration (Hall measurements) at T = 300 K reported by Watanabe et al.[5] are also given. The shape of the calculated free electron concentration
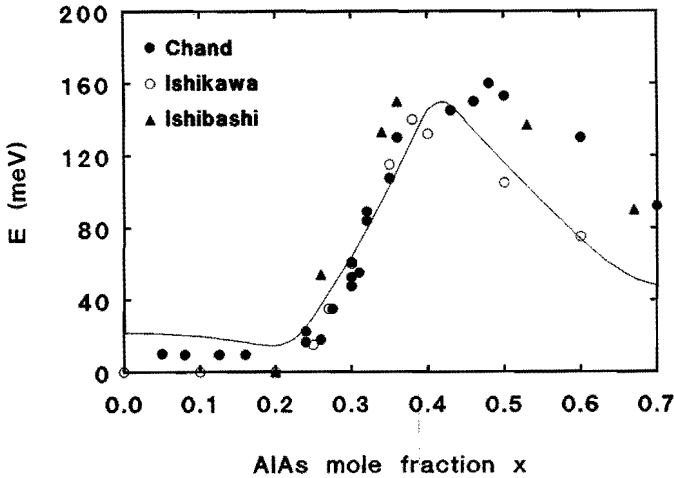
Fig. 2.3:
    Thermal activation energy as a function of AlAs mole fraction in comparison with measurements as reported by various authors[20,24,29].

agrees rather well with the experimental data. For low values of x the free electron concentration decreases due to an increasing occupancy of the deep center with increasing x. For x > 0.45 the lowest conduction band changes from Γ to X and the high effective Density Of States (DOS) of the X–band gives rise to an increasing free electron concentration. We find the minimum in the electron concentration at about x = 0.42. Ishibashi et al.[29] and Watanabe et al.[5] reported experimental values of x = 0.36 and x = 0.45 for this minimum. A precise determination of this minimum is difficult because measurements on different samples have to be compared. The results obtained at T = 100 K are plotted in Fig. 2.2 together with the DLTS data reported by Lang et al.[1]. As expected, the donor with an occupied deep ground state is dominant for 0.25 < x < 0.6. It should be noted however, that the position of the DLTS peaks, from which the occupancy has been determined, lie at different temperatures for different x. So the measured and calculated values (at one temperature) are not really comparable. Taking this into account, the calculated occupancy of the deep centers is in good agreement with the DLTS data. At T = 100 K the free electron concentration is also reduced by the high occupancies of the shallow centers.

    In order to determine the activation energy the temperature dependence of

the free electron concentration has been calculated for several values of x in the temperature range between 100 K and 300 K. For temperatures lower than 100 K no thermal equilibrium can be maintained; the electrons cannot be trapped in the deep centers anymore because of the potential barrier between the bound and ionized state. When Boltzmann statistics are applicable, the condition of charge neutrality gives[27]

$$\frac{g_r(N_A+n)n}{N_c(N_D-N_A)} = \exp\left[\frac{-E_D}{k_B T}\right] \qquad [2.8]$$

Because in our calculation zero compensation is assumed, the thermal activation energy ΔE can be defined by the relation

$$n \sim \exp\left[\frac{-\Delta E}{2k_B T}\right]$$

The calculated results for the activation energy ΔE are shown in Fig. 2.3. This curve agrees very well with the curves determined from Hall measurements[20,24,29].

2.3.1   GaAs/Al$_x$Ga$_{1-x}$As HETEROSTRUCTURE UNDER HYDROSTATIC PRESSURE

The multi–level donor model is also useful in describing the properties of a GaAs/Al$_x$Ga$_{1-x}$As heterostructure. From hydrostatic pressure measurements up to 16 kbar[30] on a GaAs/Al$_{0.3}$Ga$_{0.7}$As heterostructure the pressure dependence of the deep center can be determined. An advantage of pressure measurements is that only one sample is needed to study the changes in ionization energy of the deep center. Mercy et al.[30] neglected the free electron concentration in the L and X–band. At a pressure of about 15 kbar, however, the conduction band minimum changes from Γ to X, so for this pressure the free electron concentration in the L and X–band cannot be neglected. We assume a shallow level tied to the Γ–band and an arbitrary deep level with degeneracy factor g_{d1}. The parameters used are defined in Fig. 2.4 and Table 2.2. The position of this deep level is now defined relative to the bottom of the well by an energy E_{d1}, so no coupling between the

g_{dl}	N_A/N_D	E_c-E_{dl} (P=0)	$\partial(E_c-E_{dl})/\partial P$
		meV	meV/kbar
2	0.00	95.2	8.8
	0.10	82.7	8.7
	0.20	69.3	8.8
6	0.0	66.8	8.8
	0.1	54.3	8.7
	0.2	41.4	8.8
8	0.0	59.4	8.8
	0.1	46.8	8.7
	0.2	33.6	8.8

Table 2.3:

Calculated results for the position and the pressure dependence of the deep center as determined from measurements Mercy *et al.*[30] on a GaAs/Al$_x$Ga$_{1-x}$As heterostructure. The conduction band discontinuity in our calculations was equal to $\Delta U_c = 243$ meV.
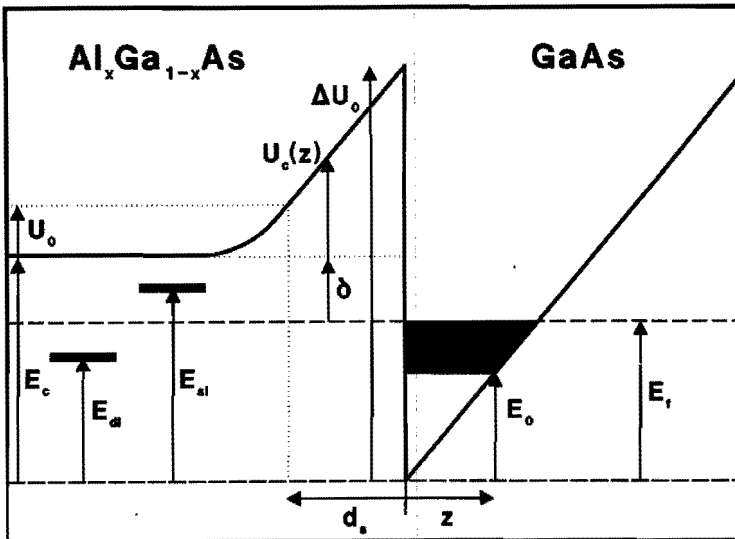
Fig. 2.4:

Band structure diagram of a GaAs/Al$_x$Ga$_{1-x}$As heterostructure.

deep level and one of the conduction bands is assumed. The pressure dependence of the deep level can be determined by calculating the positions of the deep level (E_{dl}) and the Γ–valley (E_c), both relative to the bottom of the well, as a function of pressure. In the $Al_xGa_{1-x}As$ side ($z < 0$) we have the Poisson equation

$$\frac{\partial^2}{\partial z^2} U_c(z) = \frac{e}{\epsilon_0 \epsilon_r} \cdot \rho(z)$$

The charge density is given by $\rho(z) = e \cdot [\ N_D^+(z) - N_A - n(z)\ ]$, where

$$N_D^+(z) = \frac{N_D}{1 + 2 \cdot \exp\left[\dfrac{E_f - E_{s\,1} - U_c(z)}{k_B T}\right] + 8 \cdot \exp\left[\dfrac{E_f - E_{d\,1} - U_c(z)}{k_B T}\right]} \qquad [2.9]$$

$$n_r(z) = \frac{N_{cr}}{\exp\left[\dfrac{E_{cr} - E_f + U_c(z)}{k_B T}\right] + \dfrac{1}{4}} \qquad\qquad r = \Gamma, L, X \qquad [2.10]$$

$$n(z) = \Sigma_r n_r(z)$$

Integration of the Poisson equation from $z = -\infty$ to $-d_s$ gives

$$-\left[\frac{\partial}{\partial z} U_c(z)\right]^2 \Bigg|_{z=-d_s} = \frac{2k_B T N_D e^2}{\epsilon_0 \epsilon_r} \cdot$$

$$\left\{\ln\left[\frac{2\cdot\exp\left[\dfrac{E_f - E_{s\,1}}{k_B T}\right] + 8\cdot\exp\left[\dfrac{E_f - E_{d\,1}}{k_B T}\right] + 1}{2\cdot\exp\left[\dfrac{E_f - E_{s\,1}}{k_B T}\right] + 8\cdot\exp\left[\dfrac{E_f - E_{d\,1}}{k_B T}\right] + \exp\left[\dfrac{U_0}{k_B T}\right]}\right]\right.$$

$$+ \frac{N_A U_0}{k_B T} + 4 \cdot \sum_r \frac{N_{cr}}{N_D} \left[\frac{\exp\left[\frac{E_{cr}-E_f}{k_B T}\right] + \frac{1}{4}}{\exp\left[\frac{E_{cr}-E_f}{k_B T}\right] + \frac{1}{4}\exp\left[\frac{-U_0}{k_B T}\right]} \right] \right\} \qquad [2.11]$$

Far from the junction at the $Al_x Ga_{1-x} As$ side, where $U_c(z) = 0$, charge neutrality requires

$$n(z) + N_A = N_D{}^+(z) \qquad [2.12]$$

The electrical field remains constant over the spacer, so Eq. [2.11] can be rewritten using

$$\left. \frac{\partial}{\partial z} U_c(z) \right|_{z=-d_s} = \frac{e^2}{\epsilon_0 \epsilon_r} \cdot (n_{2DEG} + n_{depl})$$

where n_{depl} is the concentration of the depletion charge on the GaAs side. From the energy band diagram we have

$$\Delta U_c = E_f + \delta + U_0 + \frac{e^2}{\epsilon_0 \epsilon_r} \cdot (n_{2DEG} + n_{depl}) \cdot d_s \qquad [2.13]$$

The Fermi energy E_f can be determined from n_{2DEG} by using the triangular well approach[31]. The energy level E_0 is then given by

$$E_0 = \left[\frac{\hbar^2}{2m^*} \right]^{1/3} \left[(3/2)\pi e <F> (i+3/4) \right]^{2/3} \qquad [2.14]$$

where $<F>$ is the average electric field felt by the electrons in the well, defined as

$$<F> = \frac{e^2}{\epsilon_0 \epsilon_r} \cdot \left[(n_{2DEG}/2) + n_{depl} \right] \qquad [2.15]$$

If we assume that $E_{sl} = 6$ meV (the shallow level plays no important role at $x = 0.3$) we have three equations. [2.11], [2.12] and [2.13], to determine the three

unknown parameters E_{d1}, U_0 and δ. When n_{2DEG} and the compensation ratio are known, the position of the deep center in the $Al_xGa_{1-x}As$ region can be calculated. Because we don't know to which conduction band the deep level is coupled, the calculation has to be done for the three possible values of g_{d1}, Table 2.2. By using the pressure dependence of n_{2DEG} at room temperature, as measured by Mercy *et al.*[30], we calculated the pressure dependence of the deep center for several compensation ratios. The results are given in Table 2.3. Mercy *et al.*[30] have chosen $N_A/N_D = 0.32$ and $\partial(E_c-E_{d1})/\partial P = 11$ meV/kbar to fit the experimental values. In our calculation no large compensation is needed to fit the experimental data. If coupled to the L–minimum ($g_{d1} = 8$), we find for $N_A = 0$ at zero pressure that $E_c-E_{d1} = 59.4$ meV. In this case the energy separation between the L–minimum and the deep center turns out to be 161.9 meV, which agrees very well with the value assumed previously in our analysis.

According to Adachi[32] the differences between the pressure coefficients of the Γ and L–band and the Γ and X–band are 8.3 meV/kbar and 11.9 meV/kbar, respectively. The calculated pressure dependence of the deep center, independent of the choice for g_{d1}, once more confirms the coupling of the deep center to the L–band.

2.4 CONCLUSIONS

In conclusion, we showed that the use of a multi–level deep donor model gives an adequate description of the general features of the deep center occupancy and the free electron concentration in bulk $Al_xGa_{1-x}As$. Using this model, no DLTS measurements are needed to determine the deep center concentration. Applying this model to a $GaAs/Al_xGa_{1-x}As$ heterostructure under hydrostatic pressure, confirms the idea that the deep center is coupled to the L–minimum with a binding energy of about 160 meV.

REFERENCES

1   D.V. Lang, R.A. Logan, and M. Jaros, Phys. Rev. B 19, 1015 (1979).

2   A.K. Saxena, Solid State Electronics 25, 127 (1982).

3   M. Tachikawa, M. Mizuta, H. Kukimoto, and S. Minomura,
     Jap. Journ. Appl. Phys. 24, L821 (1985).

4   N. Lifshitz, A. Jayaraman, and R.A. Logan, Phys. Rev. B 21, 670 (1980).

5   M.O. Watanabe, M. Morizuka, M. Mashita, Y. Ashizaway, and Y. Zohte,
     Jap. Journ. Appl. Phys. 23, L103 (1984).

6   M.F. Li, P.Y. Yu, E.R. Weber, and W. Hansen, Phys. Rev. B 36, 4531
     (1987).

7   M.F. Li, P.Y. Yu, E.R. Weber, and W. Hansen, App. Phys. Lett. 51, 349
     (1987).

8   J.C.M. Henning and J.P.M. Ansems, Semicond. Sci. Tech. 2, 1 (1987).

9   H.P. Hjalmarson and T.J. Drummond, Appl. Phys. Lett. 48, 656 (1986).

10   M. Mizuta and T. Kitano, Appl. Phys. Lett. 52, 126 (1988).

11   T.N. Theis, T.F. Kuech, L.F. Palmateer, and P.M. Mooney, "Gallium
     Arsenide and Related Compounds 1984" (Inst. Phys. Conf. Ser. 74) 241.

12   T.N. Theis, P.M. Mooney, and S.L. Wright, Phys. Rev. Lett. 60, 361 (1988).

13   D.K. Maude, J.C. Portal, L. Dmowski, T. Foster, L. Eaves, M. Nathan,
     M. Heiblum, J.J. Harris, and R.B. Beall, Phys. Rev. Lett. 59, 815 (1987).

14   T.N. Theis, B.D. Parker, P.M. Solomon, and S.L. Wright,
     Appl. Phys. Lett. 49, 1542 (1986).

15   A.K. Saxena, J. Phys. C 13, 4323 (1980).

16   E.F. Schubert and K. Ploog, Phys. Rev. B 30, 7021 (1984).

17   M.O. Watanabe and H. Maeda, Jap. Journ. Appl. Phys. 23, L734 (1984).

18   T.N. Morgan, Phys. Rev. B 34, 2664 (1986).

19   M. Cohen, "Introduction to the Quantum Theory of Semiconductors",
     (Gordon and Breach) 199

20   N. Chand, T. Henderson, J. Klem, W.T. Masselink, R. Fischer, Y. Chang,
     and H. Morkoc, Phys. Rev. B 30, 4481 (1986).

21   P.M. Mooney, N.S. Caswell, and S.L. Wright, Journ. Appl. Phys. 62, 4786
     (1986).

22   E. Calleja, A. Gomez, and E. Munoz, Appl. Phys. Lett. 52, 383 (1988).

23   H.C. Casey and B. Panish, "Heterostructure Lasers" (Academic Press, New York, 1978).

24   T. Ishikawa, J. Saito, S. Shigehiko, and S. Hiyamizu, Jap. Journ. Appl. Phys. $\underline{21}$, L675 (1982).

25   Y.P. Varshni, Physica $\underline{34}$, 149 (1967).

26   D.E. Aspnes, Phys. Rev. B $\underline{14}$, 5331 (1976).

27   J.S. Blakemore, "Semiconductor Statistics", p. 360 (Pergamon, New York, 1962).

28   W.B. Joyce, Appl. Phys. Lett. $\underline{32}$, 680 (1978).

29   T. Ishibashi, S. Tarucha, and H. Okamoto, Jap. Journ. Appl. Phys. $\underline{21}$, L476 (1982).

30   J.M. Mercy, C. Bousquet, J.L. Robert, A. Raymond, G. Gregoris, J. Beerens, J.C. Portal, P.M. Frijlinck, P. Delescluse, J. Chevrier, and N.T. Linh, Surf. Sci. $\underline{142}$, 298 (1984).

31   F. Stern, Phys. Rev. B 5, 4891 (1972).

32   S. Adachi, Journ. Appl. Phys. $\underline{58}$, R1 (1985).

CHAPTER 3

PARALLEL CONDUCTION IN A GaAs/Al$_x$Ga$_{1-x}$As HETEROSTRUCTURE

3.1 INTRODUCTION

In many GaAs/Al$_x$Ga$_{1-x}$As heterostructures parallel conduction occurs, i.e. electrical transport takes place in both the 2DEG and the Al$_x$Ga$_{1-x}$As layer. At low temperatures the electron density in the 2DEG can be increased persistently by illumination. This Persistent Photo Conductivity (PPC) effect is due to the so–called DX–center[1] formed in silicon doped Al$_x$Ga$_{1-x}$As ($0.3 < x < 0.6$). In an illuminated GaAs/Al$_x$Ga$_{1-x}$As heterostructure the photo–ionized electrons are transferred from the Al$_x$Ga$_{1-x}$As layer to the 2DEG as long as the Fermi level is positioned above the Γ–conduction band minimum in the Al$_x$Ga$_{1-x}$As layer. Due to the electric field in the spacer and the ionization of the DX–center the Fermi level rises above the Γ–conduction band minimum after a certain illumination dose. In this case free electrons are present in the Al$_x$Ga$_{1-x}$As layer and thus a second conducting channel parallel to the 2DEG is formed. See Fig. 3.1. Lin[2] has shown that parallel conduction indeed takes place in the Al$_x$Ga$_{1-x}$As layer by removing this layer part by part. In this chapter we will discuss the influence of parallel conduction on magneto–resistance measurements of a 2DEG.

At high temperatures, $T \geq 77$ K, the electrons are easily transferred from the 2DEG to the Al$_x$Ga$_{1-x}$As layer and vice versa. In this case parallel conduction can be described by a single conducting layer with two types of carriers, i.e. the low mobility electrons in the Al$_x$Ga$_{1-x}$As and the high mobility electrons in the 2DEG. Battersby *et al.*[3] have used this model successfully to describe parallel conduction in GaAs/Al$_x$Ga$_{1-x}$As heterostructures at 77 K.

Luryi and Kastalsky[4] proposed a simple electrical network to discuss the effect of parallel conduction in a GaAs/Al$_x$Ga$_{1-x}$As heterostructure on magneto–resistance measurements at low temperatures. They assumed that both conducting layers are electrical isolated from each other by the spacer layer and that the
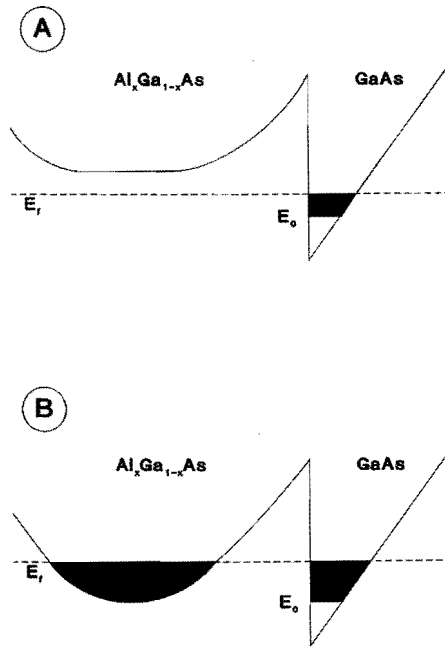
Fig. 3.1:

Schematic diagram showing the conduction band in a $GaAs/Al_xGa_{1-x}As$ heterostructure a) without and b) with parallel conduction.
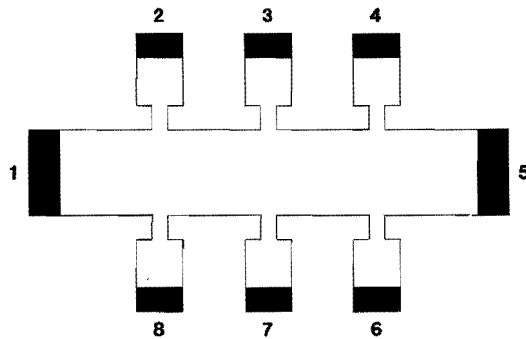

Fig. 3.2:

Sample geometry. The contacts 1 and 5 are the current probes and the other contacts are the voltage probes. The Au/Ge/Ni contacts are indicated by the black areas.

electrical contact between the two layers is only made by the current and voltages probes used to measure the Shubnikov–de Haas (SdH) and Hall resistance.

In this chapter a more sophisticated model is presented which describes parallel conduction in a GaAs/Al$_x$Ga$_{1-x}$As heterostructure at 4.2 K. We suppose that the 2DEG and the Al$_x$Ga$_{1-x}$As layer are isolated from each other and that the Hall voltage of each conducting layer acts as a voltage source which is short–circuited by the other conducting layer. This model is especially simple to use under quantum Hall conditions, where the magneto–resistivity of the 2DEG is zero and the Hall voltage of the 2DEG is exactly quantized. The theoretical description has been tested by short–circuiting two opposite Hall probes with an Ohmic resistor in the case that no parallel conduction is present in the sample.

3.2   EXPERIMENTS

The measurements have been performed on selectively doped GaAs/Al$_x$Ga$_{1-x}$As (x ≈ 0.3) heterostructures grown by Molecular Beam Epitaxy (MBE). The samples were Hall–bar shaped and the contact configuration is shown in Fig. 3.2. The samples were cooled down to 4.2 K with all contacts short–circuited. In order to illuminate the sample a red LED (HP 5082–4732, $\lambda = 650$ nm) was mounted inside the cryostat.

Fig. 3.3 shows the magneto and Hall resistivity at 4.2 K in a sample without parallel conduction. In high magnetic fields the minima of the SdH–resistivity are almost zero and the Quantum Hall plateaus have the expected quantized values: $\rho_{xy} = e^2/hi$. In Fig. 3.4 we show the SdH and Hall resistivity at 4.2 K in the same sample in the case of parallel conduction after illumination. The minima in the magneto–resistivity at high magnetic fields are no longer equal to zero. The Quantum Hall plateaus disappear and the Hall resistivity falls below the classical expected curve.

In Fig. 3.5 we show the measured SdH and Hall resistivity at 4.2 K with and without a resistor placed between the voltages probes 3 and 7. The Hall voltage is measured between contacts 3 and 7 and the SdH voltage is measured between contacts 2 and 3. A striking resemblance can be observed between the influence of a parallel resistor and that of parallel conduction in the Al$_x$Ga$_{1-x}$As layer.
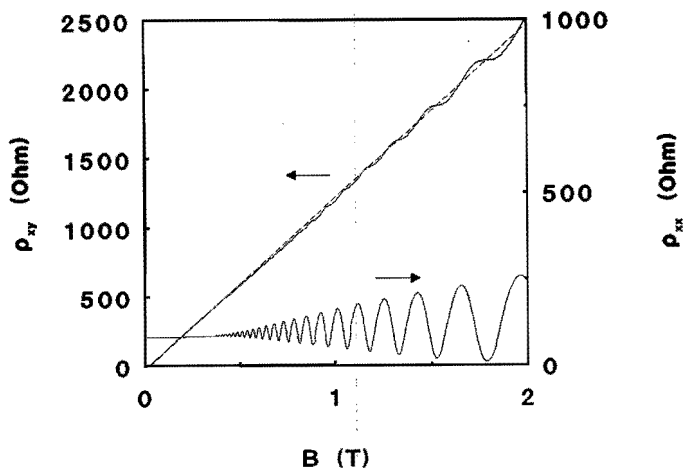
Fig. 3.3:

The magneto and Hall resistivity of a sample without parallel conduction. At 4.2 K the electron density is $5.22 \cdot 10^{11}$ cm^{-2} and the mobility is $14.8 \cdot 10^4$ cm^2/Vs. The dashed line indicates the classical Hall resistivity.
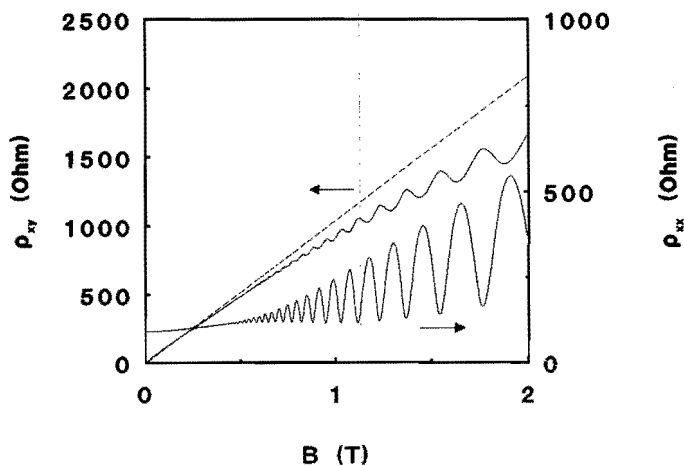

Fig. 3.4:

The magneto and Hall resistivity of the sample of Fig. 3.3 with parallel conduction after a long illumination time. The electron density is $6.00 \cdot 10^{11}$ cm^{-2} and the mobility is $20.9 \cdot 10^4$ cm^2/Vs.
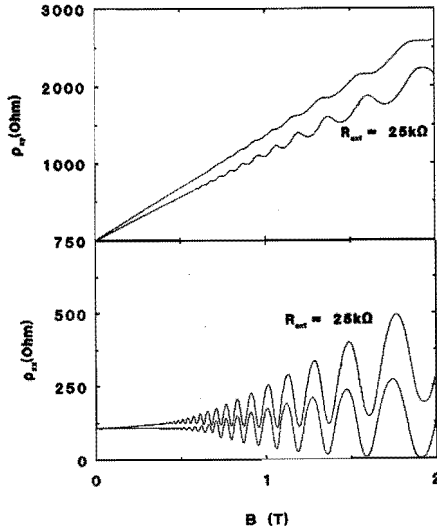
Fig. 3.5:

The magneto and Hall resistivity of a sample with and without an external resistor placed between the contacts 3 and 7. The electron density is $4.67 \cdot 10^{11}$ cm^{-2} and the mobility is $12.1 \cdot 10^4$ cm^2/Vs

3.3 DISCUSSION

The two–point resistance, R_2, of a piece of semiconductor material in a magnetic field is equal to $R_2 = R_c + R_{xx} + R_{xy}$, where R_c is the contact resistance, R_{xx} the magneto–resistance, and R_{xy} the Hall resistance. In most cases R_c is small compared to $R_{xx} + R_{xy}$. The two–point resistance contains the Hall resistance due to a different electron density in the contact and the semiconductor material[5].

Under Quantum Hall (QH) conditions $\rho_{xx} = 0$ and $\rho_{xy} = h/ie^2$. In this case the edges of the 2DEG are equipotential lines and only a discontinuity in the potential occurs at current injection and extraction points. Fig. 3.6 shows the potential distribution along the edges of a Hall bar under QH–conditions[6] when a fraction αI of the total current is extracted from the 2DEG on one side of the sample (contact 3) and injected on the other side (contact 7). The voltages between the several contacts are now given by $V_{37} = (1-\alpha)I\rho_{xy}$, $V_{23} = \alpha I\rho_{xy}$ and $V_{34} = 0$.
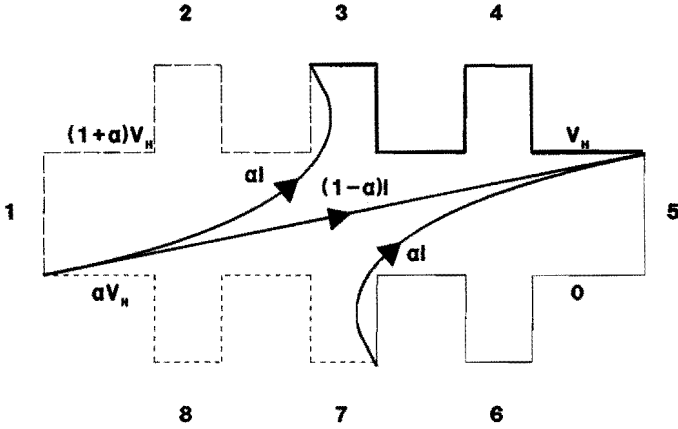
Fig. 3.6:

Schematic diagram showing the current and potential distribution in the 2DEG when a fraction αI of the current is extracted from contact 3 and injected through contact 7.
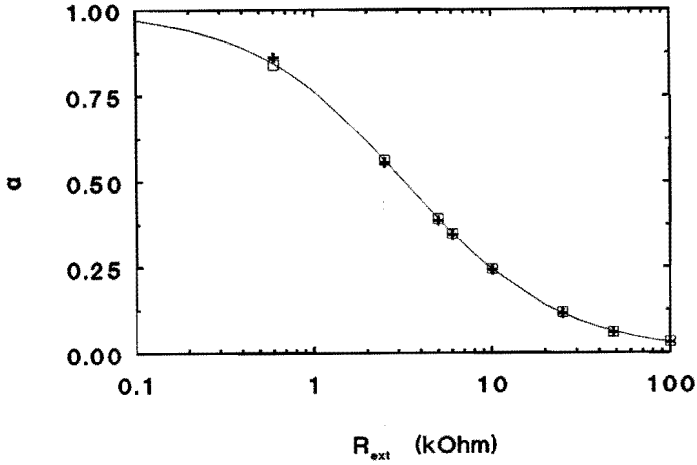
Fig. 3.7:

The current fraction α flowing through the contacts 3 and 7 as a function of the value of an external resistor placed between 3 and 7. The fraction α determined from the longitudinal voltage V_{23} and the transverse voltage V_{37} are indicated by squares and crosses, respectively.

If we connect an ohmic resistor, R_{ext}, between contacts 3 and 7 a fraction α of the current flows through these contacts. Since V_{37} is equal to $\alpha I R_{ext}$ the fraction α is given by

$$\alpha = \frac{1}{1 + (R_{ext}/\rho_{xy})} \qquad [3.1]$$

First we discuss the experiments in a sample without parallel conduction with an external resistor placed between contacts 3 and 7. The voltages were measured at contact pairs 2–3, 3–4 and 3–7 at a magnetic field corresponding to a filling factor 8. The voltage between contacts 3 and 4 is indeed zero for all values of the external resistor. We determined the current fraction α as a function of the value of the external resistor from $V_{23} = \alpha \, h/8e^2$ and $V_{37} = (1-\alpha) \, h/8e^2$. These results are shown in Fig. 3.7 together with the curve given by equation [3.1]. This excellent agreement proves that indeed only a voltage step occurs at the current injection and extraction points and that the current fraction can be determined from [3.1].

Now a heterostructure with parallel conduction will be considered as a 2DEG with the parallel conducting $Al_{1-x}Ga_xAs$ layer acting as an external resistor and vice versa. The external resistor consists in both cases of the sum of the Hall and the magneto–resistance. In Fig. 3.8 we show the current distribution in the two parallel conducting layers near the opposite contacts 3 and 7. We suppose that a fraction δ of the total current $(\beta+\delta)I$ flowing in the 2DEG splits off and leaves the 2DEG via contact 7. The fraction δ flows through the parallel $Al_xGa_{1-x}As$ layer and enters the 2DEG again through contact 3. See Fig. 3.8a. The total current flowing in the longitudinal direction (from contact 1 to 5) before and after contact pair 3–7 is constant. This is only true for contact pair 3–7 due to the symmetry of the electrical network. The distribution of the current flowing in the $Al_{1-x}Ga_xAs$ layer near contact 3 and 7 is given in Fig. 3.8b.

Although the conduction in the $Al_{1-x}Ga_xAs$ layer has a three–dimensional character we treat this layer as a two–dimensional system with a carrier density $n_{AlGaAs} = n_{3DEG} \cdot d_{AlGaAs}$. The magneto–resistivity tensor elements are then given by $\rho_{xxAlGaAs} = 1/(e \, n_{AlGaAs} \, \mu_{AlGaAs})$ and $\rho_{xyAlGaAs} = B/(e \, n_{AlGaAs})$.

In order to determine the current fractions $\beta, \gamma, \delta, \epsilon$ under QH–conditions we need four independent equations. The voltage between contacts 2 and 3 is equal
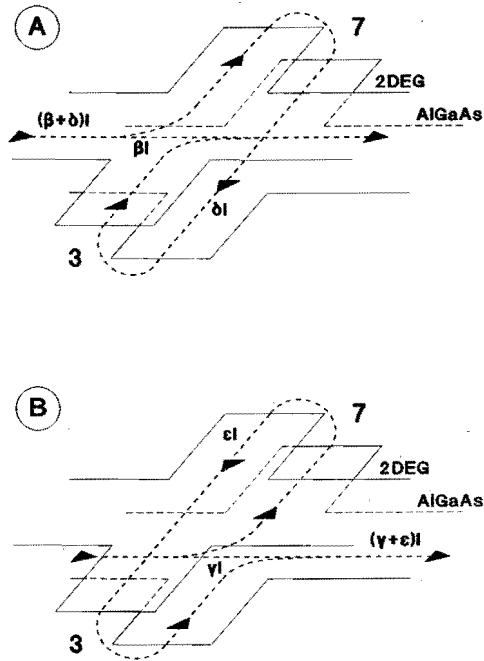
Fig. 3.8:

The current distribution in the 2DEG and the parallel conducting $Al_xGa_{1-x}As$ layer.

to the product of the injected current through contact 3 and the two–dimensional Hall resistivity (see Fig. 3.6)

$$V_{23} = (\delta - \epsilon)\, I\rho_{xy} \qquad\qquad [3.2]$$

This voltage can also be expressed in currents through and resistivity of the $Al_{1-x}Ga_xAs$ layer

$$V_{23} = 1/b\,(\gamma + \epsilon)\, I\rho_{xxAlGaAs} - (\delta - \epsilon)\, I\rho_{xyAlGaAs} \qquad\qquad [3.3]$$

where l/b is length–to–width ratio of the Hall bar between contact 2 and 3. Equations [3.2] and [3.3] give

$$(\delta - \epsilon) \cdot (\rho_{xy} + \rho_{xyAlGaAs}) = 1/b \ (\gamma + \epsilon) \ I\rho_{xyAlGaAs} \qquad [3.4]$$

Just like in the case of the external resistor between contact 3 and 7 the current δI delivered by the 2DEG is determined by the resistance of the "external" load resistor. In this case the "external" load resistor is the two–point resistance of the $Al_xGa_{1-x}As$ layer between contact 3 and 7. This two–point resistance contains the Hall and magneto–resistance of the $Al_xGa_{1-x}As$ layer. We can approximate the magneto–resistance of the $Al_xGa_{1-x}As$ layer by $2 \cdot (1/b)_c \cdot \rho_{xx}$ which is equal to two times the magneto–resistance of a contact flap. The magneto–resistance of the main channel can be neglected because of its very small length–to–width ratio. Thus the current fraction δI is given by

$$\delta I = \beta I\rho_{xy}/(\rho_{xyAlGaAs} + 2 \ (1/b)_c \ \rho_{xxAlGaAs}) \qquad [3.5]$$

A similar equation is derived for the current fraction ϵI delivered by the $Al_xGa_{1-x}As$ layer

$$\epsilon I = \gamma I\rho_{xyAlGaAs}/(\rho_{xy} + 2 \ (1/b)_c \ \rho_{xxAlGaAs}) \qquad [3.6]$$

Finally the sum of all fractions is equal to 1

$$\beta + \gamma + \delta + \epsilon = 1 \qquad [3.7]$$

At a given integer filling factor of the 2DEG the four unknown current fractions can be solved from the last four equations, [3.4] to [3.7], if $\rho_{xxAlGaAs}$ and $\rho_{xyAlGaAs}$ are known. When the current fractions are known the voltage V_{23} can be calculated from [3.2]. The voltage between contact 3 and 7 is equal to the sum of the Hall voltages in the 2DEG due to the current βI and the current ϵI

$$V_{37} = (\beta - \epsilon) \ I\rho_{xy} \qquad [3.8]$$

In Fig. 3.9 we show R_{23} and R_{37} as measured in a sample with parallel conduction. The dashed line is the classical Hall resistance for an electron density $n_{2DEG} = 6.5 \cdot 10^{11} \ cm^{-2}$ as determined from the period of the SdH–oscillations in
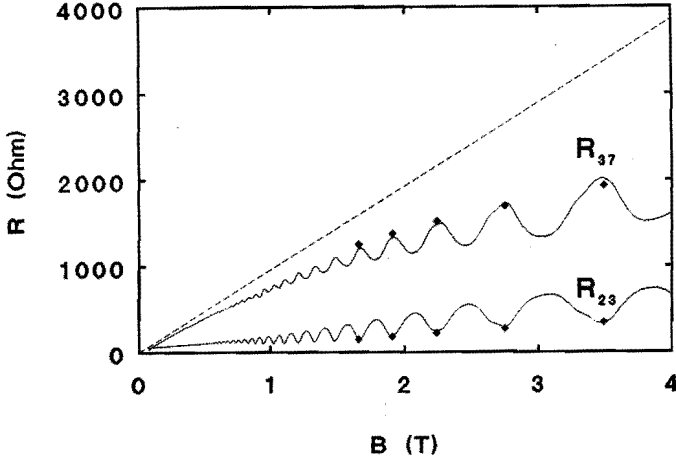
Fig. 3.9:

The measured resistances R_{23} and R_{37} in the case of parallel conduction. The electron density in the 2DEG is $6.48 \cdot 10^{11} \, cm^{-2}$ and the mobility is $\approx 21 \cdot 10^4 \, cm^2/Vs$. The calculated minima in the R_{23} and R_{37} are indicated.

R_{23}. In this sample with parallel conduction we determined the unknown values of $\rho_{xxAlGaAs}$ and $\rho_{xyAlGaAs}$ by a single fit to the measured values of both R_{23} and R_{37} at five different filling factors. As shown in Fig. 3.9 a good agreement between the calculated and measured values is obtained. From the obtained values of $\rho_{xxAlGaAs}$ and $\rho_{xyAlGaAs}$ we determined $n_{AlGaAs} = (12.5 \pm 0.6) \cdot 10^{11} \, cm^{-2}$ and $\mu_{AlGaAs} = (0.37 \pm 0.02) \cdot 10^4 \, m^2/Vs$. This value of the mobility is very reasonable for homogeneously doped $Al_xGa_{1-x}As$. The total sheet electron density $n_{2DEG} + n_{AlGaAs} = 0.19 \cdot 10^{13} \, cm^{-2}$ is far below the sheet doping density of $\approx 1 \cdot 10^{13} \, cm^{-2}$.

Finally in Fig. 3.10 we show the calculated current fractions at the five magnetic field positions used in the fit. The solid lines and dashed lines describe the current fractions in the 2DEG and $Al_xGa_{1-x}As$, respectively. The solid symbols are the longitudinal currents, the open symbols are the currents flowing through the contacts. From this figure we observe that the major part of the current flows through the 2DEG and that this fraction decreases with increasing magnetic field. The current which flows through the contacts is a minor part of the total current in both the $Al_xGa_{1-x}As$ and the 2DEG layer.
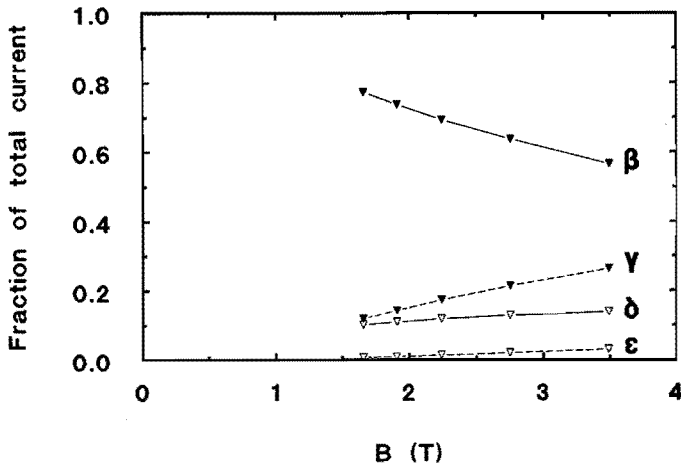
Fig. 3.10:

The calculated current fractions determined from the measurements in Fig. 3.9.

3.4 CONCLUSION

We have shown that parallel conduction in a $GaAs/Al_xGa_{1-x}As$ heterostructure at low temperatures can be described by two isolated conducting layers only connected by the voltage and current probes. From the magneto–resistance measurements of a sample with parallel conduction we were able to determine the electron density and mobility of the $Al_xGa_{1-x}As$ layer.

REFERENCES

1   S.T. Pantiledes, "Deep Centers in Semiconductors", Gordon and Beach
     Science Publishers (1986).

2   B. Lin, thesis University of Princeton, U.S.A (1985).

3   S.J. Battersby, F.M. Selten, J.J. Harris and C.T. Foxon, Solid State
     Elec. **31**, 1083 (1988).

4   S. Luryi, A. Kastalsky, App. Phys. Lett. **45**, 164 (1984).

5   G.L.J.A. Rikken, J.A.M.M. van Haaren, W.P. van der Wel,
     A.P. van Gelder, H. van Kempen, P. Wyder, J.P. André,.K. Ploog, and
     G. Weimann, Phys. Rev. B **37**, 6181 (1988).

6   D.A. Syphers and P.J. Stiles, Phys. Rev. B **32**, 6620 (1985).

CHAPTER 4

IRREVERSIBLE EFFECTS OF BACK–GATING AND WAVELENGTH
DEPENDENT ILLUMINATION ON THE TRANSPORT PROPERTIES
OF THE 2DEG IN GaAs/Al$_x$Ga$_{1-x}$As HETEROSTRUCTURES

4.1 INTRODUCTION

The electron density of the 2DEG in a GaAs/Al$_x$Ga$_{1-x}$As heterostructure can
be changed easily by either illumination or the application of a back–gate voltage.
Illumination of the sample at low temperature creates extra electrons from donor
levels or from transitions from the valence band to the conduction band in such a
way that the electron density is changed in a persistent way. The back–gate
works as a normal capacitor. This means that the electron density increases
linearly with the applied back–gate voltage.

We studied the influence of both ways to change the electron density on the
transport properties of the 2DEG in a GaAs/Al$_x$Ga$_{1-x}$As heterostructure. We
observe that the electron density and mobility are changed irreversibly when we
apply a high positive back–gate voltage. We examined these irreversible effects by
illuminating the sample with wavelengths between 0.7 μm and 1.8 μm. These
experiments show a new Negative Persistent Photo Conductivity (NPPC) effect
at a wavelength of 1.2 μm (1.0 eV). Further experiments in which we changed the
back–gate voltage indicate that the NPPC most likely arises from a trap in the
GaAs region. We present a microscopic picture to explain the physical nature of
this trap.

4.2 EXPERIMENTS

All experiments were performed on selectively doped GaAs/Al$_x$Ga$_{1-x}$As
(x $\approx$ 0.3) heterostructures which were grown by Molecular Beam Epitaxy (MBE)
on 400 μm thick semi–insulating substrates. The samples were Hall–bar shaped.

Electrical contacts to the 2DEG were made by alloying either small Sn balls or Au/Ge/Ni contacts. The samples were mounted with "epotech" in a Al_2O_3 chip–holder (Semi–Dice type HMK). The metalized bottom of this chip–holder served as the back–gate. In order to minimize the leaking resistance of the back–gate, a 20 μm mylar foil was inserted between the back of the sample and the metalized bottom of the chip–holder.

The samples were cooled down to 4.2 K with all contacts including the back–gate short–circuited. In order to illuminate the samples at a selected wavelength we used a halogen light source mounted in front of a monochromator. The monochromatic radiation was transmitted through a multi–fiber light conductor (Zeiss SLP4) from the monochromator to the sample inside the cryostat. The optical fibers were carefully shielded to insure that no infrared radiation could enter the fiber on its way from the monochromator to the cryostat. We were able to vary the wavelength between 1.8 μm and 0.7 μm (0.7 eV and 1.8 eV) and the illumination time between 75 ms and 1200 ms.
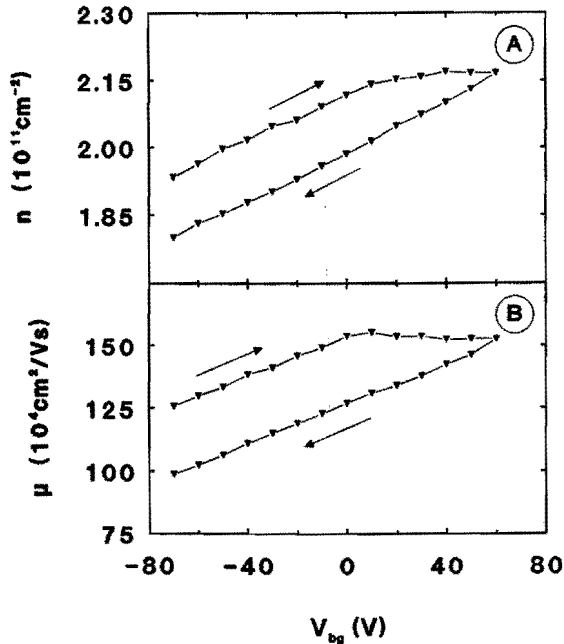
Fig. 4.1:
Electron density (a) and mobility (b) as a function of an increasing and decreasing back–gate voltage.

Fig. 4.1 shows that the electron density and mobility can be changed irreversibly if a high positive back–gate voltage of 60 V is applied. This irreversibility always occurs when the positive back–gate voltage is high enough to display a saturation of the electron density and mobility as a function of the back–gate voltage. For a negative back–gate voltage we do not observe this irreversibility. Note that outside the saturation region the slopes, dn/dV and dμ/dV, are the same for increasing and decreasing the back–gate voltage. These experiments indicate that the back–gate indeed operates as a linear capacitor as long as the electron density does not exceed a certain threshold, but that electrons are lost from the 2DEG permanently if this threshold is exceeded.
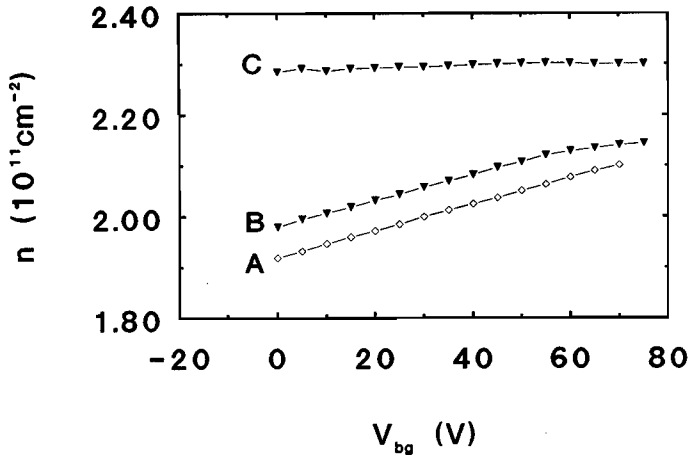
Fig. 4.2:

 The back–gate dependence of the electron density before illumination (curve A) after illumination at an energy of 0.83 eV (curve B) and after illumination at an energy of 1.63 eV (curve C).

To investigate the physical nature of the observed irreversibility we carried out a number of experiments in which we also illuminated the samples. Fig. 4.2 shows the dependence of the electron density on the back–gate voltage before illumination (curve A), after illumination with 0.83 eV radiation (curve B), and after illumination with 1.63 eV radiation (curve C). During illumination the back–gate was short–circuited. After the sample had been illuminated we waited for at least 5 min before we started the measurements. Previous to the illumina-

tion (curve A) we did not observe a saturation of the electron density. After illumination with 0.83 eV radiation (curve B) the electron density starts to saturate at a back–gate voltage of 60 V and the same irreversibility effects as discussed before are observed. After illumination with 1.63 eV radiation (curve C) the electron density appears to be independent on the back–gate voltage in the range investigated. From these experiments we suggest that the saturation of the electron density and thus the number of electrons lost from the 2DEG is sensitive to illumination of the sample. Note that Fig. 4.1 and Fig. 4.2 were taken in different runs and therefore the electron densities at zero back–gate voltage are slightly different.
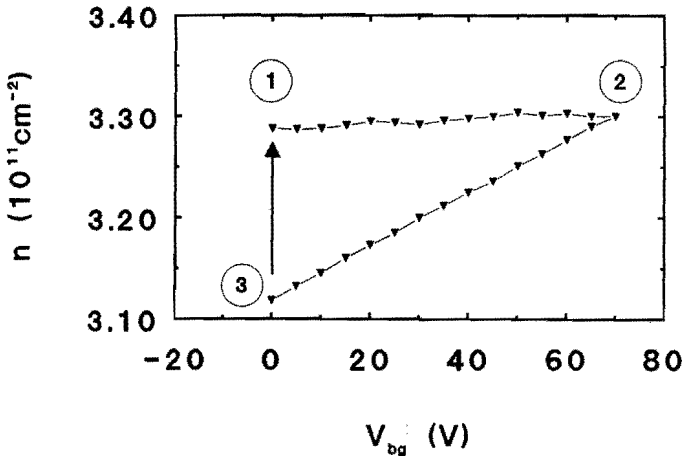
Fig. 4.3:

    The back–gate dependence of the electron density after the electron density did not change anymore with illumination at 1.63 eV. In sequence (1)–(2)–(3) the back–gate voltage is increased to 70 V and decreased to 0 V again. In sequence (3)–(1) the electron density is restored with illumination at 1.63 eV to the same value as before the back–gate voltage was applied.

We then further illuminated the sample with 1.63 eV radiation until the electron density did not change anymore. In Fig. 4.3 we present an example of a complete cycle of measurements. We measured in dark and started at zero gate voltage (1), increased the back–gate voltage to 70 V (2) and then decreased the voltage to zero again. Subsequently we turned on the illumination again until the

electron density did not change anymore bringing us back to (1). Again we observe the irreversibility effects as a function of gate voltage (during sequence (1)–(2)–(3)) but obviously the lost electrons are brought back to the 2DEG again by illumination (during sequence (3)–(1)).

Finally Fig. 4.4 shows the electron density as a function of the illumination energy after the electron density had been saturated by illumination at 1.8 eV. Surprisingly we find a dip in the electron density for radiation at 1.0 eV reminiscent to the profile of a resonance line. The dip is not sensitive to the sequence in which the data points are obtained, in particular it does not matter whether the long wavelength or short wavelength is applied first. The observation of this dip means that the electron density is decreased persistently if the sample is illuminated with the "right" wavelength. To our knowledge this is the first time that such a NPPC effect has been observed.
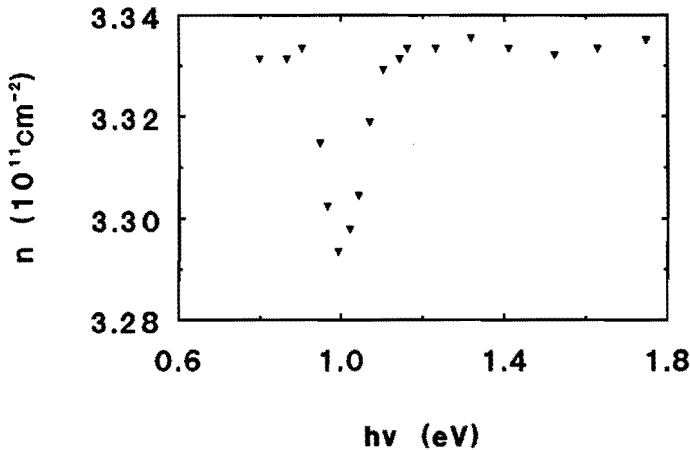
Fig. 4.4:
> The electron density as a function of the illumination energy after the electron density was saturated by illuminating at 1.8 eV.

4.3 SELFCONSISTENT CALCULATION OF THE ENVELOPE
WAVEFUNCTION AND ENERGY OF THE LOWEST SUBBAND
IN A GaAs/Al$_x$Ga$_{1-x}$As HETEROSTRUCTURE

In order to explain the effects observed we have to look at the electrostatic potential and electron distribution in the sample in detail. We start with the wellknown selfconsistent calculation of the envelope wavefunction and energy of the lowest subband and the electrostatic potential near the GaAs/Al$_x$Ga$_{1-x}$As interface. The energy and envelope wavefunction are calculated from the Schrödinger and Poisson equation. These equations are coupled through the electrostatic potential, $U_c(z)$, and the charge distribution of the electrons in the lowest subband, $n(z) = n_0\, \varphi_0^*(z)\varphi_0(z)$, see chapter 1.3. The coupled Schrödinger and Poisson equation were reduced to a set of First Order Coupled Differential Equations (FOCDE) and six boundary conditions. This set of FOCDE was solved numerically[1] with an algorithm using a multiple shooting method[2].

The following set of FOCDE has to be solved

$$\partial\, \varphi_0(z)/\partial z = \varphi_0'(z) \qquad\qquad [4.1]$$

$$\partial\, \varphi_0'(z)/\partial z =$$

$$\frac{2m^*}{\hbar^2}\left\{ U_c(z) + \Delta U_0 \cdot \theta(z) + U_{ex}(z) - E_0(z) \right\} \varphi_0(z) \qquad\qquad [4.2]$$

$$\partial\, E_0(z)/\partial z = 0 \qquad\qquad [4.3]$$

$$\partial\, N(z)/\partial z = \varphi_0^*(z)\varphi_0(z) \qquad\qquad [4.4]$$

$$\partial\, U_c(z)/\partial z = U_c'(z) \qquad\qquad [4.5]$$

$$\partial\, U_c'(z)/\partial z =$$

$$-\frac{e^2}{\epsilon_0\epsilon_r}\left\{ n_A(z) + (n_{2DEG} + n_{bg}) \cdot \varphi_0^*(z)\varphi_0(z) \right\} \qquad\qquad [4.6]$$

The equations [4.1] and [4.2] describe the Schrödinger equation and [4.5] and [4.6] describe the Poisson equation. The normalization of the envelope wavefunction is calculated from $N(z) = \int \varphi_0^*(z)\varphi_0(z)\,dz$. Since the energy of the lowest subband, $E_0(z)$, must be determined selfconsistently it is needed that the energy of the lowest subband is included in this set of FOCDE.

In order to include the influence of a back–gate voltage in the calculations we have to take into account two effects:

1) the back–gate operates as a capacitor with the back–gate and the 2DEG acting as two parallel flat electrodes. Thus the electron density increases as

$$n_{bg} = \frac{C_{bg} \cdot V_{bg}}{e} = \frac{\epsilon_0 \epsilon_r}{e} \cdot \frac{V_{bg}}{d_{bg}} \qquad [4.7]$$

where C_{bg} is the capacitance and d_{bg} is the distance between the 2DEG and the back–gate electrode.

2) the electric field between the 2DEG and the back of the sample increases with

$$E_{bg} = \frac{V_{bg}}{d_{bg}} = \frac{e}{\epsilon_0 \epsilon_r} \cdot n_{bg} \qquad [4.8]$$

The third term in [4.2] describes the exchange and correlation effects. There are various models to include these effects[3-5]. Here we used the potential proposed by Gunnarson and Lundqvist[5]

$$U_{ex} = -\frac{2m^*Ry}{m_e \epsilon_0 \epsilon_r{}^2 \pi \alpha r_s} \left[1 + 0.0545\, r_s \ln(1 + 11.4/r_s) \right] \qquad [4.9]$$

where

$$1/r_s = \sqrt[3]{4\pi n(z)/3}\; r_0\, \epsilon_r\, m_e/m^*$$

$$r_0 = 5.29177 \cdot 10^{11}\,\text{m} \quad \text{and} \quad \alpha = \sqrt[3]{4/9\pi}$$

This set FOCDE was solved in the interval $[A,B] = [-100 \text{ Å}, 500 \text{ Å}]$ where $z = 0$ is coincident with the $GaAs/Al_xGa_{1-x}As$ interface. We only calculated the solution in this interval because at 500 Å away from the interface the amplitude of the envelope wavefunction is almost zero, see Fig. 4.5. The remaining part of the electrostatic potential is easily calculated analytically. The selfconsistent solution was calculated with the following boundary conditions

$$\varphi_0(A) = 0 \qquad\qquad\qquad [4.10]$$

$$\varphi_0'(B) = 0 \qquad\qquad\qquad [4.11]$$

$$N(A) = 0 \qquad\qquad\qquad [4.12]$$

$$N(B) = 1 \qquad\qquad\qquad [4.13]$$

$$U_c(A) = 0 \qquad\qquad\qquad [4.14]$$

$$U_c'(B) = \frac{e}{\epsilon_0 \epsilon_r} \left\{ n_{depl} - n_{bg} \right\} \qquad\qquad\qquad [4.15]$$

The computer program started an iteration procedure with the Fang–Howard envelope wavefunction[6] as the initial solution.

We calculated the selfconsistent envelope wavefunction of the lowest sub-band and the electrostatic potential for a $GaAs/Al_xGa_{1-x}As$ heterostructure with an electron density of $3.0 \cdot 10^{11} \text{ cm}^{-2}$ at $V_{bg} = 0$ and a depletion charge of $0.2 \cdot 10^{11} \text{ cm}^{-2}$ for several positive back–gate voltages up to 150 V ($d_{bg} = 400 \ \mu m$). Fig. 4.5 shows the envelope wavefunction of the lowest subband and the electrostatic potential for $V_{bg} = 0$ V, 60 V and 120 V. The electrostatic potential at a distance of several hundred Å from the interface appears to be a strong function of the back–gate voltage. This figure clearly shows that the electrostatic potential is nearly flat for $z > 200$ Å if $V_{bg} = 120$ V. We think this to be an important issue for the experiments described in this chapter.
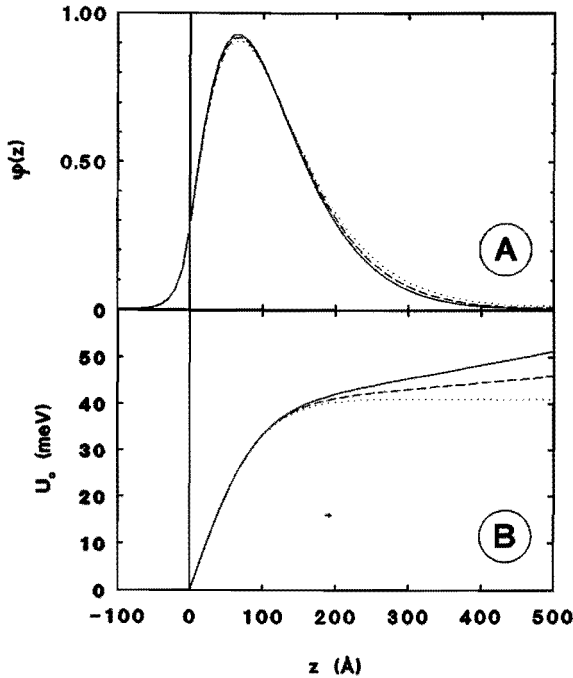
Fig. 4.5:

Calculated envelope wavefunction (a) and electrostatic potential (b) for $V_{bg} = 0$ V, 60 V, and 120 V. The electron density at $V_{bg} = 0$ is $3.0 \cdot 10^{11}$ cm^{-2}, the depletion charge is $2 \cdot 10^{10}$ cm^{-2} and $d_{bg} = 400$ μm.

4.4 DISCUSSION

In Fig. 4.1 we observed that the electron density saturates and shows some irreversible behaviour as a function of the back–gate voltage. The calculations indicate that the electrostatic potential in the GaAs is flat far away from the GaAs/Al$_x$Ga$_{1-x}$As interface for a certain positive back–gate voltage. In case that the back–gate voltage is increased further the gradient in the electrostatic potential far away from the interface becomes even negative. In this case electrons are pulled out of the confining well and flow towards the GaAs substrate. We believe that this flow of electrons from the 2DEG towards the GaAs substrate is responsible for the observed saturation of the electron density. In order to explain the observed irreversibility we propose that the electrons are trapped somewhere in the GaAs substrate. The electrons must be trapped far away from the 2DEG

because the mobility remains constant when electrons are trapped. If we assume that the flow of electrons starts for an electric field on the back–gate side, [4.15], such that $n_{depl} \approx n_{bg} = C_{bg} \cdot V_{bg}$, we can estimate the corresponding back–gate voltage. For example for a sample with $d_{bg} = 400 \, \mu m$ and a depletion charge of $2 \cdot 10^{10} \, cm^{-2}$ this back–gate voltage is ≈ 100 V. This value is close to the experimentally observed value from curve A in Fig. 3.2. In this model a negative back–gate voltage does not lead to a saturation of the electron density, as observed in our experiments.

Within this model we can also explain the measurements presented in Fig. 4.2. When we illuminate the sample (see curve B and C) the electron density in the 2DEG increases due to the Persistent Photo Conductivity (PPC) effect[7] of the Si–donors in the $Al_xGa_{1-x}As$ layer. Thus the Fermi level rises. This means that electrons are able to flow to the GaAs substrate already at a lower back–gate voltage and thus give rise to a saturation of the electron density at this lower back–gate voltage. This situation occurs at all illumination wavelengths we studied. Besides the PPC effect of the Si–donors, which is observed at all illumination wavelengths, a second mechanism occurs when the illumination energy exceeds the bandgap of GaAs. In this case electron–hole pairs are created in the GaAs layer. While the holes flow towards the GaAs substrate the electrons flow towards the 2DEG. This mechanism is due to the built–in electric field and it occurs until flat band conditions are reached in the GaAs layer (see curve C).

Also the measurements shown in Fig. 4.3 can be explained with this model. The electrons which have been pulled out of the 2DEG and have been trapped in the GaAs substrate can be transferred back to the 2DEG if they are detrapped by illumination. This model is clearly consistent with our observations at all the illumination energies studied, i.e. from 0.7 eV to 1.8 eV. We conclude that the energies involved in a possible detrapping mechanism are smaller than 0.7 eV.

In Fig. 4.4 we showed the electron density as a function of illumination energy. In order to explain the observed dip at 1.0 eV we propose the following model that somewhere in the sample there is a trap which is resonantly populated at 1.0 eV. There is indeed evidence that such a trap is present. Puencher et al.[8] have reported the observation of a level at 1.0 eV above the valence band which is due to a Ga–vacancy formed at low concentrations in MBE–grown GaAs. By illuminating the sample it then happens that the electron density of the 2DEG decreases if the holes, created by the illumination, recombine with electrons from

the 2DEG. Depopulation of this level originating from the Ga–vacancy is possible at illumination energies larger than 0.5 eV (The bandgap of GaAs at 4.2 K is 1.5 eV). This explanation implies that a depletion charge is formed in the GaAs layer.

We have shown that the depletion charge in the GaAs determines the saturation value of the electron density when a positive back–gate voltage is applied, see [4.15]. Fig. 4.6 shows the dependence of the electron density on the back–gate voltage after successive illumination at 1.57 eV, 1.04 eV and 0.85 eV. We conclude that, according to our model, the conduction band in the GaAs layer is flat after illumination at 1.57 eV and 0.85 eV since we observe a constant electron density for $V_{bg} > 0$. After illumination at 1.04 eV, however, we do not achieve flat band conditions, since we are able to increase the electron density for $V_{bg} > 0$. The maximum change of the electron density obtained as a function of the back– gate voltage is equal to the depletion charge in the GaAs layer. This is consistent with the idea that all electrons trapped after illumination at 1.04 eV are transferred from the 2DEG to the GaAs layer.
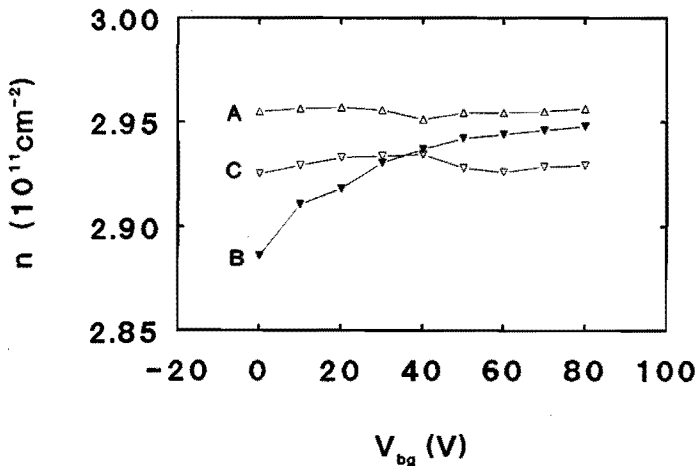
Fig. 4.6:

    Back–gate dependence of the electron density after illumination at 1.57 eV, 1.04 eV and 0.84 eV after the electron density was saturated by illumination at 1.8 eV.

4.5 CONCLUSIONS

We measured the back–gate dependence of the electron density in $GaAs/Al_xGa_{1-x}As$ heterostructures as a function of the back–gate voltage. We observed that the electron density and mobility saturate at a certain positive back–gate voltage. We further observed that the electron density as a function of the back–gate voltage can display irreversible effects. The saturation is most likely due to the fact that the electrons induced by the back–gate flow to the GaAs substrate. We also presented a model which explains the irreversibility effects by means of trapping of electrons in the GaAs. We found a new NPPC effect which most likely is due to a resonant level associated with a Ga–vacancy level in the GaAs.

REFERENCES

1   The computer program was kindly provided by R.M.M. Mattheij.

2   U.M. Asher, R.M.M. Mattheij, and R.D. Russel, "Numerical solutions of boundary value problems for ordinary differential equations", Englewood Cliffs, Prentice–Hall (1988).

3   W. Kohn and L.J. Sham, Phys. Rev. __140__, A1133 (1965)

4   L. Hedin and B.I. Lundqvist, J. Phys. C __4__, 2064 (1971)

5   O. Gunnarson and B.I. Lundqvist, Phys. Rev. B __13__

6   F. Fang and W.E. Howard, Phys. Rev. Lett. __16__, 797 (1966)

7   M.I. Nathan, Solid State Elec. __29__, 167 (1986)

8   R.A. Puecher, D.A. Johnson, and G.N. Maracas, App. Phys. Lett. __53__, 1952 (1988)

CHAPTER 5

ASYMMETRY OF THE AMPLITUDE OF THE SHUBNIKOV–DE HAAS OSCILLATIONS IN A TWO–DIMENSIONAL ELECTRON GAS

5.1 INTRODUCTION

From measurements of the Shubnikov–de Haas (SdH) and the Quantum Hall effect in GaAs/Al$_x$Ga$_{1-x}$As heterojunctions it is well known that the magneto-resistivity ρ_{xx} and Hall resistivity ρ_{xy} can be non–ohmic and apparently dependent on the spin–state of the electrons in the two–dimensional electron gas (2DEG). Recently, Haug et al.[1] showed that the asymmetry in the line shape of ρ_{xx} and the width of the quantized Hall plateaus can be modified by applying a back–gate voltage. The authors explained the asymmetry in terms of a changing interaction with positive and negative scatterers. Regarding their experiments, however, the question arises, whether electron–impurity interaction is the only mechanism which leads to the observed asymmetry. Also it is not clear, whether the observed asymmetry is also affected by the change of the electron density induced by the back–gate voltage.

In this chapter measurements on samples with different mobilities are reported. The electron density was changed either by applying a back–gate voltage or by the use of the Persistent–Photo–Conductivity effect (PPC). In this way the electron concentration in a sample was increased to the same value either by back–gating or illumination. These tools were used to study the influence of the electron–impurity interaction on the asymmetry of the SdH–oscillations.

5.2 EXPERIMENTS

The experiments were carried out in the temperature range from 1.2 K to 4.2 K with magnetic fields up to 6 T. The MBE–grown GaAs/Al$_x$Ga$_{1-x}$As hetero-structures were Hall–bar shaped and provided with a back–gate as discussed in
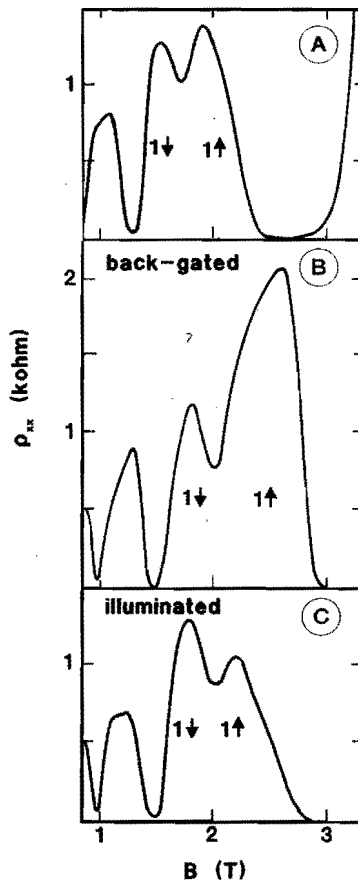
Fig. 5.1:

The magneto–resistivity of sample A at 1.5 K measured with a current of 0.1 μA:

a) without a back–gate voltage or illumination,

b) with a back–gate voltage of +20 V and without illumination,

c) without a back–gate voltage after illumination with a LED during 9.2 μs.

chapter 4. The samples were cooled down to 4.2 K with all electrical contacts and the back–gate short–circuited. The sample specifications are given in Table 5.1. In order to illuminate the samples a LED ($\lambda = 650$ nm) was mounted inside the cryostat. The electron density increases both through ionization of DX–centers in the $Al_xGa_{1-x}As$ layer and the creation of electron–hole pairs in the GaAs–region[2].

	spacer $\mathring{A}$	n 10^{11} cm^{-2}	μ cm^2/Vs
A	360	1.2	$36 \cdot 10^4$
B	400	2.0	$160 \cdot 10^4$

Table 5.1:

Spacer and transport properties of sample A and B at 4.2 K.

Fig. 5.1 presents measurements of ρ_{xx} on sample A under various back–gating and illumination conditions. The initial electron density and mobility at 1.5 K are $1.22 \cdot 10^{11}$ cm^{-2} and $36 \cdot 10^4$ cm^2/Vs. For a back–gate voltage of $+20$ V these become $1.38 \cdot 10^{11}$ cm^{-2} and $41 \cdot 10^4$ cm^2/Vs, respectively; after illumination during 9.2 μs these become $1.41 \cdot 10^{11}$ cm^{-2} and $40 \cdot 10^4$ cm^2/Vs. The sample was illuminated with short pulses until the electron density was nearly the same as for the back–gate voltage of $+20$ V.

Measurements on sample B are shown in Fig. 5.2. Here the initial electron density and mobility at 1.2 K are $2.00 \cdot 10^{11}$ cm^{-2} and $161 \cdot 10^4$ cm^2/Vs. For a back–gate voltage of $+30$ V these become $2.09 \cdot 10^{11}$ cm^{-2} and $175 \cdot 10^4$ cm^2/Vs, respectively; after illumination during 11.1 μs these become $2.09 \cdot 10^{11}$ cm^{-2} and $161 \cdot 10^4$ cm^2/Vs.

The most striking difference between the cases b) and c) for both samples is the height of the spin–up peak. This predominantly observable for the N = 1 peaks. For both samples the N = 1 spin–up peak increases with the back–gate voltage as has been observed by Haug *et al.*. Comparing the results after illumination, we observe that in sample A the N = 1 spin–up peak decreases whereas in sample B the N = 1 spin–up peak does not change significantly. Fig. 5.3 shows ρ_{xx} in sample B before and after a long illumination time. This figure clearly shows that after a longer illumination time the spin–up peak increases with illumination.

5.3 DISCUSSION

Below 4.2 K electron scattering is mainly due to ionized impurity scattering on ionized donors in the $Al_xGa_{1-x}As$ layer and charged background impurities in the GaAs layer (normally C–acceptors); see chapter 1.4. The scattering on acoustic phonons is also of some importance at temperatures below 4.2 K. The relative importance of these scattering mechanisms in sample A and B was determined from the temperature dependence of the mobility between 4.2 K and 1.2 K.
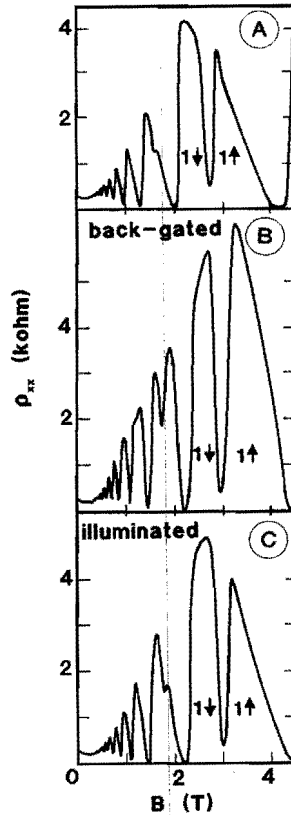
Fig. 5.2:

The magneto–resistivity of sample B at 1.2 K measured with a current of 0.2 μA:

a) without a back–gate voltage or illumination,

b) with a back–gate voltage of +30 V and without illumination,

c) without a back–gate voltage after illumination with a LED during 11.1 μs.

In Figs. 5.4 and 5.5 the temperature dependence of the mobility between 1.2 K and 4.2 K is shown for sample A and B, respectively. Note that the data of sample B were obtained after illumination of the sample. In the calculations[3] we did not account for alloy or surface roughness scattering. The concentration of the background impurities was the only adjustable parameter in the calculations. As is shown in Figs. 5.4 and 5.5 a good agreement between the measured and calculated mobility could be obtained when the concentration of background impurities in sample A and B is assumed to be $10 \cdot 10^{14}$ cm^{-3} and $3.3 \cdot 10^{14}$ cm^{-3}, respectively. This result proves that in both samples ionized impurity scattering on charged donors and background impurities is the main scattering mechanism
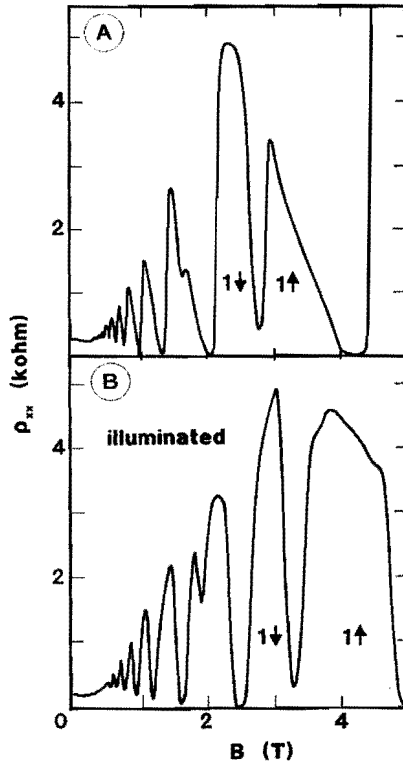
Fig. 5.3:

The magneto–resistivity of sample B at 1.2 K measured with a current of 0.2 μA:

a) before illumination,

b) after a long illumination.
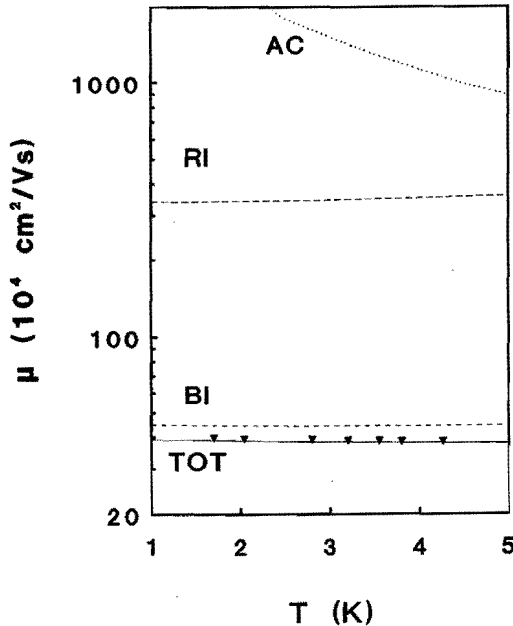
Fig. 5.4:

The temperature dependence of the mobility in sample A. The lines indicate the calculated mobility due to remote ionized (RI) impurity scattering, background ionized (BI) impurity scattering, and acoustic (AC) phonon scattering.

below 2.0 K. In sample B before illumination, we obtained with almost the same concentration of background impurities good agreement between the measured and the calculated mobility. This indicates that, although most acceptors in the GaAs are neutralized by the illumination (see chapter 4 and ref. 2) the scattering on the background impurities nearly remains constant. This is not surprising, since only the acceptors far away from the 2DEG are neutralized. Remember that the depletion layer is several microns thick.

The influence of the various scattering mechanisms on the electrical transport properties was studied in further detail. The mobility at 4.2 K as a function of the electron density in sample A and B is shown in Fig. 5.6 and Fig. 5.7, respectively. The electron density was increased either by the application of a back—gate voltage or by illumination of the sample. The variation of the illumination data of sample B is partly due to the fact that the data were obtained in several
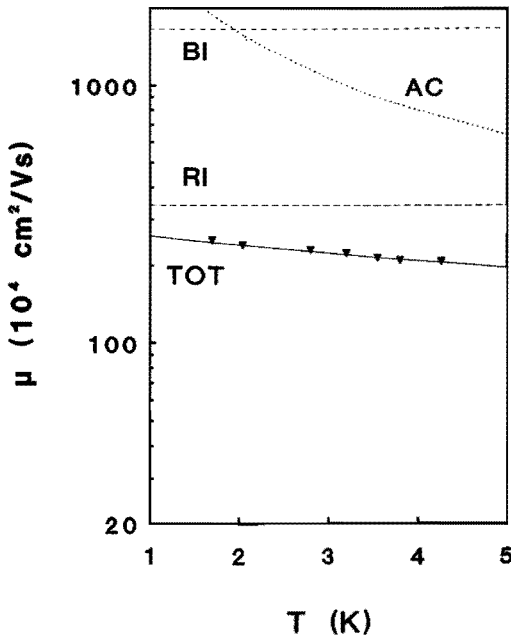
Fig. 5.5:

The temperature dependence of the mobility in sample B. The lines indicate the calculated mobility due to remote ionized (RI) impurity scattering, background ionized (BI) impurity scattering, and acoustic (AC) phonon scattering.

runs. In Sample A the mobility shows nearly the same dependence on the electron density for both illumination and the application of a back–gate voltage. But the data of sample B, presented in Fig. 5.7, clearly show a stronger dependence of the mobility on the electron density in the case that the electron density is increased by the application of a back–gate voltage.

By applying a back–gate voltage or illumination both the electron density and the envelope wavefunction of the 2DEG change. By performing selfconsistent calculations, as described in the previous chapter, we investigated the effects of illumination and the application of a back–gate voltage on the envelope wavefunction of the electrons in the lowest subband of a $GaAs/Al_xGa_{1-x}As$ heterostructure. In the calculations we assumed that in the case of illumination only DX–centers in the $Al_xGa_{1-x}As$ layer are ionized and thus no electron–hole pairs are generated in the GaAs layer. Fig. 5.8 shows the averaged distance of the
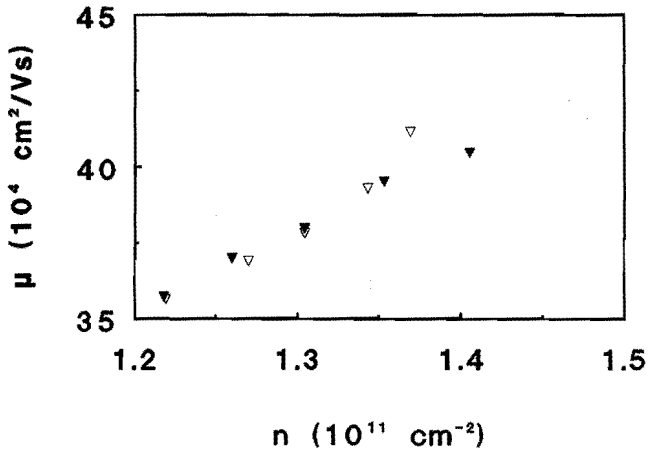
Fig. 5.6:

Dependence of the mobility on the electron density in sample A. The electron density is increased either by illumination (solid symbols) or by the application of a back–gate voltage (open symbols).
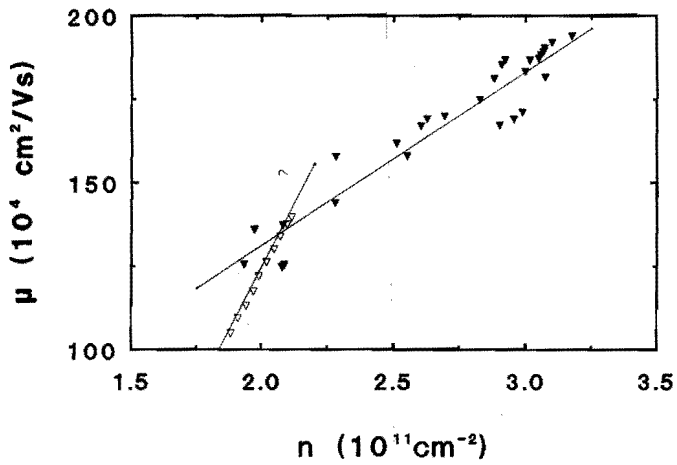
Fig. 5.7:

Dependence of the mobility on the electron density in sample B. The electron density is increased either by illumination (solid symbols) or by the application of a back–gate voltage (open symbols).

envelope wavefunction from the GaAs/Al$_x$Ga$_{1-x}$As interface, $<z>$, and the width of the envelope wavefunction, var(z) $= \sqrt{<(z-<z>)^2>}$, as a function of the electron density. The average distance of the envelope wavefunction from the GaAs/Al$_x$Ga$_{1-x}$As interface increases with a positive back–gate voltage whereas it decreases after illumination. Thus by comparing two measurements at the same electron density, achieved either by the application of a back–gate voltage or by illumination, it turns out that the envelope wavefunction is closer to the GaAs/Al$_x$Ga$_{1-x}$As interface in the latter case.

If scattering on the GaAs/Al$_x$Ga$_{1-x}$As interface, i.e. surface roughness or alloy scattering, was important, we would expect that in both samples the mobility would increase strongest as a function of the electron density, when the electron density is increased by application of a positive back–gate voltage.
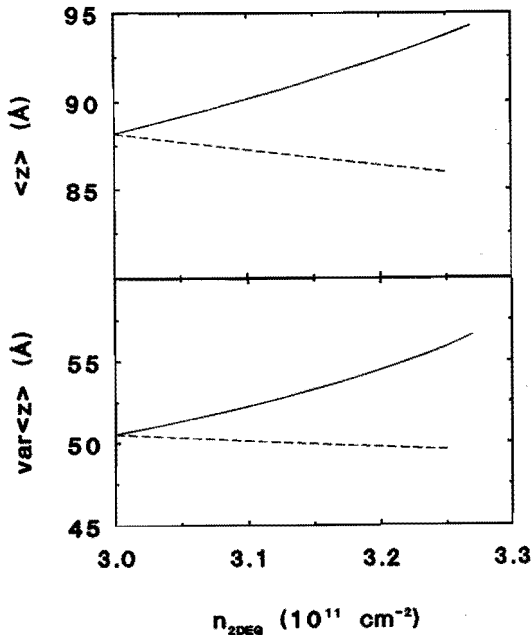
Fig. 5.8:

The calculated averaged distance, $<z>$, from the GaAs/Al$_x$Ga$_{1-x}$As interface and the width, var(z), of the envelope wavefunction in a GaAs/Al$_x$Ga$_{1-x}$As heterostructure as a function of the electron density. The electron density was increased either by illumination (dashed line) or the application of a positive back–gate voltage (solid line).

The experiments on sample A which has a low mobility and therefore might suffer from surface roughness scattering ,however , tell us that this is not the case. We therefore believe that the dependence of the mobility on the electron density is mainly determined by the interaction with the ionized donors in the $Al_xGa_{1-x}As$ layer and the charged acceptors in the GaAs layer.

When the electron density is increased by the application of a positive back-gate voltage, the envelope wavefunction shifts away from the interface thus leading to a smaller interaction with the positively charged donors in the $Al_xGa_{1-x}As$ layer. After illumination the envelope wavefunction is shifted towards the GaAs/$Al_xGa_{1-x}As$ interface and photo–ionization of the DX–centers, i.e. the Si–donors in the $Al_xGa_{1-x}As$ layer, results in more positively charged scattering centers in the $Al_xGa_{1-x}As$ region. Both these effects, the shift of the envelope wavefunction and the increased number of ionized donors, lead to a stronger interaction with the positively charged scatterers in the case of illumination compared to the case of the application of a back–gate voltage. Thus, we expect that the mobility increases strongest when the electron density is increased by a positive back–gate voltage. In this argumentation we assume that the interaction with the charged acceptors is nearly constant. The results obtained in sample B, see Fig. 5.6, where we know from the fit of calculated mobility on the temperature dependence of the measured mobility that the scattering on the charged acceptors is nearly constant as a function of the illumination time, agree well with this picture.

In sample A, see Fig. 5.6 we observed the same dependence of the mobility on the electron density for the cases of illumination and back–gating. As can be seen from Figs. 5.4 and 5.5 the relative importance of the background impurity scattering is much more important in sample A as in sample B. Thus the influence of the neutralization of the charged acceptors, due to creation of electron–hole pairs by illumination, on the mobility is more important in sample A as in sample B. Since we observed the same dependence of the mobility on the electron density in the cases of illumination and back–gating, we conclude that in sample A the reduction of the mobility due to the stronger interaction with ionized donors after illumination is regained due to the reduced number of charged acceptors.
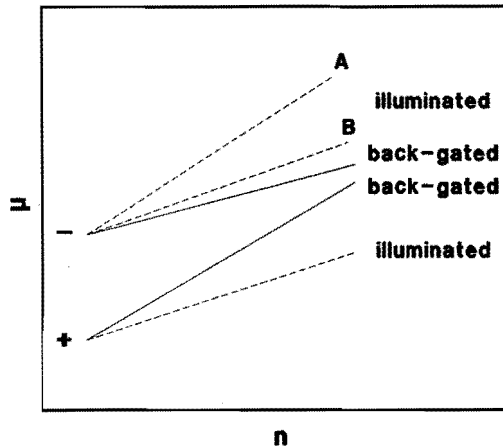
Fig. 5.9:

   Schematic diagram showing the electron mobility as a function of the electron density. The electron density dependence in the case of illumination and the application of a positive back–gate voltage are shown by the dashed and solid line, respectively.

   Now we turn to the magneto–resistivity measurements. In order to explain the observations we use Fig. 5.9. The figure shows qualitatively the behaviour of the remote and background mobility with increasing positive back–gate voltage and illumination. As discussed before the remote and background impurity scattering are due to the positively charged donors in $Al_xGa_{1-x}As$ layer (indicated by +) and the negatively charged background impurities in the GaAs–region (indicated by −), respectively. In all cases the mobility increases due to a stronger screening of the electrons at higher densities and due to a larger k–vector of the electrons at the Fermi energy[4]. With an increasing positive back–gate voltage (indicated by the solid lines) the relative contribution of the positively charged donors to the total mobility becomes less important due to the shift of the envelope wavefunction. At a positive back–gate voltage, case b) of Figs. 5.1 and 5.2, we observed in both samples that the spin–up peak increased. This is consistent with the observations of Haug *et al.* who proposed that the spin–up peak increases for a decreasing interaction with the positive scatterers. The question ,however , remains whether the observed asymmetry is also affected by the change of the electron density.

After illumination the envelope wavefunction shifts towards the interface, the number of ionized impurities changes and the electron density increases. Thus by comparing measurements at the same electron density obtained either by illumination or by the application of a back–gate voltage we can exclude electron density effects. Comparison of b) and c) in Figs. 5.1 and 5.2 shows that the height of the $N = 1$ spin–up peak of ρ_{xx} is decreased. The $N = 1$ spin–down peak remains almost unchanged. As discussed above the interaction with the positively charged donors, at the same electron density, is strongest after illumination (case c). We conclude that indeed a stronger interaction with the positively charged donors leads to a reduction of the value of the spin–up peak.

In Fig. 5.9 the change of background and remote mobility due illumination is shown (indicated by the dashed lines). The mobility due to scattering on the positively charged donors does not increase as strong as in the case of back–gating due to the shift of the envelope wavefunction and the increased number of ionized donors. The change of the background mobility in sample A and B is dependent on the reduction of the number of negatively charged acceptors. Thus after illumination the relative interaction with the positive scatterers can increase or decrease depending on the reduction of the negatively charged acceptors. In sample A the number of negatively charged acceptors reduces stronger than in sample B. This results in a stronger increase of the relative importance of the positively charged donors on the total mobility in sample A. This is consistent with the observation that in sample A spin–up peak decreases after illumination whereas in sample B the height of the spin–up peak is constant, see case c) of Figs. 5.1 and 5.2.

From various experiments it is well known that the number of negatively charged acceptors in the GaAs layer does not change after a certain illumination dose whereas it is still possible to increase the electron density by the ionization of DX–centers. For instance, Ensslin et al.[5] and Dobers et al.[6] observed that only the first illumination dose significantly changes the number charged acceptors. This is also in nice agreement with our experiments described in chapter 4. There we observed, from the back–gate dependence, that the acceptors are neutralized after a short illumination time whereas we were still able to increase the electron density by ionization of the DX–centers. In sample A as well as in sample B we observed that the spin–up peak increased after a longer illumination time, see Fig. 5.3. Since we know that the change of the spin–up after illumination is

dependent on the neutralization rate of the charged acceptors, we suppose that the growth of the spin–up peak after a long illumination time is due to the fact that the neutralization of the charged acceptors ceases after a certain illumination time.

5.4 CONCLUSIONS

We conclude that the asymmetry of the Shubnikov–de Haas oscillations is dependent on the relative interaction with negatively charged acceptors in the GaAs region and positively charged donors in the $Al_xGa_{1-x}As$ region.

REFERENCES

1   R.J. Haug, K. von Klitzing and K. Ploog, Phys. Rev. B <u>35</u>, 5933 (1987).

2   J.J. Harris, D.E. Lacklison, C.T. Foxon, F.M. Selten, A.M. Suckling, R.J. Nicholas and K.W.J. Barnham, Semicond. Sci. Technol. <u>2</u>, 783 (1987).

3   P.J. van Hall, private communications and P.J. van Hall, T. Klaver, and J.H. Wolter, Semicond. Sci. Technol. <u>3</u>, 120 (1988).

4   W. Walukiewicz, H.E. Ruda, J. Lagowski and H.C. Gatos, Phys. Rev. B <u>30</u>, 4571 (1984).

5   K. Ensslin, D. Heitmann, and K. Ploog, "The Application of High Magnetic Fields in Semiconductor Physics II", Würzburg, p. 289, ed. by G. Landwehr (Springer Verlag, 1989).

6   M. Dobers, F. Malcher, G. Lommer, K. von Klitzing, U. Rössler, K. Ploog, and G. Weimann, "The Application of High Magnetic Fields in Semiconductor Physics II", Würzburg, p.386, ed. by G. Landwehr (Springer Verlag, 1989).

CHAPTER 6

INFLUENCE OF ELECTRON–IMPURITY INTERACTION ON ρ_{xx} AND ρ_{xy}
IN THE INTEGER AND FRACTIONAL QUANTUM HALL REGIME

6.1 INTRODUCTION

In order to study the influence of the electron–impurity scattering on the integer and the fractional Quantum Hall Effect (QHE) in a GaAs/Al$_x$Ga$_{1-x}$As heterostructure we extended the measurements described in the previous chapter to lower temperatures and higher magnetic fields. Until now the influence of electron–impurity interaction on the integer and fractional QHE has only been studied by comparing measurements performed on different samples and different electron densities[1,2]. We, for the first time, compared measurements performed on the same sample and at the same electron density[3]. The results clearly show a different influence of the electron–impurity interaction on the integer and fractional QHE. In this chapter we also give a tentative explanation for the observed influence of the electron impurity interaction on ρ_{xx} and ρ_{xy}.

7.2 EXPERIMENTS

We used GaAs/Al$_x$Ga$_{1-x}$As heterostructures grown by Molecular Beam Epitaxy. The samples had a spacer layer thickness of ≈ 400 Å, since high mobilities can be achieved at this spacer thickness, see Fig. 1.9. The magneto-resistivity, ρ_{xx}, and Hall resistivity, ρ_{xy}, were measured on standard Hall–bar shaped samples. The samples were provided with a back–gate as discussed in chapter 4. The measurements were carried out at 200 mK in a He$_3$/He$_4$ dilution refrigerator in a 20 T Bitter magnet. A LED ($\lambda = 650$ nm) mounted inside the dilution refrigerator was used to illuminate the sample. Due to the Persistent Photo Conductivity of Si–doped Al$_x$Ga$_{1-x}$As the effect of the illumination is permanent.

Firstly, we increased the electron density in the 2DEG by applying a positive back–gate voltage and measured ρ_{xx} and ρ_{xy}. Then the back–gate was short–circuited and the electron density was increased by illuminating the sample pulse by pulse until the same electron density was reached as in the back–gated situation. The results obtained at 230 mK after illumination and back–gating are shown in Fig. 6.1. The initial electron density and mobility are $1.27 \cdot 10^{11}$ cm^{-2} and
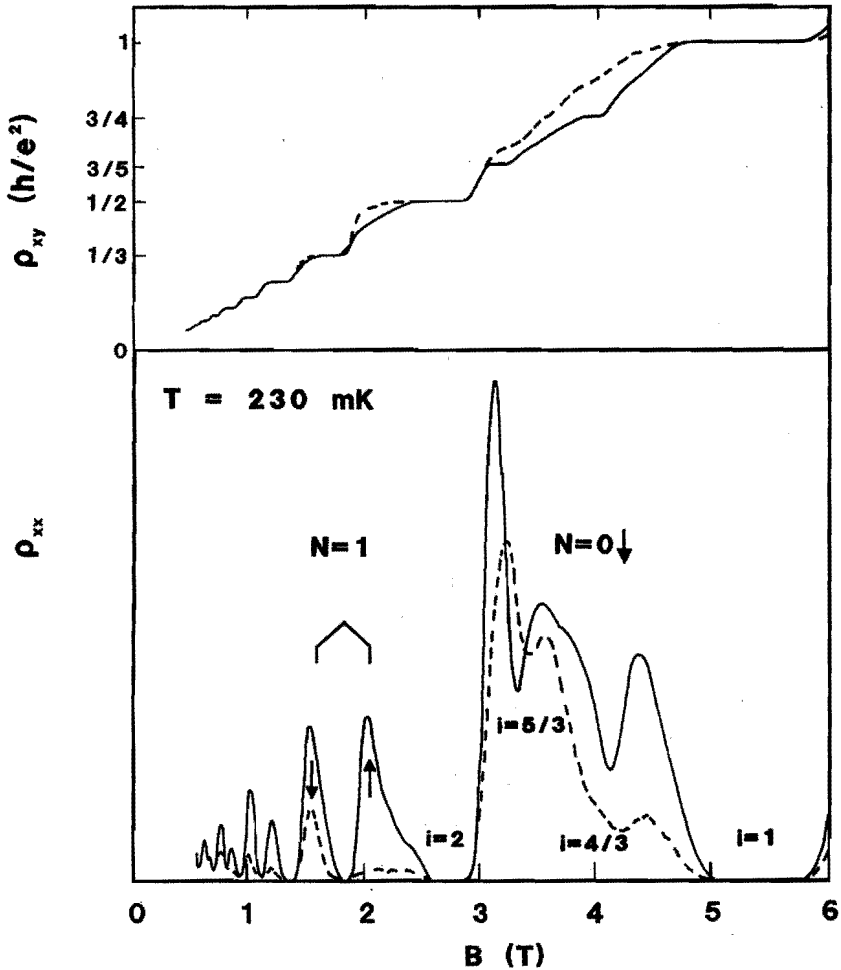

Fig. 6.1:

Magneto and Hall resistivity at 230 mK for a back–gate voltage of +25 V (solid line) and after 7.0 μs illumination (dashed line).

$55 \cdot 10^4$ cm^2/Vs. For back–gating at $+25$ V these become $1.33 \cdot 10^{11}$ cm^{-2} and $60 \cdot 10^4$ cm^2/Vs and after 7.0 μs illumination $1.33 \cdot 10^{11}$ cm^{-2} and $58 \cdot 10^4$ cm^2/Vs. The solid and dashed lines represent the back–gated and illuminated sample, respectively. The figure clearly shows that after illumination the spin splitted N $= 1$ peak and the N $= 0$ spin–down peak have become more asymmetric and that the integer Quantum Hall (QH) plateaus i $= 1$ and 2 have broadened. On the other hand, the fractional QH–plateaus i $= 4/3$ and $5/3$ and the corresponding minima in ρ_{xx} have almost disappeared.

6.3 DISCUSSION

The measurements show that the fractional quantized Hall plateaus and the integer quantized Hall plateaus behave different when the interaction with the impurities is changed. This means that the integer and fractional QHE have a different physical origin. Our observations are consistent with the idea that the fractional QHE is due to electron–electron interaction which is destroyed when the electron–impurity interaction becomes too strong and the integer QHE, on the other hand, is due to electron–impurity interaction.

Now we present a tentative model which explains the observed asymmetries in the spin splitting. In a simple classical picture we explain the width of a Landau level as due to potential fluctuations in the xy–plane induced by the ionized impurities. On the left side in Fig. 6.2 we show the potential energy in the x–direction, $-eV(x)$, and the local total energy, $-eV(x) + (N+\frac{1}{2})\hbar\omega_c$, for the two lowest Landau levels. On the right side we show the Density Of States (DOS) for this potential distribution. This classical picture gives a good description in the case of long range scattering potentials, i.e. the cyclotron orbit is smaller than the range of the scattering potential. In this simple classical picture[4] the width of a Landau level can be approximated by $\Gamma_n^2 = 4 < (V(\vec{r}) - <V(\vec{r})>)^2 >$ in the case the scattering potentials are enough long range. Localization can be understood in this simple classical picture. The Lorentz force due to the gradient of the electrostatic potential and the perpendicular magnetic field gives a centrifugal force which points towards the center of a potential hill or valley. This Lorentz force compels the electrons to move around an attractive or repulsive potential. These electrons are thus localized and do not participate in the electrical current through the 2DEG. When the Fermi level rises through a Landau level, first the

regions with the deepest potentials are filled with electrons. The deepest potentials induce the strongest localization. In a nearly filled Landau level the electrons are localized by the potential hills. These localized states appear in the wings of the Landau level as indicated in Fig. 6.2 by the black areas.
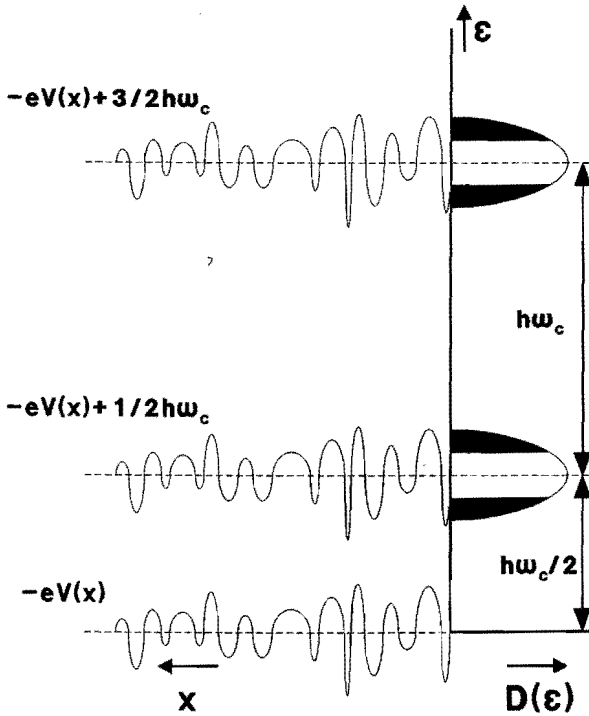
Fig. 6.2:

On the left side the surface potential energy and the local total energy is shown. On the right side the DOS is shown for this potential distribution. The localized states are indicated by the black areas.

This model is also useful to explain the asymmetric shape of a Landau level when a small number of either attractive or repulsive scattering centers is present[5,6]. Fig. 6.3a shows just like Fig. 6.2 the surface potential energy and a symmetrical broadened Landau level. An equal number of attractive and repulsive scattering centers are present. When a small extra number of strong attractive scattering centers is present we expect an extra number of states on the low

energy side of the Landau level and thus an asymmetric DOS, see Fig. 6.3b. In the case of a large surplus of attractive scattering centers the DOS becomes symmetric again and is shifted to a lower energy, see Fig. 6.4c. Although in ref. 5 and 6 short range scattering potentials are treated, these results are in good agreement with those calculations, see chapter 1.6.
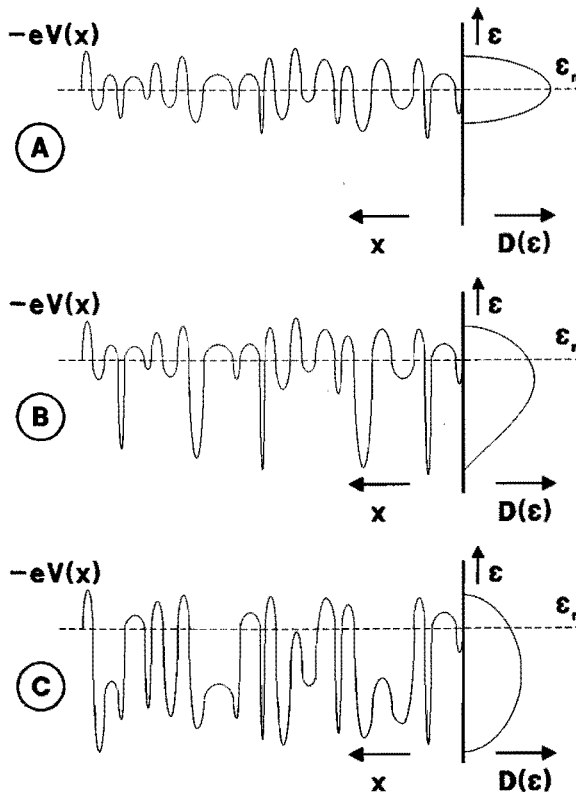
Fig. 6.3:

Schematic representation of the surface potential energy and DOS in the case of

a) an equal number of attractive and repulsive scatterers,

b) a small surplus of attractive scatterers,

c) a large surplus of attractive scatterers.

Normally the energy difference of the spin–up and spin–down level is smaller than the width of each level and thus these levels overlap with each other. In case of a small surplus of attractive scatterers the overlap at the center of spin–up level is stronger than at the center of the spin–down level, see Fig. 6.4a. When the number of repulsive scatterers is larger than the number of attractive scatterers the overlap is strongest at the center of the spin–down level, see Fig. 6.4b.
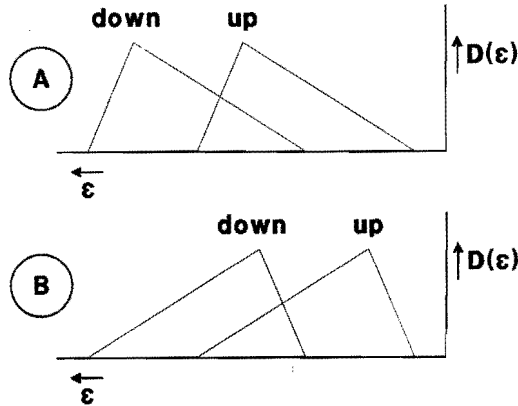
Fig. 6.4:

 Schematic representation of the overlapping DOS of the spin–up and spin–down Landau levels in the case of a surplus of

 a) attractive scatterers,

 b) repulsive scatterers.

If the interaction with the positively charged donors becomes stronger, we observe a reduction of the spin–up peak in ρ_{xx} and the growth of the QH–plateau in the same magnetic field region just as it has been described in the previous chapter. As shown in Fig. 6.4 the overlap at the center of the spin–up Landau level increases when the number of attractive scattering centers increases. Therefore we suggest that this increased overlap is responsible for the reduction of ρ_{xx} and the fact that the integer quantized Hall plateaus broaden asymmetrically (on the side of the spin–up peak).

In Fig. 6.5 we plot the overlapping Landau levels and the local total energy when the Fermi level is situated in the spin–up peak. We observe that the electrons in the spin–down peak are trapped in the deepest scattering potentials.

Thus the electrons in the spin–down level are situated on top of the strongest scattering centers. These electrons will reduce the depth of the potential and extend the range of the scattering potential, i.e. the potential becomes flatter. Ando and Uemura[7] have shown that localization increases when the scattering potential becomes more long range: this explains the growth of the integer quantized Hall plateaus. They also showed that the peak value of ρ_{xx} reduces when the range of the potential increases[4]. This reduction of the peak value of ρ_{xx} does not occur for the spin–down peak, because in that case the Fermi level is situated at the center of the spin–down Landau level. As can be observed from Fig. 6.5 there is no overlap with the spin–up Landau level at that energy and the spin–up Landau level will be totally filled. Such a totally filled Landau cannot contribute to a reduction of the scattering potentials because the electrons in that Landau level are distributed homogeneously in space.
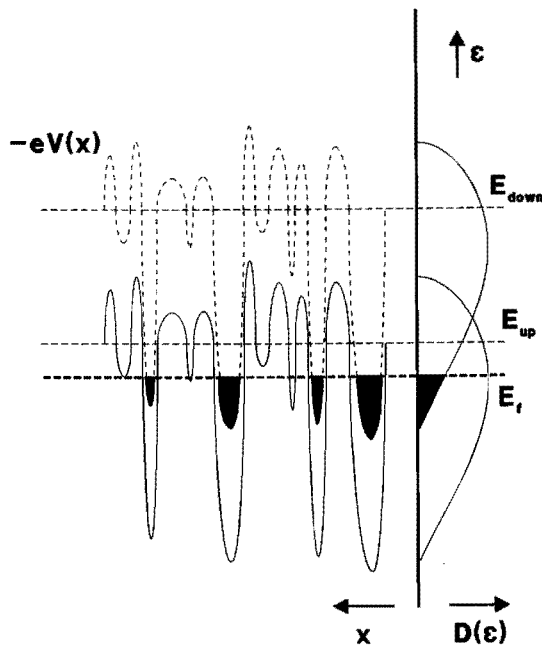
Fig. 6.5:
    Schematic representation of the local total energy and DOS in the case of an overlapping spin–up and spin–down level due to a surplus of attractive scatterers. The Fermi level is situated at the center of the spin–up level.

It is well known that the observed asymmetry of the spin–up and spin–down peak in ρ_{xx} is current dependent, i.e. at a high current density the asymmetry disappears[8]. Due to the higher power dissipation more phonons are generated which reduce the scattering lifetime. Since phonon scattering leads to a symmetric DOS for both the spin–up and spin–down levels, the overlap becomes equal for both levels. In this case there is no longer a different overlap at the centers of both Landau levels. Thus the influence of the both levels on each other is equal for the case that the Fermi level is situated at the center of the spin–up or spin–down Landau levels. In view of this picture we can understand why the asymmetry disappears at high current densities.

Although our model seems to describe a number of observations quite satisfactory, there still remain experiments which do not fit within this model. For example Zheng et al.[9] reported on measurements on a Hall–bar structure with wide as well as narrow channels. They found that in the wide channel the spin–up and spin–down peak are almost symmetrical while in the narrow channel the spin–up and spin–down peak are strongly asymmetric. Our model does not give an explanation for this behiaviour.

7.5 CONCLUSION

To our knowledge this is the first direct observation that in the same sample for the same electron density the IQHE and the FQHE respond completely different to a change in the electron interaction with impurities. This confirms that the integer and fractional QHE have a different physical origin.

We think that the reduction of the ρ_{xx} peak and the corresponding broadening of the quantized Hall plateau is due to the increased screening of the overlapping spin–down level with the spin–up level. This model does not explain the asymmetry of the spin–up and spin–down peak which is observed in a narrow Hall–bar shaped samples.

REFERENCES

1   R.G. Clark, J.R. Mallet, A. Usher, A.M. Suckling, R.J. Nicholas,
     S.R. Hayes, Y. Journaux, J.J. Harris, and C.T. Foxon, Surf. Sci. **196**, 219
     (1988)

2   R.J. Haug, K. von Klitzing, and K. Ploog, Phys. Rev. **B35**, 5933 (1987)

3   P.M. Koenraad, F.A.P. Blom, P.A.M. Blom, C.T. Foxon, E.N.M. Frijns,
     J.J. Harris, G. Weimann, and J.H. Wolter, Supl. Micros. **5**, 519 (1989)

4   T. Ando, and Y. Uemura, Journ. Phys. Soc. Jap. **36**, 959 (1974)

5   E. Brézhin, D.J. Gross, and C. Itzykson, Nucl. Phys. **B235**, [FS11] 24 (1984)

6   T. Ando, Journ. Phys. Soc. Jap. **53**, 3126 (1984)

7   T. Ando, Journ. Phys. Soc. Jap. **53**, 3101 (1984)

8   R. Woltjer, J. Mooren, J. Wolter, J.P. André, and G. Weimann,
     Physica **134B**, 532 (1985)

9   H.Z. Zheng, K.K. Choi, D.C. Tsui, and G. Weimann, Phys. Rev. Lett. **55**,
     1144 (1985)

CHAPTER 7

OBSERVATION OF HIGH MOBILITY IN
20 Å SILICON δ–DOPED GaAs GROWN BY MBE AT 480 °C

7.1 INTRODUCTION

Recently there has been a lot of interest in the physics of sharply confined doping layers (δ–doping). Until now δ–doping has been used successfully for Si–layers in GaAs and $Al_xGa_{1-x}As$[1,5], Sb–layers in Si[2] and S–layers in InP[3]. Both, Molecular Beam Epitaxy (MBE) and Metal Organic Chemical Vapor Deposition (MOCVD) have been used to grow such δ–doped layers. The two–dimensional nature of the electrons confined in the potential well, induced by the δ–doped donor layer, was first shown from Shubnikov–de Haas (SdH) measurements by Zrenner et al.[1]. It has been shown from Secondary Ion Mass Spectrometry (SIMS)[4] and subband population measurements[5,6] that the spreading of the donors is strongly reduced when the growth temperature is lowered. Recently, Gillman et al.[7] presented Hall effect measurements of the electron density and mobility in Si δ–doped GaAs samples grown at 590 °C. They reported a maximum Hall mobility of 2000 cm^2/Vs at 4.2 K.

By growing at low temperature, 480 °C, we are able to enhance the mobility at 4.2 K to 6760 cm^2/Vs. In this chapter we present measurements on the Hall effect and subband population carried out on Si δ–doped GaAs samples grown at 480 °C, 530 °C and 620 °C. We also report Cyclotron Resonance (CR) measurements on δ–doped samples for the first time.

7.2 EXPERIMENTS

The δ–doped samples were grown in our computer controlled Varian Modular MBE system. The semi–insulating GaAs [100] substrates were carefully cleaned and etched before they were introduced into the MBE system. The substrates
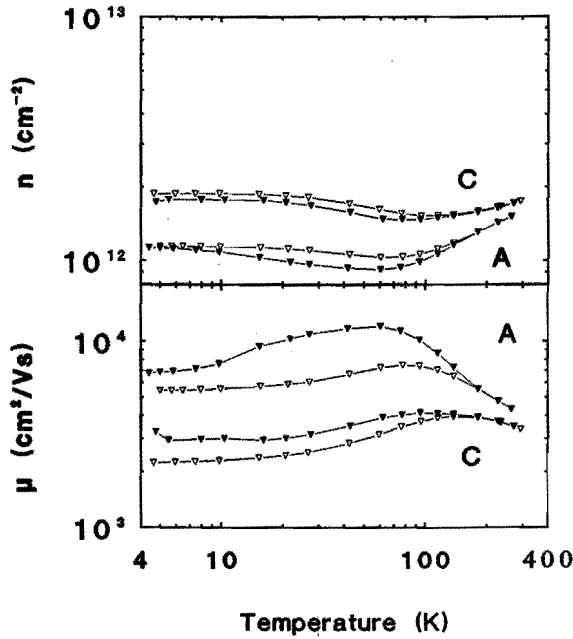
Fig 7.1:

The measured temperature dependence of the Hall electron density and mobility between 4.2 K and 300 K before illumination (open symbols) and after illumination (solid symbols) with a red LED in sample A and C, see table 7.1.

were annealed at 630 ^{0}C in As$_4$–flux in the MBE prior to growth in order to remove the oxide layer from the substrate surface. The samples were grown at substrate temperatures between 480 ^{0}C and 620 ^{0}C. The As/Ga beam equivalent pressure ratio was close to 1.5 and the GaAs growth rate close to 1 μm/h. In these samples the background acceptor concentration was lower than $1 \cdot 10^{14}$/cm^3 as determined from "Polaron profiler" and CV measurements. In order to obtain a planar doping layer on a smooth surface the growth of GaAs was interrupted by closing the Ga–shutter and waiting for 10 s; then the Si–furnace was opened either for 7.5 s or 30 s to deposit the doping layer of $2 \cdot 10^{12}$ or $8 \cdot 10^{12}$ atoms per cm^2 respectively, see Fig. 1.3. During the growth of GaAs the Si–furnace was kept at 1400 ^{0}C in order to obtain a Si–flux as high as possible. The samples were
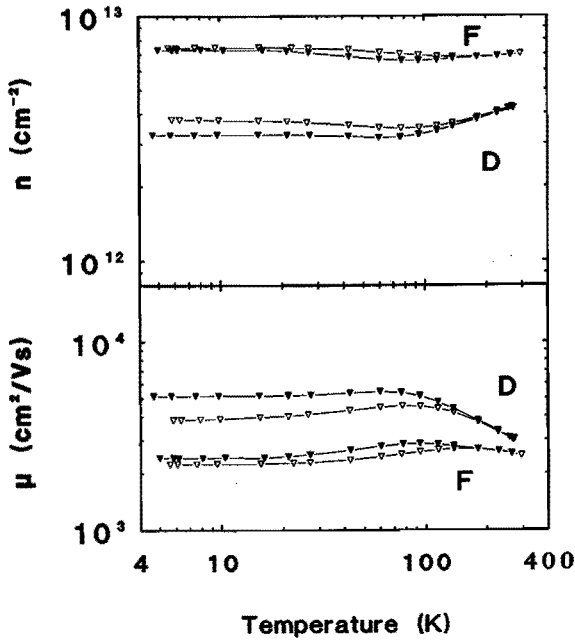
Fig 7.2:

    The measured temperature dependence of the Hall electron density and mobility between 4.2 K and 300 K before illumination (open symbols) and after illumination (solid symbols) with a red LED in sample D and F, see Table 7.1.

grown with a buffer layer between the doping layer and the substrate of 2.5 μm and a top layer of 1 μm.

    We first used the Van der Pauw method for the characterization of the electrical transport properties of the samples. The subband population measurements were performed on Hall bar shaped samples. Ohmic contacts were made by annealing small Sn balls at 400 ^{0}C during 1.5 minutes under a N_2:H_2 = 4:1 flux. The Hall mobility and electron density were measured between 4.2 K and 300 K. The samples were illuminated with GaAs outgap radiation of a red LED (λ = 650 nm) mounted inside the cryostat.

    We have grown two sets of samples with doping concentrations of $2 \cdot 10^{12}$ cm^{-2} and $8 \cdot 10^{12}$ cm^{-2} at three different substrate temperatures, 480 ^{0}C,

	N_D 10^{12} cm^{-2}	T growth ^0C	electron density 10^{12} cm^{-2}		mobility cm^2/Vs	
			dark	light	dark	light
A	2	480	1.14	1.13	5450	6760
B	2	530	1.13	1.14	5170	6540
C	2	620	1.87	1.73	2230	3270
D	8	480	3.76	3.27	3850	5150
E	8	530	5.70	5.05	2260	2800
F	8	620	7.46	7.30	2240	2430

Table 7.1:

    The sheet doping concentration, N_D, growth temperature, Hall electron density and Hall mobility at 4.2 K before and after illumination
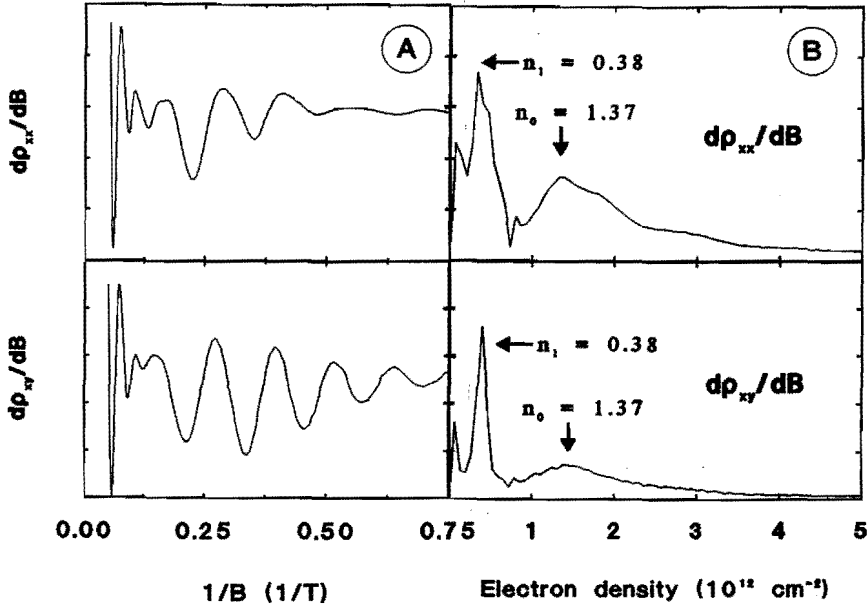
Fig. 7.3:

    a) The measured derivative of the SdH and Hall resistance, $d\rho_{xx}/dB$ and $d\rho_{xy}/dB$, versus 1/B at 1.3 K for sample A.

    b) The calculated Fast Fourier Transform of the SdH and Hall resistance shown in a).

530 ⁰C and 620 ⁰C, see Table 7.1. This table also shows the measured Hall densi-
ty and mobility of the samples at 4.2 K. The results clearly show that the Hall
mobility at 4.2 K increases by about a factor of 2 when the growth temperature is
decreased from 620 ⁰C to 480 ⁰C. The Hall electron density decreases when the
growth temperature is lowered. After illumination the mobility in all samples
increases whereas the electron density stays almost equal. The observed mobility
of 6760 cm²/Vs in sample A and 5150 cm²/Vs in sample D are the highest Hall
mobilities in Si δ–doped GaAs samples at a sheet donor concentration of
$2 \cdot 10^{12}$ cm⁻² and $8 \cdot 10^{12}$ cm⁻² reported thus far[7,8].

Figs. 7.1 and 7.2 show the temperature dependence of the Hall electron den-
sity and mobility of the samples A,C,D, and F between 4.2 K and 300 K before
and after illumination. In the temperature range between 4.2 K and 100 K the
Hall mobility in the samples A and D, grown at 480 ⁰C, appears to be much
higher as in the samples C and F, grown at 620 ⁰C. In samples C and F, grown at
620 ⁰C, the electron density below 100 K compares very well to the sheet doping
concentration. On the other hand for samples A and D, grown at 480 ⁰C, for both
doping concentrations the electron density below 100 K appears to be smaller by
almost a factor of 2. We note however, as discussed in chapter 1.2.2, that in
δ–doped structures normally more than one subband is populated. These sub-
bands have a different mobility. They thus add in a complicated way to the
measured Hall voltage[9]. Hall measurements therefore in general give only limited
information on the total electron density.

A method which is able to determine the electron density in the different
subbands separately is based on the SdH–effect. We carried out measurements on
Hall–bar shaped samples in magnetic fields up to 20 T. The weak oscillations in
ρ_{xx} and ρ_{xy} were resolved by measuring $d\rho_{xx}/dB$ and $d\rho_{xy}/dB$ with a modulation
field of 0.03 T at a frequency of 70 Hz. Fig. 7.3a shows $d\rho_{xx}/dB$ and $d\rho_{xy}/dB$
versus 1/B for sample A. The subband population has been determined by taking
the Fast Fourier Transform (FFT) of $d\rho_{xx}/dB$ and $d\rho_{xy}/dB$, Fig. 7.3b. In sample
D it was difficult to determine the exact population of the lowest subband due to
the small number of weak oscillations visible in $d\rho_{xx}/dB$ and $d\rho_{xy}/dB$. The
results for sample A and D are given in Table 7.2. The total electron density, i.e.
the sum of the electron densities in all the subbands, is smaller than the number
of doping atoms deposited during growth for these samples. The total electron
density in sample D is less than four times the total electron density in sample A

		$d\rho_{xx}/dB$	$d\rho_{xy}/dB$	calc.
A	n_0	1.37	1.37	1.38
	n_1	0.38	0.38	0.37
	n_{tot}	1.75	1.75	1.75
A ill	n_0	1.50	1.53	
	n_1	0.45	0.42	
	n_{tot}	1.95	1.95	
D	n_0	3.50	?	3.60
	n_1	1.23	1.24	1.29
	n_2	0.51	0.52	0.46
	n_{tot}	5.24	?	5.25
D ill	n_0	3.50	?	
	n_1	1.29	1.30	
	n_2	0.56	0.55	
	n_{tot}	5.35	?	

Table 7.2:

The measured and calculated subband population, n_i (10^{12} cm^{-2}), at 4.2 K in the samples A and D before and after illumination. The total electron density is given by n_{tot}. A square donor distribution of 20 Å and a background impurity concentration of $1 \cdot 10^{14}$ cm^{-3} are used in the calculation.
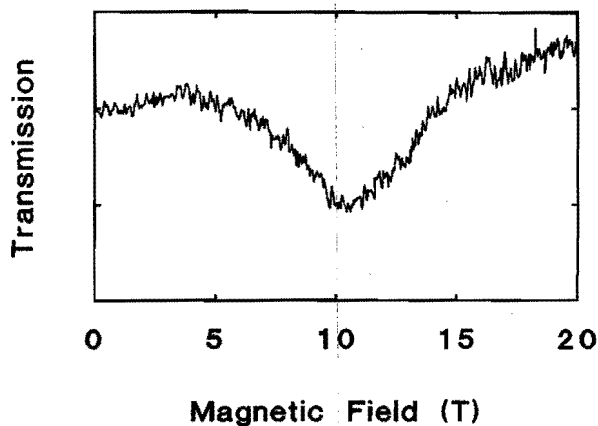
Fig. 7.4:

A measured FIR absorption profile as a function of the magnetic field at wavelength of 77.4 μm at 1.3 K.

although the doping concentration is four times higher. This indeed confirms that the Hall measurements do not yield the correct numbers. Illumination of sample A and D with a red LED only changed the subband population slightly.

On the high mobility samples A and D we also performed Cyclotron Resonance (CR) measurements. To our knowledge these are the first CR–measurements on δ–doped samples reported thus far. The measurements were done in magnetic fields up to 20 T with an optically–pumped FIR laser. Fig. 7.4 shows a typical example of a measured CR–profile. All measured CR–profiles were very broad and some of them had an asymmetric shape. In Fig. 7.5 we have plotted the apparent cyclotron effective mass derived from the transmission minimum for sample D as a function of energy. Similar measurements on sample A showed a smaller value. The effective mass shows a complicated behavior as a function of energy for both sample A and D.
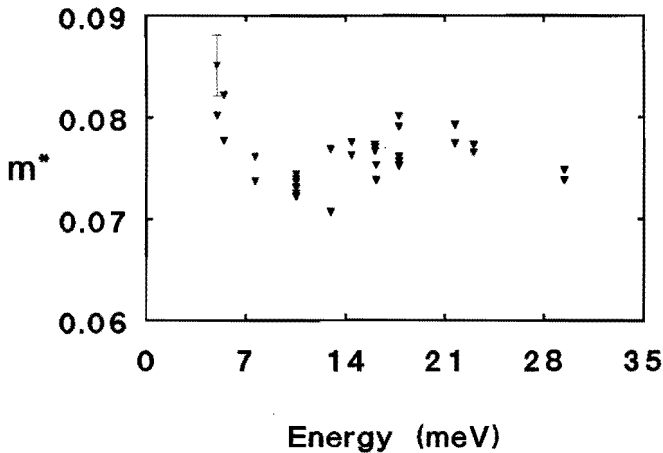
Fig. 7.5:

    The effective mass determined from the magnetic field position of the minimum in the FIR absorption profile as a function of the energy of the CR at 1.3 K.

7.3 SELFCONSISTENT CALCULATION OF THE SUBBAND
ENERGIES AND ENVELOPE WAVEFUNCTIONS

We calculated the confining potential, subband energies and envelope wave-functions self–consistently by solving simultaneously the Poisson and Schrödinger equations, see chapter 1.3. Due to the high electron density in a δ–doped structure more than one subband is populated. Therefore we have to solve the following one–dimensional Schrödinger equation for each subband separately

$$\left\{ -\frac{\hbar^2}{2m^*} \frac{\partial^2}{\partial z^2} + U(z) \right\} \varphi_i(z) = E_i \, \varphi_i(z) \qquad [7.1]$$

where i is the subband index. The potential $U(z)$ consists of only two terms in the case of a δ–doped structure

$$U(z) = U_c(z) + U_{ex}(z) \qquad [7.2]$$

The first term describes the electrostatic potential defined by the Poisson equation.

$$\frac{\partial^2}{\partial z^2} U_c(z) = \frac{e\rho(z)}{\epsilon_0 \epsilon_r} \qquad [7.3]$$

In the case of a δ–doped structure the charge distribution, $\rho(z)$, is the sum of the negatively charged acceptors (background impurities) on both sides of the doping layer, the positively charged donors in the doping layer, and the electron density of the 2DEG.

The second term in [7.2] describes the exchange and correlation effects. There are various models to include these effects[9-11]. Here we used the potential proposed by Gunnarson and Lundqvist[11]

$$U_{ex} = -\frac{2m^* Ry}{m_e \epsilon_0 \epsilon_r^2 \pi \alpha r_s} \left[1 + 0.0545 \, r_s \ln(1 + 11.4/r_s) \right] \qquad [7.4]$$

where

$$1/r_s = \sqrt[3]{4\pi n(z)/3} \; r_0 \; \epsilon_r \; m_e/m^*$$

$$r_0 = 5.29177 \cdot 10^{11} \, m \quad \text{and} \quad \alpha = \sqrt[3]{4/9\pi}$$

In order to solve the Schrödinger and Poisson equation self–consistently we proceeded as follows; we took a donor distribution of a certain width and estimated the subband wavefunctions. Then the electrostatic potential was calculated from the Poisson equation by a double integration over the charge distribution. We did not calculate the electrostatic potential in the total depletion layer. We only calculated the potential within 500 Å from the center of the doping layer because the electron envelope wavefunctions spread only over about 400 Å on each side. Although the remaining part of the confining potential can be calculated analytically it is not needed in further calculations.

$$D_{don} = 40 \; Å \qquad D_{don} = 180 \; Å$$
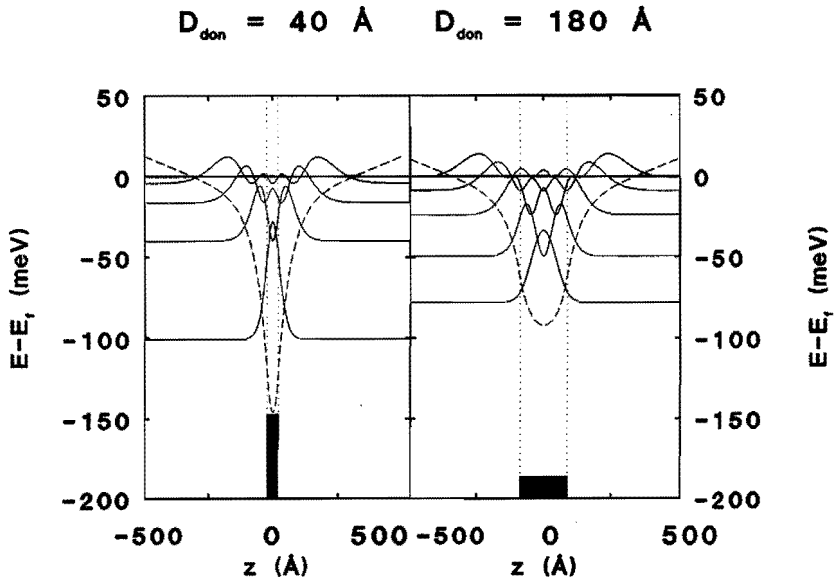
Fig. 7.6:

The calculated energy and probability distribution, $|\varphi_i(z)|^2$, of each subband (solid lines) and the electrostatic potential (dashed line) for a δ–doped structure. The $4.5 \cdot 10^{12}$ cm^{-2} donors are distributed over 40 Å or 180 Å as indicated by the black box.

The calculated electrostatic potential was used in the Schrödinger equation to find the envelope wavefunction of each subband. We calculated only one envelope wavefunction at a time from a set of 4 coupled differential equations. This was done with the same computer program as described in chapter 3 with the electrostatic potential kept constant during the calculation. The envelope wavefunctions of the other subbands, and the population of the subbands were also not changed during the calculations. After the separate calculation of all subband wavefunctions and energies had been completed the distribution of the electrons over the subband was calculated taking into account the non–parabolicity of the Γ–conduction band[13]. Using this distribution the electrostatic potential was calculated again. This cycle was repeated until we reached convergence in the electron distribution. In Fig. 7.6 we show as an example the probability distribution, $|\varphi_i(z)|^2$, and E_i in a δ–doped structure in which $4.5 \ 10^{12} \ cm^{-2}$ donors are spread over 40 Å and 180 Å.

N_{2DEG} 10^{12} cm^{-2}	i	relative subband population			lowest subband E_0 (meV)		
		1	2	3	1	2	3
1.0	0	0.797	0.775	0.771	13.55	12.94	13.45
	1	0.203	0.225	0.229			
4.5	0	0.594	0.583	0.581	25.60	25.16	27.43
	1	0.293	0.288	0.284			
	2	0.100	0.105	0.110			
	3	0.013	0.023	0.025			
10.0	0	0.508	0.502	0.502	35.14	34.84	39.51
	1	0.304	0.299	0.293			
	2	0.136	0.136	0.139			
	3	0.049	0.053	0.054			
	4	0.004	0.010	0.012			

Table 7.3:

The relative population, n_i, of the subbands and energy of the lowest subband, E_0, calculated for;

1) a square donor distribution of 100 Å with exchange intercation.

2) a square donor distribution of 100 Å without exchange interaction.

3) a Gaussian donor ditribution of $25\sqrt{\pi}$ Å with exchange interaction.

It is clear from these figures that the distribution of the electrons over the levels is dependent on the width of the donor distribution. The width of the donor distribution thus can be used as a fitting parameter in the calculations to obtain the same subband population as measured.

We also studied the influence of the exchange and correlation effects on the subband energies and envelope wavefunctions. Table 7.3 gives the calculated subband population and the energy of the lowest subband with and without the exchange interaction included, for samples with a width of the donor distribution of 100 Å (column 1 and 2). The calculations show that the influence of the exchange interaction on the subband population and energy is only weak.

We also studied the changes of the subband population and energies for the case of a Gaussian distribution of the donor atoms, $N_D(z) = 2/\sigma\sqrt{\pi}\cdot\exp{-(z/\sigma)^2}$, instead of a square distribution[1,5,14]. Calculations show that a Gaussian distribution with a half width $\sigma = (d/4)\sqrt{\pi}$ gives nearly the same subband population as a square distribution with a width d. This is shown in column 1 and 3 in Table 6.3 in the case of a square distribution with a width of 100 Å and a Gaussian distribution with a half width of $25\sqrt{\pi}$ Å. On the other hand the subband energy is sensitive to the donor distribution if the electron density is high. We conclude that the shape of the donor distribution influences the calculated subband energy at high electron densities only.

7.4 DISCUSSION

The subband population measured in sample A and D is in good agreement with the calculations for a square donor distribution donor with a width of 20 Å, see Fig. 7.7 and Table 7.2. It is difficult to give a very accurate value for the width because below 20 Å the subband population is nearly independent on the width of the donor distribution. The total electron density found in sample A by the FFT on $d\rho_{xx}/dB$ and $d\rho_{xy}/dB$ is nearly equal to the intended donor concentration. Only a small fraction of the electrons is missing probably due to the formation of a depletion layer on both sides of the δ–doped layer, see Table 7.2. In sample D, however, the total electron density is much smaller than the sheet doping concentration. Zrenner *et al.*[5], found that the electron density is not only dependent on the sheet doping concentration but also on the width of the donor distribution. They argued that this is due to the DX–center at 200 meV
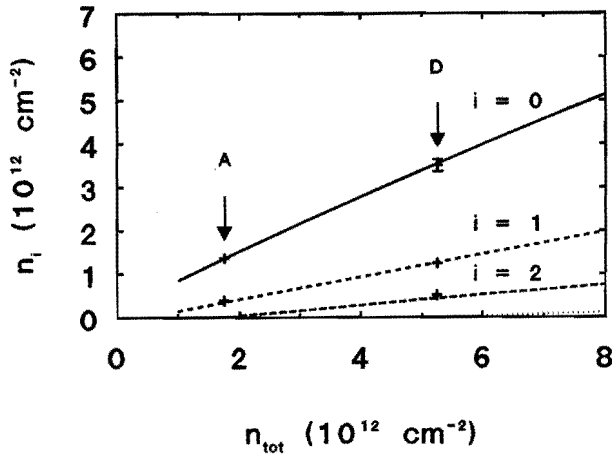
Fig. 7.7:
   The population of the subbands as a function of the total electron density in the 2DEG when the donor are distributed over 20 Å. The measured subband populations in sample A and D are indicated in this figure.

n_{don}	T_{growth}		
cm^{-2}	480 ^{0}C	530 ^{0}C	620 ^{0}C
$2 \cdot 10^{12}$	20 Å	30 Å	60 Å
$8 \cdot 10^{12}$	20 Å	80 Å	?

Table 7.4:
   The width of the donor distribution in all samples as determined from the SdH measurements.

above the Γ–band. For the same number of electrons originating from the same sheet doping concentration subbands at higher energies are populated in samples with a narrower donor distribution. Thus a threshold of 200 meV is reached at a lower doping concentration than for a wider donor distribution. In this way the DX–center levels off the maximum attainable electron concentration. In sample A the total electron density is such that the corresponding Fermi–level is well lying

below 200 meV whereas in sample D it is not.

If indeed DX–centers were responsible for the discrepancy of the electron density as described above one should expect to observe the PPC effect. Surprisingly however the electron concentration has hardly changed after illumination of the sample. This means that there are no DX–centers at all and the arguments given above are wrong.

Recently Beall *et al.*[15] presented SIMS and CV–measurements on δ–doped GaAs structures in the same range of growth temperatures and doping concentrations. They found evidence that at doping concentrations above $4 \cdot 10^{12}$ cm^{-2} only a fraction of the silicon is deposited on electrically active sides. The remainder of silicon forms clusters or at higher growth temperatures, above 590 ^{0}C, even small droplets. In view of their results we think that this mechanism is also responsible for the discrepancies between the electron concentration and the sheet doping concentrations found in our samples.

We already discussed the discrepancy between the electron density derived from van der Pauw and SdH–measurements. The Hall electron density in sample A and D is much smaller than the electron density derived from the FFT measurements. As stated before this is due to the different mobilities in the different subbands. It is likely that the width of the donor distribution is larger in samples C and F, grown at high temperature, than in samples A and D, grown at low temperatures. Table 7.4 shows that this is indeed true in the samples investigated. In this case for sample A and D a strong overlap between the envelope function and the scatterers exists only for the lowest subband, see Fig. 7.7. As a consequence we expect that the mobility in the various subbands differs more strongly in samples A and D than in samples C and F [16]. This is consistent with the observation that samples A and D show the strongest discrepancy between the van der Pauw and the SdH measurements.

Note that at room temperature the differences in electron densities determined from van der Pauw measurements for sample A and C are much smaller than at low temperature. This is not surprising, because at room temperature the scattering of electrons on optical phonons is the dominant scattering mechanism for all subbands involved. Thus the mobility in these subbands are not expected to differ that much.

When the subband population is known and only two subbands are populated we are able to calculate the subband mobility from the Hall electron density

and mobility[14], see Table 7.5. This proves that the mobility in the higher sub-
bands increases when the distribution of the ionized donors becomes narrower.
After illumination of sample A the mobilities in the first and second subband
become 2150 cm^2/Vs and 10900 cm^2/Vs respectively. We think that the mobility
in the highest subband increases because the electron distribution is shifted away
from the donors after illumination. This shift is due to the flat band conditions in
the GaAs depletion layer which exist after neutralization of the charged acceptors
due to bandgap excitation, see chapter 4. In sample D, where three subbands are
populated, we can only estimate the mobility in the subbands. The mobility in
the lowest subband at 4.2 K is $\approx$ 1500 cm^2/Vs and in the other subbands
$\approx$ 5500 cm^2/Vs.

	A	B	C
μ_0	2210	2030	2230
μ_1	9250	8500	2230

Table 7.5:
  The mobility in the two subbands of the samples A,B, and C each with a
  sheet doping concentration of $2 \cdot 10^{12}$ cm^{-2}.

Note that the mobilities observed in the narrow δ–doped conduction layers of
sample A and D are much higher than the mobilities reported thus far[5,7]. In addi-
tion to the mechanism described above there might be a second mechanism which
enhances the mobility. As van Hall et al.[17] have shown that in a heterostructure
the electron scattering is determined by the fluctuations in the distribution of the
ionized scattering centers. It is likely that in samples grown at low temperature,
like samples A and D, these fluctuations are smaller than in samples grown at
high temperature, like samples C and F.

We now turn to measurements of the CR. As mentioned already the width of
the CR are very broad compared to the width of the CR in a GaAs/Al$_x$Ga$_{1-x}$As
heterostructure. There are at least three reasons for this broadening. First, the
mobility and hence the scattering time of the electrons in the δ–doped layer is low
compared to the case of a heterostructure. Second, the high electron density gives
rise to considerable dielectric broadening of the CR (see ref. 16 and especially Fig.
4 therein). Third, the overlap of several CR may also give rise to an apparent

broadening of the CR–profile. Remember that more than one subband is populated.

In the case that the minimum in the FIR absorption is due to a CR in only one subband we can determine the effective mass of the electrons. We find that the effective mass in sample D is considerably enhanced above the effective mass at the Γ–conduction band minimum. Since the electron density is very high in these structures and the confining potential is very narrow it is likely that this enhancement is due to the non–parabolicity of the Γ–conduction band. The effective mass, however, which we obtained is lower than that expected from the calculations of Rössler[11]. In sample A the effective mass is smaller than in sample D and very close to the effective mass determined in bulk GaAs. This is also consistent within the picture of non–parabolicity because the electron density in sample A is much smaller as in sample B. At present we cannot explain the complicated behavior of the effective mass as a function of the CR energy.

7.5 CONCLUSION

In conclusion we have shown that for the growth of narrow silicon δ–doped layers in GaAs a lower substrate temperature is fortuitous. Measurements on the subband population using the SdH–effect show that the δ–doped samples we have grown at 480 ^{0}C display very narrow doping profiles, down to 20 Å. In these very narrow δ–doped layers the mobility is enhanced strongly. To our knowledge these samples show the highest mobility reported to date. We think that the enhancement of the mobility is due to a smaller overlap of the ionized donors with the electrons in the higher subbands. In these very narrow δ–doped layers we were able to determine the effective mass by CR measurements for the first time. The results show that in a sample with a high electron density the effective mass is considerably enhanced.

REFERENCES

1   A. Zrenner, H. Reisinger, F. Koch, and K. Ploog, Proceedings of the 17th International Conference on the Physics of Semiconductors, San Fransisco, 1984, ed. by J.P. Chadi and W.A. Harrison (Springer–Verlag, New York, 1985), p.325.

2   H.P. Zeindl, T. Wegehaupt, I. Eisele, H. Oppolzer, H. Reisinger, G. Tempel and F. Koch, App. Phys. Lett. $\underline{50}$, 1164 (1987).

3   Wenchao Cheng, A. Zrenner, Qiu–Yi Ye, F. Koch, D. Grützmacher and P. Balk, Semicond. Sci. Technol. $\underline{4}$, 16 (1989).

4   R.B. Beall, J.B. Clegg and J.J. Harris, Semicond. Sci. Technol. $\underline{3}$, 612 (1988)

5   A. Zrenner, F. Koch, R.L. Williams, R.A. Stradling, K. Ploog and G. Weimann, Semicond. Sci. Technol. $\underline{3}$, 1203 (1988).

6   M. Santos, T. Sajoto, A. Zrenner, and M. Shayegan, App. Phys. Lett. $\underline{53}$, 2504 (1988)

7   G. Gillman, B. Vinter, E. Barbier, and A. Tardella, App. Phys. Lett. $\underline{52}$, 972 (1988).

8   K. Ploog, Journ. of Crystal Growth, $\underline{81}$, 304 (1987).

9   R.A. Smith, "Semiconductors" (Cambridge University Press, Cambridge, 1978).

10   W. Kohn and L.J. Sham, Phys. Rev. $\underline{140}$, A1133 (1965).

11   L. Hedin and B.I. Lundqvist, J. Phys. C $\underline{4}$, 2064 (1971).

12   O. Gunnarson and B.I. Lundqvist, Phys. Rev. B $\underline{13}$, 4274 (1976).

13   U. Rössler, Solid State Commun. $\underline{49}$, 943 (1984).

14   B. Ullrich, E.F. Schubert, J.B. Stark and J.E. Cunningham, App. Phys. A $\underline{47}$, 123 (1988).

15   R.B. Beall, J.B. Clegg, J. Castagné, J.J. Harris, R. Murray and R.C. Newman, to be published in Semicond. Sci. and Technol.

16   E.F. Schubert, J.E. Cunningham and W.T. Tsang, Solid State Com. $\underline{63}$, 591 (1988).

17   P.J. van Hall, T. Klaver and J.H. Wolter, Semicond. Sci. Technol. $\underline{3}$, 123 (1988).

18   C.J.G.M. Singleton, P.J. v.d. Wel, J.A.A.J. Perenboom, D.J. Barnes, M.A. Hopkins, R.J. Nicholas and C.T.B. Foxon, Phys. Rev. B $\underline{38}$, 13133 (1988)

SUMMARY

In this thesis experiments on two–dimensional electron gases (2DEG) in GaAs/$Al_xGa_{1-x}As$ heterostructures and Si–δ–doped GaAs structures are treated. In these experiments we are mainly interested in the influence of ionized impurities on the transport properties of a 2DEG. In a GaAs/$Al_xGa_{1-x}As$ heterostructure the electrons in the 2DEG are separated from the ionized donors in the $Al_xGa_{1-x}As$ layer by a so–called $Al_xGa_{1-x}As$ spacer layer. In a Si–δ–doped GaAs structure the electrons and ionized donors are confined to the same two–dimensional layer.

In a GaAs/$Al_xGa_{1-x}As$ heterostructure we study two ways to change the interaction between the electrons and the charged impurities: 1) illumination of the heterostructure, and 2) the application of a back–gate voltage. In a Si–δ–doped GaAs structure we have studied the influence of the charged impurities on the electrons in the various populated subbands.

Due to the Persistent Photo Conductivity (PPC) effect in Si–doped $Al_xGa_{1-x}As$ ($0.25 > x > 0.60$) the electron density in GaAs/$Al_xGa_{1-x}As$ heterostructures persistently increases during illumination. This PPC effect is due to the formation of the still hardly understood DX–center in Si–doped $Al_xGa_{1-x}As$. In this thesis we presented a three level donor model in order to calculate the occupancy of the DX–center.

When a GaAs/$Al_xGa_{1-x}As$ heterostructure is illuminated it is possible that a second conducting channel is formed in the $Al_xGa_{1-x}As$ layer parallel to the 2DEG conducting channel. The influence of this parallel conduction on the Hall resistivity and the magneto–resistivity is studied experimentally and compared with model calculations.

In a GaAs/$Al_xGa_{1-x}As$ heterostructure the electron density increases when a positive back–gate voltage is applied. Self–consistent calculations shows that the distance of the envelope wavefunction to the GaAs/$Al_xGa_{1-x}As$ interface increases. Since also the slope of the Γ–conduction band in the GaAs decreases it is possible that electrons flow from the 2DEG to the semi–insulating GaAs sub-

strate. Experiments in which we measured the electron density as a function of the back–gate voltage show that indeed charge is transferred to the GaAs substrate.

By using illumination as well as the application of a back–gate voltage we are able to change the interaction between the electrons in the 2DEG and the ionized donors in the $Al_xGa_{1-x}As$ layer. In the case that a positive back–gate voltage is applied, the number of ionized donors remains constant and the envelope wavefunction is shifted away from the $GaAs/Al_xGa_{1-x}As$ interface. After illumination the number of ionized donors increases and the envelope wavefunction shifts towards the $GaAs/Al_xGa_{1-x}As$ interface. When both methods are used to increase the electron density to the same value the interaction with the ionized donors is strongest after illumination. From these experiments we prove that the interaction of the electrons with the ionized donors in the $Al_xGa_{1-x}As$ layer is responsible for the observed asymmetry in the height of the spin–up and spin–down peak in the magneto–resistivity. In this thesis a tentative explaination of this asymmetry by a simple model is given.

In the same way we also study the influence of the ionized donors on the integer and fractional Quantum Hall Effect (QHE). We find that the integer quantized plateaus braoden while the fractional quantized plateaus disappear when the interaction with the ionized donors increases. This clearly shows that the integer and fractional QHE have a different physical origin.

In the literature it has been shown that the growth temperature is an important parameter for the broadening of the Si–doping profiles in Si–δ–doped GaAs structures. By growing these structures at 480 ^{0}C we succeeded in narrowing down the width of the doping profile to 20 Å or smaller. The characterization of these structures, i.e. the width of the doping profiles and the mobility in the various subbands is carried out by magneto–transport measurements. Due to the narrow doping profile in our samples the mobility in the various subbands differs strongly.

SAMENVATTING

In dit proefschrift worden experimenten aan twee–dimensionale elektronen-gassen (2DEG) in GaAs/$Al_x Ga_{1-x}$As heterostructuren en Si–δ–gedoteerde GaAs structuren behandeld. In deze experimenten is voornamelijk gekeken naar de invloed van geladen onzuiverheden op de transporteigenschappen van een 2DEG. In een GaAs/$Al_x Ga_{1-x}$As heterostructuur zijn de elektronen in het 2DEG en geladen onzuiverheden in de Si–gedoteerde $Al_x Ga_{1-x}$As laag gescheiden door een zogenaamde $Al_x Ga_{1-x}$As "spacer" laag. In een Si–δ–gedoteerde GaAs structuur bevinden zowel de elektronen als de geladen onzuiverheden zich in één en dezelfde twee–dimensionale laag.

In een GaAs/$Al_x Ga_{1-x}$As heterostructuur hebben we de volgende twee methodes onderzocht die de interactie tussen de elektronen en de geladen onzui-verheden beïnvloeden: 1) belichting van de heterostructuur en 2) het aanleggen van een positieve back–gate spanning. In een Si–δ–gedoteerde structuur hebben we onderzocht wat de invloed is van de geladen onzuiverheden op de elektronen in de verschillende bezette subbanden.

In een GaAs/$Al_x Ga_{1-x}$As heterostructuur zal door het aanleggen van een positieve back–gate spanning de elektronendichtheid toenemen. Zelfconsistente berekeningen laten zien dat de gemiddelde afstand van de omhullende golffunktie tot het GaAs/$Al_x Ga_{1-x}$As grensvlak toeneemt. Omdat tevens de helling van de Γ–geleidingsband in het GaAs wordt verlaagd is het mogelijk dat door een te hoge gatespanning elektronen vanuit het 2DEG naar het semi–isolerende GaAs sub-straat kunnen toestromen. Experimenten, waarbij de elektronendichtheid als funktie van de back–gate spanning wordt gemeten, laten zien dat er inderdaad op een lading vanuit het 2DEG naar het GaAs substraat toestroomt.

Dankzij het persistente fotogeleidingseffect in Si–gedoteerd $Al_x Ga_{1-x}$As ($0.25 > x > 0.6$) neemt de electronendichtheid in een GaAs/$Al_x Ga_{1-x}$As hetero-structuur na belichting blijvend toe. De nog nauwelijks begrepen oorzaak van dit persistente fotogeleidingseffect ligt in de vorming van het zogenaamde DX–cen-trum in Si–gedoteerd $Al_x Ga_{1-x}$As. In dit proefschrift wordt door ons een drie-niveauschema gepresenteert om de bezetting van het DX–centrum te berekenen.

In een GaAs/Al$_x$Ga$_{1-x}$As heterostructuur is het mogelijk dat ten gevolge van belichting, naast de geleiding in het 2DEG, ook parallele geleiding ontstaat in de Si-gedoteerde Al$_x$Ga$_{1-x}$As laag. De invloed van parallele geleiding op de Hall weerstand en magnetoweerstand bij 4.2 K is experimenteel onderzocht en vergeleken met modelberekeningen.

Door gebruik te maken van zowel belichting als het aanleggen van een back-gate spanning is het mogelijk om in een GaAs/Al$_x$Ga$_{1-x}$As heterostructuur de interactie tussen de elektronen en het 2DEG te beïnvloeden. In het geval dat een positieve back–gate spanning wordt aangelegd blijft het aantal geïoniseerde donoren gelijk en wordt de afstand tussen de omhullende golffunktie en het GaAs/Al$_x$Ga$_{1-x}$As grensvlak groter. Na belichting neemt het aantal geïoniseerde donoren toe en wordt de afstand tussen de omhullende golfunktie en het GaAs/Al$_x$Ga$_{1-x}$As grensvlak kleiner. Als beide methode worden gecombineerd zodanig dat de elektronendichtheid in de twee experimenten gelijkis dan zal de interactie met de geïoniseerde donorenhet grootst zijn na belichting.

Met behulp van dergelijke experimenten hebben we gevonden bepaald dat de asymmetry van de spin–op en spin–neer piek in de magnetoweerstand van het 2DEG wordt bepaald door de interactie met de positief geladen donoren in het Al$_x$Ga$_{1-x}$As. In dit proefschrift wordt tevens een mogelijke verklaring gegeven voor deze verandering van de asymmetrie ten gevolge van de interactie tussen geïoniseerde donoren en de elektronen in het 2DEG.

Hetzelfde soort experimenten werd uitgevoerd om de afhankelijkheid van het geheeltallige en het fractionele quantum Hall effect (QHE) van de geladen onzuiverheden te bepalen. Het bleek dat het geheeltallige QHE sterker wordt met toenemende interactie de geïoniseerde donoren terwijl in dat geval het fractionele QHE in dat geval juist zwakker wordt. Dit toont op een duidelijke wijze aan dat beide effekten een verschillende fysische oorzaak hebben.

Uit de literatuur is bekend dat de groeitemperatuur een belangrijke parameter is voor de verbreding van Si–doterings profielen in Si–δ–gedoteerde GaAs structuren. Door deze structuren te groeien bij een temperatuur van 480 ^{0}C zijn we er in geslaagd om de breedte van de doteringsprofielen te verkleinen tot 20 Å of minder. De karakterisatie van deze structuren, d.w.z. de breedte van de doteringsprofielen en de mobiliteit in de verschillende subbanden, werd verricht door magneto–transport metingen. Vanwege de kleine breedte van de doteringsprofielen in onze structuren is de mobiliteit in de verschillende subbanden erg groot.

LIST OF PUBLICATIONS

1   J.H. Wolter, F.A.P. Blom, P.M. Koenraad, and P.F. Fontein,
     "The Influence of Impurities on the Shubnikov–de Haas and Hall Resistance
     of Two Dimensional Electrongases in GaAs/$Al_xGa_{1-x}As$ heterostructures
     investigated by Back–gating and Persistent Photoconductivity.",
     NATO ASI series B **183**, "Physics of Impurity States in Superlattice
     Semiconductors", p. 297, ed. C.Y. Fong (Plenum Press,1988).

2   P.M. Koenraad, F.A.P. Blom, P.W.M. Blom, C.T. Foxon, E.N.M. Frijns,
     J.J. Harris, G. Weimann, and J.H. Wolter.
     "Dependence of Spin–Asymmetry in the Shubnikov–de Haas Resistance on
     Back–Gating, Illumination and Uni–Axial Stress",
     Superlatt. and Micro., **5**, 519 (1989).

3   P.M. Koenraad. F.A.P. Blom, J.P. Cuypers, C.T. Foxon,
     J.A.A.J Perenboom, S.J.R.M. Spermon, and J.H. Wolter,
     "Different behaviour of Integral and Fractional Quantum–Hall Plateaus in
     GaAs/AlGaAs heterostructures under Back–Gating and Illumination",
     Proceedings "High Magnetic Fields in Semiconductors II", Würzburg, p. 150,
     ed. by G. Landwehr (Springer–verlag, 1989).

4   P.W.M. Blom, P.M. Koenraad, F.A.P. Blom, and J.H. Wolter,
     "Analysis of the Shallow and Deep Occupancies in Si–doped $Al_xGa_{1-x}As$
     using a Multilevel Donor Model",
     accepted for publication in Journ. App. Phys.

5   P.M. Koenraad, A.P.J. Voncken, J. Singleton, F.A.P. Blom,
     C.J.G.M. Langerak, M.R. Leys, J.A.A.J Perenboom, S.J.R.M. Spermon,
     W.C. van der Vleuten, and J.H. Wolter,
     "Characterization of Silicon δ–doped GaAs grown by MBE at various
     Temperatures.", accepted for publication in Surf. Sci.

6   P.M. Koenraad, F.A.P. Blom, C.J.G.M. Langerak, M.R. Leys,
     J.A.A.J. Perenboom, J. Singleton, S.J.R.M. Spermon, W.C. van der Vleuten,
     A.P.J. Voncken, and J.H. Wolter,
     "The Observation of High Mobility and Cyclotron Resonance in 20 Å Silicon

δ–doped GaAs grown by MBE at 480 ^{0}C.",
accepted for publication in Semicond. Sci. Technol.

7   P.M. Koenraad, B. Wolfs, F.A.P. Blom,and J.H. Wolter,
"Parallel Conduction in GaAs/Al$_x$Ga$_{1-x}$As heterostructures",
to be submitted.

8   P.M. Koenraad, G.H.C. van Werkhoven, F.A.P. Blom, J.H. Wolter,
"Irreversible Effects of Back–gating and Wavelength Dependent Illumination
on the Transport Properties of the 2DEG in GaAs/Al$_x$Ga$_{1-x}$As
Heterostructures", to be submitted.

CURRICULUM VITAE

geboren: 13 oktober 1959 te Vught

middelbaar onderwijs: Maurick College te Vught
                        HAVO 1977
                        Atheneum 1979

doctoraal examen: Rijksuniversiteit Utrecht
                        Faculteit Natuurkunde
                        14 september 1986
                        Hoofdvak: Experimentele Natuurkunde
                        Bijvakken:Wiskunde en Mathematische fysica

promotie onderzoek: Technische Universiteit Eindhoven
                        Faculteit Technische Natuurkunde
                        van 15 september 1986 tot 16 februari 1990
                        Het onderzoek is gedeeltelijk verricht op het
                        Laboratorium voor Hoge Magneetvelden van de
                        Katholieke Universiteit Nijmegen.

Stellingen

behorende bij het proefschrift

**The Influence of Ionized Impurities on the
Transport Properties of a Two–Dimensional Electron Gas**

1) De berekening van de elektronendichtheid in Si–gedoteerd $Al_xGa_{1-x}As$ met behulp van onafhankelijke donortoestanden is onjuist.
   - N. Lifschitz, A. Jayaraman, and R.A. Logan, Phys. Rev. B <u>21</u>, 21 (1980)
   - M. Tachikawa, M.Mizuta, H. Kukimoto, and S. Minomura,
     Jap. Journ. Appl. Phys. <u>24</u>, L821 (1985)
   - hoofdstuk 2 van dit proefschrift

2) Het gecombineerde gebruik van een back–gate en belichting maakt het mogelijk om in hetzelfde sample en bij dezelfde elektronendichtheid de interactie met de geladen onzuiverheden te manipuleren.
   - hoofdstuk 5 van dit proefschrift

3) Na 13 jaar intensief onderzoek is het microscopisch gedrag van Si in $Al_xGa_{1-x}As$ $(0.25 > x > 0.60)$ nog steeds niet begrepen.
   - D.V. Lang and R.A. Logan, Phys. Rev. Lett. <u>39</u>, 635 (1977)
   - D.J. Chadi and K.J. Chang, Phys. Rev. Lett. <u>61</u>, 873 (1988)
   - J.C.M. Henning and Ansems, Semicond. Sci. Technol. <u>2</u>, 1 (1987)

4) "Scanning Tunneling Microscopy" biedt een zeer interessante mogelijkheid om rechtstreeks de breedte van de elektronenverdeling en de energieniveaus in Si–δ–gedoteerde GaAs structuren te bepalen.
   - H.W.M. Salemink, H.P. Meier, R. Ellialtioglu, J.W. Gerritsen, and
     P.R.M. Muralt, Appl. Phys. Lett. <u>54</u>, 1112 (1989)

5) De breedte van niet–coïncidente elektronenenergiespectra bij Li⁺–He botsingen voor een botsingsenergie van 2keV zijn niet het gevolg van een moleculaire autoïoniserende toestand.

   – P. van der Straten, P. Koenraad, R. Morgenstern, A. Niehaus,
     Z. Phys. A <u>320</u>, 81 (1985)

6) De ruis in $GaAs/Al_xGa_{1-x}As$ heterostructuren is sterk afhankelijk van de vulfactor van het Landau–niveau.

   – A.J. Kil, R.J.J. Zijlstra, P.M. Koenraad, J.A. Pals, and J.P. André,
     Solid State Comm. <u>60</u>, 831 (1986)

7) Met plaatselijke front–gates op de contactarmen in een Hall–bar structuur moet het mogelijk zijn om parallele geleiding in $GaAs/Al_xGa_{1-x}As$ heterostructuren bij 4.2 K te onderdrukken.

8) De bepaling van de halve lange as van meteoorbanen aan de hand van fotografische simultaan opnamen is zeer moeilijk voor meteoren met een snelheid nabij de hyperbolische waarde.

9) Om het imago van de Technische Universiteit Eindhoven te bevorderen dient op centraal niveau een fietsenmaker aangesteld te worden.

10) Veel hondenfokkers besteden meer aandacht aan de voeding van hun honden dan aan hun eigen voeding.

16 februari 1990, Eindhoven   Paul Koenraad